Phil. Trans. R. Soc. Lond. B **310**, 573–609 (1985) [573]
Printed in Great Britain

THE OLIVARY PRETECTAL NUCLEUS: EXPERIMENTAL ANATOMICAL STUDIES IN THE RAT

By G. CAMPBELL AND A. R. LIEBERMAN

Department of Anatomy and Embryology, University College London, Gower Street, London WC1E 6BT, U.K. and Institute of Anatomy B, University of Aarhus, DK-8000 Aarhus C, Denmark

(*Communicated by E. G. Gray, F.R.S.* – *Received* 21 *September* 1984)

[Plates 1–19]

CONTENTS

 [Published 14 October 1985

The olivary pretectal nucleus (OPN) is one of several pretectal nuclei with direct input from the eye, but is the only one containing neurons whose rate of firing is linearly related to the intensity of light falling on the retina. It is thus the first central station in the pupillary light reflex. We report experimental light (l.m.) and electron microscope (e.m.) studies of this nucleus in adult albino and pigmented rats, the first extensive study of this or of any other mammalian pretectal nucleus.

The more cytoarchitecturally distinct rostral part of the nucleus (*pars oralis* of F. Scalia (*J. comp. Neurol.* **145**, 223–253, 1972)), which is approximately 350 μm in diameter in coronal sections was analysed. It displays a peripheral shell of closely packed neurons and a central core in which cell density is lower and in which there are very few myelinated fibres. Cellular and synaptic organization appear to be identical in albino and pigmented animals but the nucleus is more superficially situated in albinos because the brachium of the superior colliculus is thinner than in pigmented animals.

Two major cell types were recognized in Golgi preparations. Class I cells were large (somal diameter 15–30 μm) with three to six radiating dendrites which were sparsely branched and sparsely spined, and an axon, arising either from the soma or a proximal dendrite and impregnated for only 20–40 μm from its origin. Class II cells were smaller and commonly bipolar (somal diameter 7–10 × 15–20 μm) with few minimally branched dendrites bearing complex dendritic appendages. The latter were particularly numerous close to the distal extremities of the dendrites and were often also conspicuous close to the origin of the dendrites. One subpopulation of class II cells (class IIa cells) were bipolar with dendrites showing a predominantly dorsomedial to ventrolateral orientation; class IIb cells had smaller, often spherical somata and their dendrites tended to curve around the parent cell body to establish a restricted dendritic domain. Few class II cells give rise to unequivocal axons.

By e.m., class I cells bodies were characterized by pale, organelle-rich cytoplasm and pale, extensively indented nuclei. Their cell bodies, dendrites and dendritic spines were exclusively postsynaptic. Class II cell bodies were variable in size but generally smaller, less rich in organelles and more irregularly shaped than the cell bodies of class I cells, and their cytoplasm and nuclei more electron dense. Their cell bodies and dendritic shafts contained focal clusters of, and their dendritic appendages and the terminal parts of smaller dendrites, large numbers of, pleomorphic electron lucent synaptic vesicles: these cellular domains were all presynaptic as well as postsynaptic.

The neuropil of OPN was characterized by extensive areas of small, closely packed neural profiles engaged in complex synaptic relationships, surrounded by a simpler neuropil in which axodendritic synapses predominated. In addition to the dendrites and appendages of class I neurons (D-profiles) the neuropil contained four principal presynaptic components. RP-boutons (36%) contained spherical synaptic vesicles and large pale mitochondria, made Gray type 1 synaptic contacts and were shown by experimental degeneration after eye enucleation and by labelling after intravitreal injection of HRP (DAB-cobalt chloride method) to be retinal in origin. RD-boutons (3%) contained spherical vesicles and small dark mitochondria, made Gray type 1 synaptic contacts outside the areas of complex neuropil and experimental evidence to be reported elsewhere shows that many and possibly all RD-boutons originate in the superior colliculus. F-boutons (8%) were varied in size and shape, contained closely packed flattened synaptic vesicles, and made Gray type 2 synaptic contacts. Their origins were not ascertained. P-boutons (18%) irregularly shaped and pale, containing loosely packed pleomorphic synaptic vesicles, and sometimes ribosomes, were both postsynaptic and presynaptic (at small specializations resembling Gray type 2 contacts but with a slightly thicker postsynaptic density) and were identified as the dendrites and dendritic appendages of class II cells. RP-boutons, RD-boutons, F-boutons and P-boutons were all presynaptic to both D-profiles and P-boutons. In addition the cell bodies of class II cells were presynaptic to the dendrites and cell bodies of class I cells and F-boutons made synaptic contact with the cell bodies, somal spines and dendritic shafts of both class I and class II cells and with the axon hillocks and initial axon segments of the former. RP-, RD- and P-boutons were only rarely presynaptic to cell bodies.

Analysis of serial sections of the neuropil revealed the presence of serial synapses of variable composition and remarkable complexity, all based on the dual postsynaptic and presynaptic properties of P-boutons. Triplet synapses

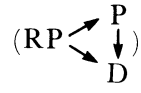

were characteristic of the complex neuropil and may be concerned with feed-forward inhibition of projection cells, as has been previously suggested for thalamic nuclei, although the functional significance of these and the rather complex synaptic interactions that occur in OPN neuropil remains to be established.

The organization of the retinal projections to OPN was analysed by l.m. after unilateral intravitreal injections of HRP or radioactive amino acids. Previous findings that the input is predominantly contralateral were confirmed and evidence obtained that there may be some overlap between the inputs from the two eyes. We have also demonstrated that in parasagittal sections the contralateral retinal terminal fields form a folded sheet resembling a W facing rostrodorsally and have confirmed that the ipsilateral terminal field in the lateral part of the nucleus is larger in pigmented than in albino animals.

Radioautographs of transneuronal labelling following injections of [^{3}H]proline and [^{3}H]fucose into one eye revealed a bundle of efferent fibres, which emerged from the ventromedial border of OPN, ran medially and then turned to pass ventrocaudally through the periaqueductal grey to the Edinger–Westphal nucleus.

Electron-microscope studies of OPN 1–15 days after contralateral eye enucleation showed the earliest degenerative changes in RP-boutons to consist of vesicle enlargement and an increase in the number of neurofilaments. Massive neurofilamentous hyperplasia associated with loss and clumping of synaptic vesicles was seen in many boutons (and preterminal axons) from 3 to 12 days after enucleation. Moderately electron dense flocculent material also appeared in some affected terminals within two or three days of enucleation, and electron dense degenerating terminals (first seen,

but rare, at three days) were common by six days and predominated after about eight days. Glial engulfment of degenerating boutons involved only those showing the dense form of degeneration. 'Vacated' postsynaptic densities and signs of their reoccupation by F- or P-boutons were seen at, and after, 11 days.

These findings strengthen the evidence for a central role of the OPN in the pathway for the pupillary light reflex. The surprising complexity of the neuropil of OPN, which resembles the neuropil of the dorsal lateral geniculate nucleus, and the existence of inputs from several sources other than the retina (including superior colliculus and ventral lateral geniculate nucleus) suggest that extensive processing of luminance information may occur within the OPN.

1. Introduction

The mammalian pretectum is an area of complex cytoarchitecture in the rostral brain stem at the junction between the mesencephalon and the diencephalon. It comprises several distinct nuclear groups, the connections and functional associations of which are different from one another, but most of which appear to be concerned with eye reflexes, eye movements, and visually guided behaviours (Sprague *et al.* 1973; Collewijn 1975). Experimental anatomical studies of the pretectum to date have been concerned chiefly with the projections to and from the pretectal area as a whole, or in relation to specific pretectal nuclei (Giolli & Guthrie 1971; Scalia 1972; Carpenter & Pierson 1973; Kanaseki & Sprague 1974; Itoh 1977; Berman 1977; Graybiel & Berson 1980; Weber & Harting 1980; Holstege & Collewijn 1982). There have been published no systematic ultrastructural studies of the pretectum in any species.

Of the various nuclear groups in the pretectal region, the one with the most distinctive cytoarchitecture and the most clearly established role, is the olivary pretectal nucleus (OPN). It is the major and possibly the sole pretectal nucleus involved in the pupillary light reflex. Like other parts of the pretectum, including the nucleus of the optic tract and the posterior pretectal nucleus (nomenclature according to Scalia 1972) the OPN receives direct input from the retina in many species: rat (Nauta & Van Straaten 1947; Viktorov 1969; Scalia 1972; Repérant 1975; Colman *et al.* 1976; Scalia & Arango 1979; Perry & Cowey 1979; Campbell & Lieberman 1980); cat (Kanaseki & Sprague 1974; Berman 1977); primates (Hendrickson *et al.* 1970; Pierson & Carpenter 1974; Tigges & O'Steen 1974; Santos-Anderson *et al.* 1976; Graham *et al.* 1979). But although several pretectal nuclei receive retinal input, the OPN alone among such nuclei, in the cat and rat at least, contains 'luminance detector units', neurons whose rate of firing is directly related to the intensity of light falling on the retina (Loewy 1979; Clarke & Ikeda 1981; Trejo & Cicerone 1984). Furthermore, there is evidence that the OPN sends axons directly to the Edinger–Westphal (accessory oculomotor) nucleus. This appears to be the case in the monkey (Carpenter & Pierson 1973; Pierson & Carpenter 1974; Benevento *et al.* 1977; Steiger & Büttner-Ennever 1979), cat (Breen *et al.* 1983) and rat (Itaya & Van Hoesen 1982; Campbell 1982), and recent evidence has shown this to be so for the pigeon, in which the area pretectalis (the avian homologue of the mammalian OPN) projects directly to the Edinger–Westphal nucleus (Gamlin *et al.* 1984). From the Edinger–Westphal nucleus arise the preganglionic parasympathetic fibres which induce pupillary constriction via their connection with the neurons of the ciliary ganglion. In some species, however, a proportion of pretectal afferents to the Edinger–Westphal nucleus possibly originating from the nucleus of the optic tract (Berman 1977) may reach the Edinger–Westphal nucleus via a relay in the

nucleus of the posterior commissure rather than directly from OPN (cat (Graybiel & Hartwieg 1974; Berman 1977; see also Breen *et al.* 1983); tree shrew (Weber & Harting 1980)). In addition, OPN, in the cat at least, appears to play a central role in the mediation of the visually triggered blink reflex via direct projections to the facial motor nucleus (Itoh *et al.* 1983).

The first part of this paper deals with the morphology and cytology of cell types in OPN and the main features of synaptic organization in this nucleus. In the second part, we describe the organization of the retinal input to OPN in the albino and pigmented rat by using a sensitive anterograde tracing method using horseradish peroxidase (HRP) and tetramethylbenzidine (TMB) (Mesulam 1978) and add to previous accounts of these projections based on the degeneration method (Scalia 1972) and on the radioautographic method (Scalia & Arango 1979). We also report radioautographic observations of transneuronally transported radioactive label which reveal a direct projection from OPN to the region of the Edinger–Westphal nucleus in the albino rat. And finally, we report on the identification by electron microscopy of retinal terminals in OPN following section of the optic nerve or injection of HRP into the eye, on the synaptic organization of retinal terminals, and on the sequence of degenerative changes in retinal terminals after optic nerve section. Brief accounts of parts of this work have appeared (Campbell & Lieberman 1979, 1980, 1982; Pegg *et al.* 1982).

2. Materials and methods

(*a*) *Animals*

Adult albino rats of the Wistar strain, 150–300 g in body mass, and pigmented rats of the Lister–PVG strain of similar mass were used.

Four animals were used for cell and myelin staining; 97 for the Golgi procedures; and 26 for studies of the fine structure of the normal nucleus, 4 of them pigmented and the remainder albinos. For studies of the retinal input to OPN, 56 albino rats and 2 pigmented rats were used. Seventeen albinos and 2 pigmented rats were used for studies by light microscopy (l.m.) of retinal projections following intravitreal injection of HRP and material from 7 of these animals was also processed for electron microscopy (e.m.). Four animals were used in radioautographic experiments, two for tracing primary retinal projections, and two for tracing transneuronal projections. For the study of retinal input by e.m., 35 animals with unilateral optic nerve section or enucleation, were used, after postoperative survival periods of between 1 and 15 days.

(*b*) *Control material*

(i) *Light microscopy*

For cell and myelin staining animals were anaesthetized with ether and perfused with 4% phosphate-buffered formaldehyde (4 g/100 ml). After one to five days in the same fixative at 4 °C, brains were trimmed, dehydrated in ethanol and embedded in Fibrowax (Raymond Lamb) at 56 °C. Wax sections were cut at 10 μm in the frontal plane. After clearing in xylene and dehydrating in ethanol the sections were stained overnight at 60 °C with methasol fast blue in ethanol (0.1 g/100 ml) and counterstained with cresyl violet.

Brains to be stained for the rapid Golgi method (Valverde 1970) were perfused with 4% phosphate-buffered formaldehyde (4 g/100 ml) and trimmed into 3–5 mm blocks. After the removal of the cerebral cortex the blocks were suspended for at least seven days in an aqueous solution of osmium tetroxide (0.25 g/100 ml) potassium dichromate (2 g/100 ml) in the dark

with daily agitation. After the required time, the OsO_4–dichromate solution was rinsed from the jar, lid and blocks with distilled water and replaced with aqueous silver nitrate solution (0.75 g/100 ml). The blocks remained in this solution for 7–14 days in the dark with daily agitation. The blocks were then dehydrated in ethanol, cleared in xylene and shelled in paraffin wax. Sections were cut at 90 μm in the frontal plane, collected in ethanol, cleared in xylene and coverslipped by using DPX. Of the 97 rats used for the Golgi procedure, 21 had well impregnated, reliably localized and recordable neurons in the OPN, 49 of which were drawn and analysed. Drawings of impregnated neurons were made with a camera lucida attached to a Zeiss standard microscope.

(ii) *Electron microscopy*

Animals were anaesthetized with ether and perfused, with the aid of a peristaltic pump, through the left cardiac ventricle and ascending aorta with a mixture of 4 % paraformaldehyde (Fisons; 4 g/100 ml) and 0.5 % glutaraldehyde (2 ml of 25 % glutaraldehyde (Emscope) per 100 ml of Millonig's 0.1 M phosphate buffer) at pH 7.4 and at approximately 37 °C (modified from Karnovsky 1965). The perfusate was delivered at flow rates of between 15 and 30 ml min^{-1} maintained by a peristaltic pump (Watson-Marlow, MHRE II) through a debevelled hypodermic needle pushed into the ascending aorta through an incision in the left ventricle, and clamped in position with a crocodile clip. The right atrium was cut and the descending aorta clamped. Perfused animals were left in sealed polythene bags at 4 °C overnight. The fixed brains were then removed and sectioned at 100 μm in the frontal plane by using a Vibratome (Oxford Instruments). Sections were collected in buffer, postfixed in aqueous osmium tetroxide (2 g/100 ml) in the same buffer, stained in aqueous uranyl acetate (2 g/100 ml) at 4 °C, dehydrated in a graded series of ethanols, and embedded flat in Araldite. Thin sections of OPN, cut in the frontal plane, were stained with lead citrate (Reynolds 1963) and examined in Philips 300 or 301 electron microscopes. Attention was concentrated on the rostral portion of the nucleus (*pars oralis* of Scalia) since this part of the nucleus can be reliably recognised in 100 μm, Araldite-embedded sections (see figures 1, 2*a*, *b* and *c*, plate 1) and in toluidine blue-stained 1 μm plastic sections (see figure 2*d*).

(iii) *Quantitative analysis*

The frequency and mean area of synaptic vesicle-containing profiles were obtained by using an Apple graphics tablet interfaced with an Apple II microcomputer. Data were colleted from four animals. Electron micrographs were taken at a print magnification of × 23000 of strips of OPN neuropil covering an entire grid window. Care was taken not to overlap adjacent photographs in a strip or to overlap strip edges. Only grid windows that included nothing but OPN neuropil and cells were photographed in this way (two to six grid windows per section for a 200 mesh grid). One ultrathin section from each animal was analysed in this way.

In each micrograph all profiles containing synaptic vesicles were counted and their area measured. Profiles with poorly defined plasma membranes or which were not satisfactorily made visible for some other reason were excluded. Classification into RP-, RD-, F- and P-profiles (see §3*a*ii) was done according to the following characteristic features of these elements; round vesicles and pale mitochondria (RP-profiles), round vesicles and dark mitochondria (RD-profiles), densely packed flattened vesicles (F-profiles), and loosely packed less flattened vesicles (P-profiles). Elements containing round vesicles but not displaying mitochondrial profiles were

placed in an unclassified, round-vesicle (UR) category and ambiguous elements with flattened vesicles were placed in an unclassified, flat-vesicle (UF) category. In all 1839 profiles were counted and measured in a total neuropil area of 10000 μm^2.

The analysis of synaptic vesicles was performed manually. Electron microscope negatives at instrumental magnifications of $\times$ 20000–50000 were projected by a Zeiss microfilm reader at a magnification of $\times$ 6.5, onto a sheet of paper, on which vesicle outlines were traced. Measurements were made from these tracings of the minimum and maximum diameter of each vesicle. Mean maximum diameter and ellipticity ratios (maximum diameter: minimum diameter) were calculated. Eleven terminals that established synaptic contact, containing 1714 vesicles, were analysed in this manner.

(*c*) *Experimental material*

(i) *HRP experiments*

Animals were anaesthetized by brief exposure to ether followed by induction and maintenance of full anaesthesia by a mixture of nitrous oxide, halothane and oxygen, or by intraperitoneal injection of sodium pentobarbitone. A single intravitreal injection of 3–5 µl of 30–50 % HRP solution (Sigma type VI, 3–5 mg/10 µl of sodium chloride solution; 0.9 g/100 ml) was made in one eye, by using a 5 µl Hamilton microsyringe. Care was taken to position the bevelled tip of the 30 gauge needle of the syringe behind the lens without damaging the retina. The HRP was injected over a period of 1 min, and the needle was left in place for a further minute before being withdrawn.

The animals were allowed to recover from the anaesthetic and 17–24 h after injection were again anaesthetized (with ether) and killed by perfusion through the left cardiac ventricle of fixative solution (1 % paraformaldehyde (1 g/100 ml) and 1.25 % glutaraldehyde (5 ml of 25 % glutaraldehyde (Emscope) in Millonig's 0.1 M phosphate buffer at pH 7.3), as described above. When tissue was to be examined only by l.m., 300 ml of fixative (at room temperature) were perfused over a period of approximately 15 min, followed immediately by 200 ml of Millonig's buffer at the same temperature. The brain was then removed and placed in phosphate buffer solution containing sucrose (20 g/100 ml) for 24–48 h. Frozen sections were cut in the coronal plane at a thickness of 20–50 µm on a sliding microtome, by using solid CO_2, and collected in Millonig's buffer. When tissue was also to be used for e.m., perfusion with fixative was carried out as above but the brain was then removed, placed in fresh fixative for approximately 12 h at 4 °C, and cut in the coronal plane at 100 µm in a Vibratome. The sections were collected in Millonig's buffer and in most cases alternate sections were processed using the tetramethylbenzidine (TMB) and diaminobenzidine (DAB) methods.

Sections for l.m. were processed by using TMB according to the recommendations of Mesulam (1978, 1982), and by using 3 ml of 0.3 % H_2O_2 (1 ml of 30 % H_2O_2 (BDH) in 100 ml distilled water) per 100 ml of incubation solution. Reacted solutions were rinsed, immediately mounted on gelatinized slides, air-dried and lightly counterstained with neutral red. Sections for l.m. and e.m. were processed by using the DAB method described by Graham & Karnovsky (1966) with the cobalt intensification modification of Adams (1977) and by using the same amount of H_2O_2 as for the TMB method. Reacted sections were either rinsed in distilled water, mounted on gelatinized slides, lightly counterstained with cresyl violet, coverslipped and examined by l.m. or were washed in Millonig's buffer and then processed for e.m. as described in §2*b*ii, with the exception that the staining step in uranyl acetate was occasionally omitted.

(ii) *Radioautography experiments*

For tracing the primary visual pathways a single injection of 2.5 μl of a solution containing 80 μCi of [^{3}H]proline was made into the vitreous body. For tracing secondary pathways 4.0 μl of a solution containing 75 μCi of [^{3}H]proline and 75 μCi of [^{3}H]fucose was injected on each of three successive days (that is, total dose administered was 225 μCi of [^{3}H]proline and 225 μCi of [^{3}H]fucose). The radioisotopes ([^{3}H]proline, specific activity 27 Ci mmol^{-1}; [^{3}H]fucose, specific activity 26 Ci mmol^{-1}) were obtained from Amersham International and were concentrated by evaporation in a stream of nitrogen. The injections were made as for the injections of HRP, with the difference that the syringe and all glassware containing solutions for injection were sterilized before use and sterile conditions were maintained throughout the operations.

After one day (for tracing primary visual pathways) or 9 and 20 days (for tracing secondary projections; counted from the day on which the first injection was given), the animals were again anaesthetized (with ether), and perfused as described above, with 300 ml of buffered formalin (Pease 1964) over a period of approximately 20 min. The brains were removed, kept in Pease's fixative for 12–24 h at 4 °C and then sectioned in the coronal or parasagittal plane at 40 μm, by using a freezing sliding microtome and solid CO_2. The sections were collected in distilled water, mounted on gelatinized slides, air-dried and exposed to formaldehyde vapour for 12 h at 37 °C. The sections were then cleared in xylene, hydrated through a series of ethanol solutions, stored in distilled water, and coated with Ilford K5 emulsion. The slides were dried, exposed and developed as recommended by Cowan *et al.* (1972), stained with thionin and coverslipped. In addition, similar preparations were kindly made available from the laboratory of Professor K. E. Webster, King's College, London. These included three series of frontal sections and one series of sagittal sections derived from four albino adult rats which each received intravitreal injections of [^{3}H]proline–[^{3}H]fucose radioactive tracer cocktail at total doses of 200–250 μCi and which survived for 10 days after the injections.

(iii) *Optic nerve section and enucleation*

Animals were anaesthetized as for intravitreal injections and the cornea irrigated with Amethocaine until the corneal reflex was completely abolished. The optic nerve was then approached by dissecting through orbital connective tissue from the lateral aspect of the eye, exposed, and transected with fine scissors. The extraocular muscles were not cut and the eye was left *in situ*. Alternatively and in most cases, the optic nerve was exposed, clamped with fine artery forceps, cut above (distal to) the clamp and the eye removed by cutting through the extraocular muscles. The clamp was then released and the eyelids sutured together.

After postoperative survival times of 1–15 days the animals were again anaesthetized, perfused as described in §2*b*ii and the OPN on both sides of the brain prepared for study in the e.m. as described in §2*b*ii.

3. Results

(*a*) *Normal material*

(i) *Light microscopy*

(a) *Cytoarchitecture and myeloarchitecture.* The OPN is a small nucleus. Its rostrocaudal extent is approximately 300 μm and at the level at which its cross-sectional area is greatest, it is

Description of plate 1

Figures 1–4. Light microscopy. Cytoarchitecture, myeloarchitecture and cell types of OPN.

Figure 1. Frontal 10 μm paraffin section, stained with cresyl violet and methasol fast blue, through the brain of an adult albino rat at the level of *pars oralis* of the OPN (arrows). APN, anterior pretectal nucleus; LP, lateral posterior nucleus; LGd, dorsal lateral geniculate nucleus; br., brachium of the superior colliculus; *, fasciculus retroflexus; v., third ventricle. Magn. × 19.8.

Figure 2 (*a*) Enlargement of left OPN *pars oralis* from figure 1, showing the clear, 'gelatinous' neuropil of OPN beneath the myelinated fibres of the brachium of the superior colliculus (br.). A large blood vessel penetrates the nucleus from its dorsolateral aspect (arrow). d., Dorsal; l., lateral. Unless otherwise stated or shown, all l.m. photographs and drawings of the OPN are displayed in the same orientation as in this figure. Magn. × 72.
(*b*) Frontal section of OPN *pars oralis* (technical details as for figure 1) at a more rostral level and at a higher magnification, showing the clusters of cells at the centre of the nucleus and the small bundles of myelinated fibres radiating across the gelatinous neuropil. Magn. × 180.
(*c*) Frontal, Vibratome slice, 100 μm thick, osmicated and embedded in Araldite and from approximately the same level as that depicted in figure 1. The OPN (arrow) is seen as a pale, oval region dorsolateral to the posterior commissure (p.c.). Thin sections for e.m. analysis were cut from such slices. LGd, dorsal lateral geniculate nucleus. Magn. × 11.7.
(*d*) Frontal, 1 μm thick toluidine-blue stained section of the OPN, with its conspicuously myelin-poor neuropil, cut from a 100 μm slice such as that shown in figure 2*c*. All series of thin sections for e.m. analysis were cut at this size and shape between two such semi-thin sections. Magn. × 72.

Figures 3 and 4. Rapid-Golgi preparations. All figures are from 90 μm frontal sections of the OPN *pars oralis*.

Figure 3. (*a*) Three class I cells with their perikarya in the peripheral shall of densely packed cell bodies. Magn. × 72. (*b*)–(*d*) Initial segments of axons (arrows) arising from the cell body (figure 3*b*) and proximal dendrites (figure 3*c*, *d*) of class I cells. A dendrite arising from the cell body in figure 3*b* bears two, small, forked spines (arrowheads). A drawing of the cell in figure 3*b* appears in figure 5. Figure 3*b* magn. × 720; figure 3*c* magn. × 450; figure 3*d* magn. × 450.

Figure 4. (*a*)–(*c*) A class II cell lying close to the ventromedial border of OPN (figure 4*a*). The cell has two dendrites. The one directed dorsolaterally emits a thin, beaded, axon-like process, which is shown at greater magnification and at a different plane of focus, in figure 4*b*. The other dendrite gives rise to several irregularly shaped appendages, the most complex of which (in the region indicated by the arrow) are enlarged in figure 4*c*. Figure 4*a* magn. × 72; figure 4*b* magn. × 450; figure 4*c* magn. × 450. (*d*)–(*e*) Bipolar class IIa cell with two long, straight dendrites, one with a cuff of complex appendages around its proximal portion (arrow). Other, irregularly shaped protrusions arising more distally from this same dendrite, are enlarged in a through-focus series in figure 4*e*. This region is also shown in the drawing of the cell in figure 6*a*, in which the proximal cuff of protrusions is indicated by arrow 1 and the more distal appendages by arrow 2. This cell is also illustrated in the abstract of Pegg *et al.* (1982). Figure 4*d* magn. × 288; figure 4*e* magn. × 1080. (*f*) Complex dendritic appendages of a long, thin tertiary dendrite (seen also at arrow 3 in figure 6*b*) branching from a thick secondary dendrite (arrow) of a class IIb cell. Magn. × 1080.

Description of plate 2

Figures 5 and 6. Light microscopy. Golgi-impregnated class I and class II cells. Composite camera lucida drawings of Golgi-impregnated class I (figure 5), class IIa (figure 6*a*) and class IIb (figure 6*b*) neurons. The outlines of OPN are indicated by the dashed lines. Note the long, sparsely spined dendrites of the class I cells, and the axon initial segment (arrow) illustrated in figure 3*b*. The complex dendritic appendages of class II cells are evident and those indicated by numbered arrows are illustrated further in figures 4*d* (arrow 1), 4*e* (arrow 2) and 4*f* (arrow 3). Magn. × 270. Drawing by D. J. Pegg.

(*Facing p.* 580)

Description of plate 3

Figures 7–9. Electron microscopy. Cell bodies of class I neurons.

Figure 7. Large neuron with prominent granular endoplasmic reticulum (g.e.r.) and moderately indented nuclear outline. A series of three extremely flattened parallel cisterns of granular reticulum from the stack at the top right of the figure is enlarged in the inset. Magn. ×4500; inset ×32400.

Figure 8. Neuron with an eccentrically located nucleus, prominent nucleolus and nuclear infoldings facing into the cytocentrum, in which elements of the Golgi apparatus are prominent. Magn. ×5400.

Figure 9. A cluster of neurons in the peripheral shell of OPN, showing parts of three class I cells (I) and of two class II cells (II). Note the relatively greater diameter, cytoplasm:nucleus ratio, and extent of nuclear infolding in the class I cells. The large, centrally situated class I cell is contacted by two terminals (large arrow and enlargement in inset), one containing spherical synaptic vesicles and identifiable as an RD-terminal (see §3*a*iic), the other flattened synaptic vesicles. Much of the surface of this and the other cells shown is related to narrow sheets of astrocytic cytoplasm. A transversely sectioned cilium is indicated by the small arrow. Magn. ×7200; inset 33750.

Description of plate 4

Figures 10–12. Electron microscopy. Axosomatic synapses and somal spines of class I cells.

Figure 10. Parts of two class I cells, both with deeply folded nuclei, are shown in figure 10*a*. The lower cell, which has a prominent nucleolus and a large dendrite extending to the right, receives a large number of axosomatic synapses from a variety of boutons, some of which are enlarged in figures 10*b* (region of arrow) and 10*c* (region of arrowhead). Boutons containing flattened synaptic vesicles and making Gray type 2 contacts predominate (F-boutons; see §3*a*iic) but some contain spherical vesicles and make Gray type 1 contacts (figure 10*c*; RD-bouton). Figure 10*a* magn. ×2700; figure 10*b* magn. ×25650; figure 10*c* magn. ×32850.

Figure 11. Axon terminals containing flattened synaptic vesicles in Gray type 2 synaptic contact with class I cell bodies. The terminal in figure 11*a* is densely packed with vesicles, the two in figure 11*b* rather less so. The terminal to the right in figure 11*b* makes both a synaptic and a long adherens-like contact (arrow). The arrow in figure 11*a* indicates short adherens-like contact (arrow). The arrow in figure 11*a* indicates short adherens-like specializations between perineuronal astrocytic processes and between the innermost such process and the plasma membrane of the neuron. Arrowheads in figure 11*a* show the preterminal axon. Figure 11*a* magn. ×14850; figure 11*b* magn. ×27000.

Figure 12. Part of the cell body and base of a dendrite of a large class I cell (figure 12*a*). At the arrow the cell gives rise to a large branched spine enlarged in figure 12*b* and from a serial section in figure 12*c*. Note the flocculent moderately electron-dense material within the spines (S). The isolated spine profile marked S1 in figure 12*b* is revealed as part of S in figure 12*c*. The spine is surrounded by a cluster of axon terminals, including two F-terminals (F) and one RP-terminal (RP, see §3*a*iic). Figure 12*a* magn. ×3600; figures 12*b*, *c* magn. ×25200.

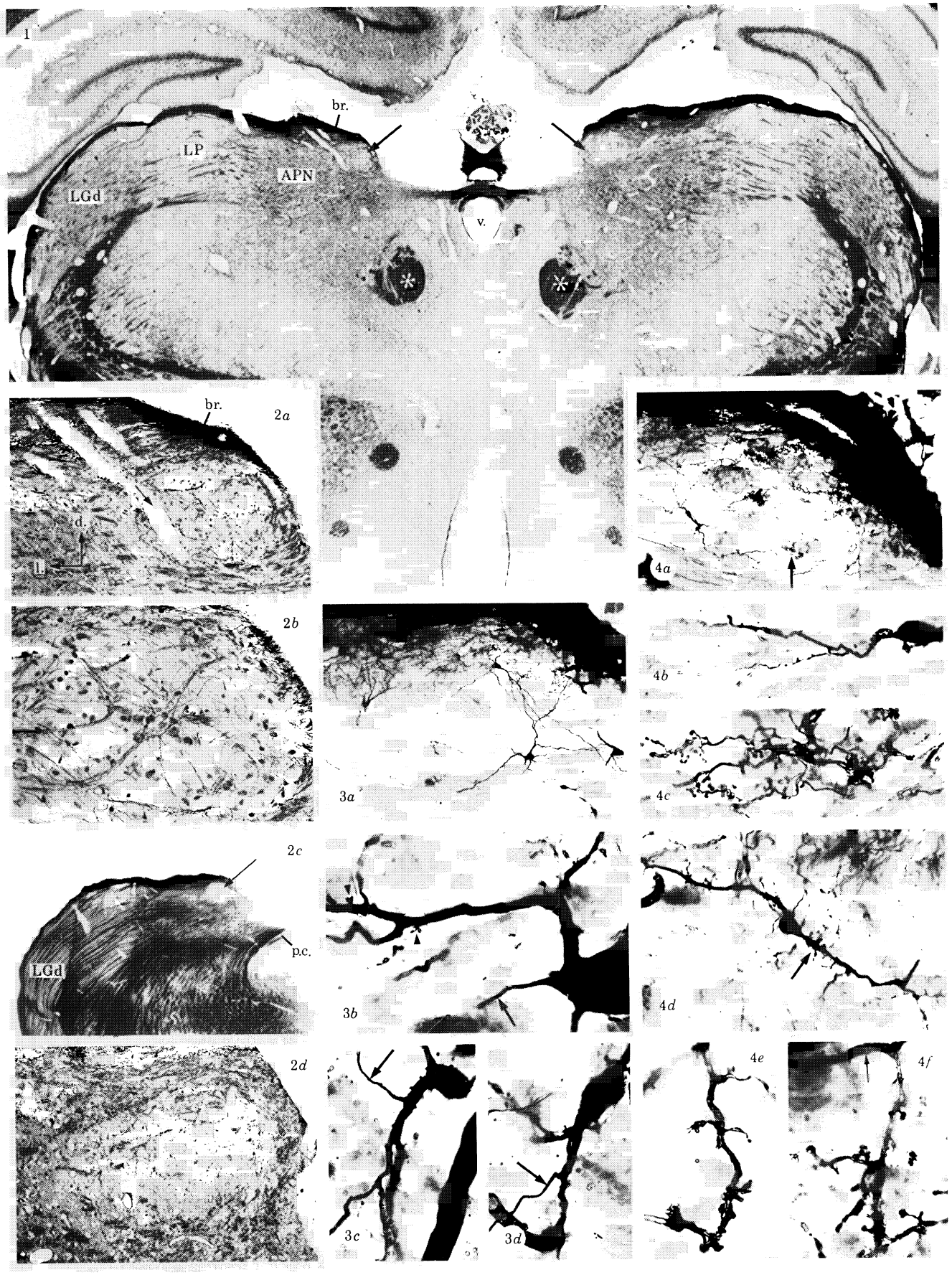

FIGURES 1–4. For description see facing p. 580.

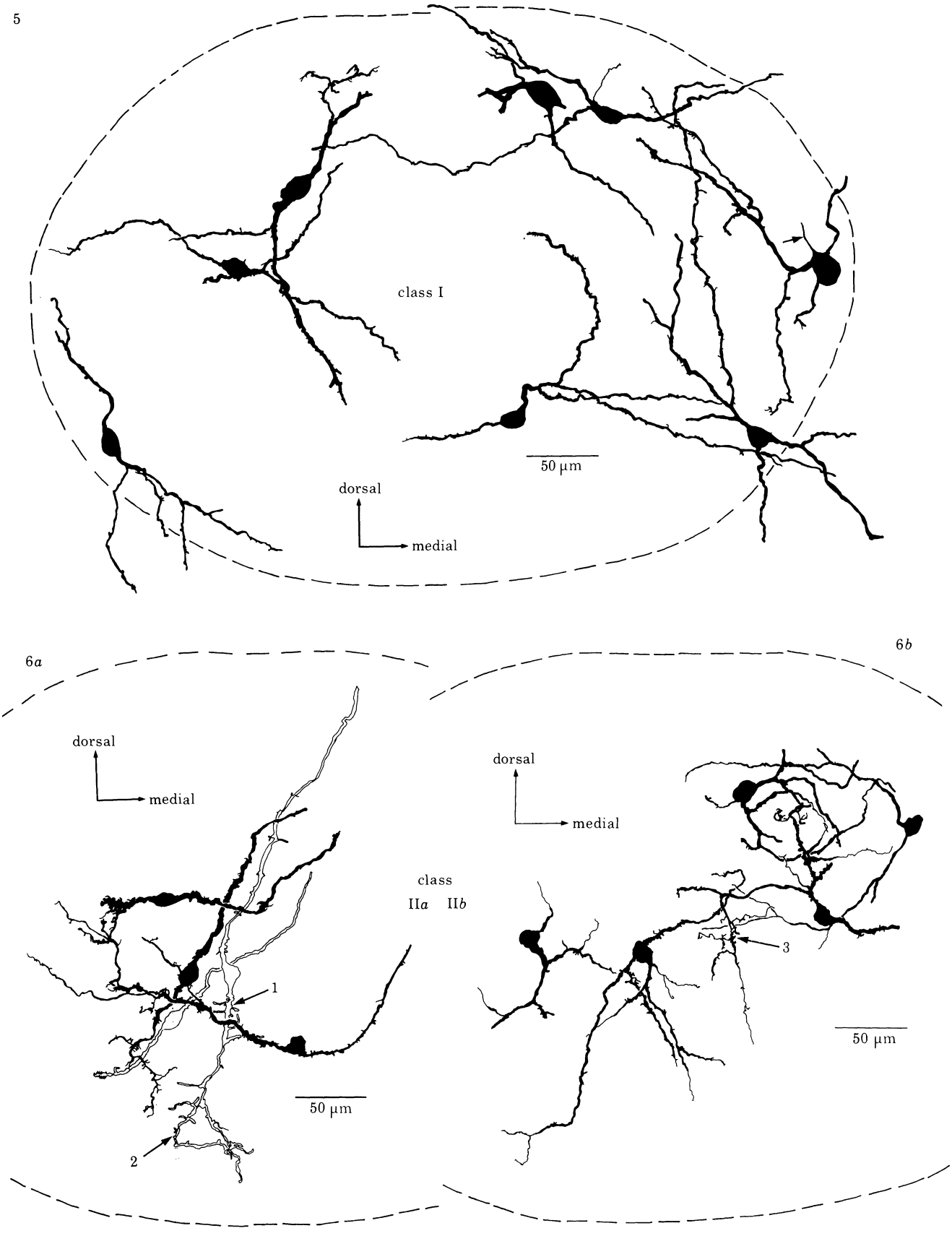

FIGURES 5 AND 6. For description see facing p. 580.

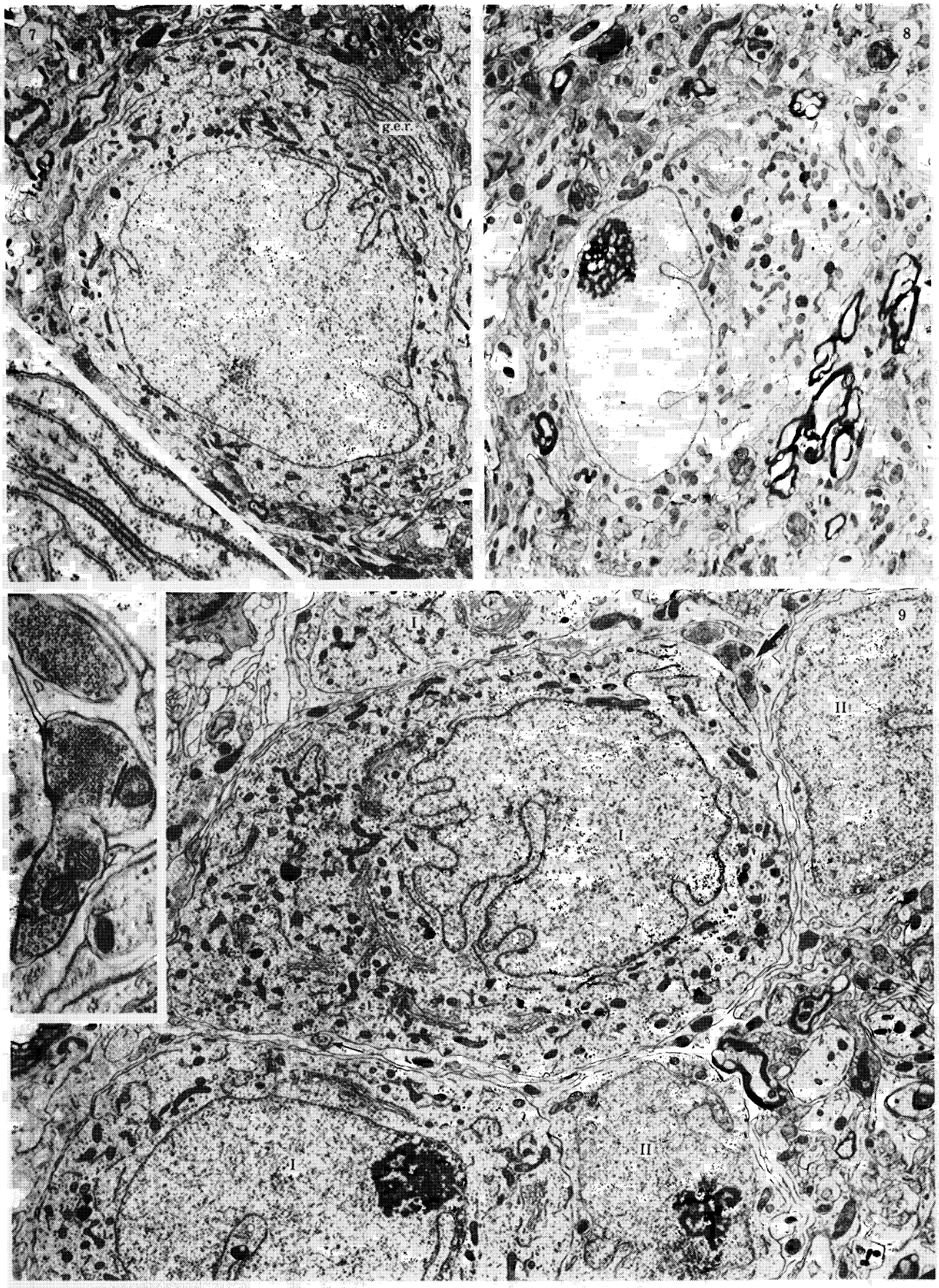

FIGURES 7–9. For description see facing plate 1.

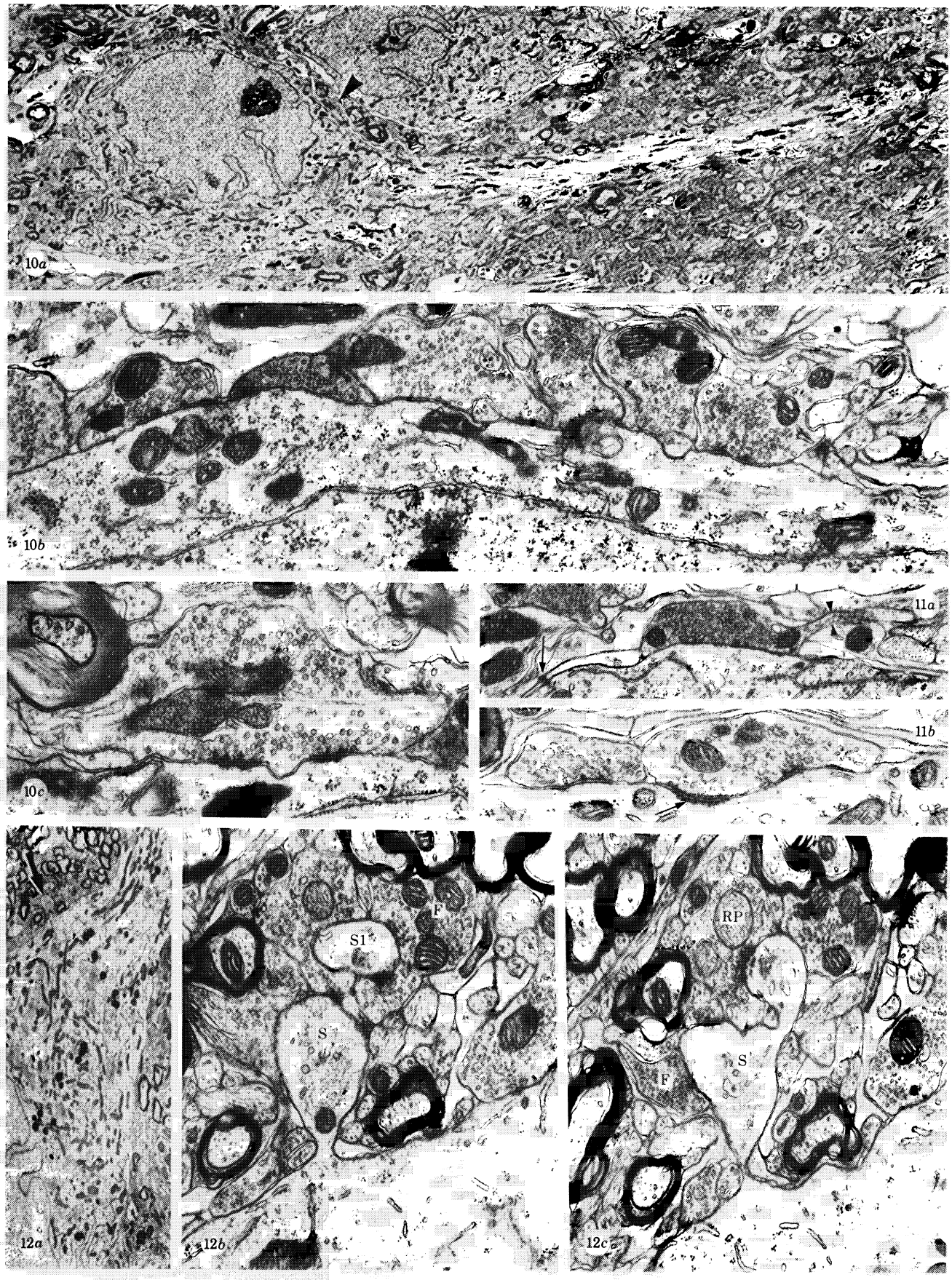

FIGURES 10–12. For description see facing plate 1.

Description of plate 5

Figures 13–16. Electron microscopy. Dendrites, dendritic spines and axons of class I cells.

Figure 13. Transversely sectioned dendrite (D) of a class I cell. The dendrite receives a synaptic contact from an F-bouton (F) and bears a large, long-necked spine (S) which receives synaptic contacts from two other F-boutons one of which also establishes synaptic contact with an adjacent small dendrite. Part of the spine head and of the larger F-bouton contacting it, are shown at greater enlargement in the inset. An unidentified bouton containing round vesicles (arrow) also contacts the same spine head. Magn. ×16650; inset ×32400.

Figure 14. Dendritic spines (arrows) stemming from the dendrites of class I cells. The unusually large and irregularly shaped spine in figure 14*a* is contacted by several terminal profiles; the simple drumstick-like spine in figure 14*b* receives a synaptic contact from an RP-bouton (RP); the shaft and two of the three bulbous protrusions arising from the dendrite marked with an asterisk, and the large irregularly shaped spine stemming from the dendrite at the right of figure 14*c* are contacted by RP-boutons (RP). Figure 14*a* magn. ×10800; figure 14*b* magn. ×9450; figure 14*c* magn. ×14400.

Figure 15. Figure 15*a* shows part of the cell body (c.b.) the axon hillock (a.h.), the initial segment of the axon (i.s.), and part of the first internode of the myelinated portion of the axon (m.a.) of a class I cell. The inset, from a serial section, shows more clearly continuity between the initial segment and the myelinated part of the axon. An unusual bulbous protrusion of the initial segment (arrow) invaginates the cell body of an adjacent astrocyte (as.). This protrusion and the initial segment from which it arises are seen more clearly in a serial section at higher magnification in figure 15*b*. Note that the plasma membrane of the protrusion does not have a continuous undercoating, although patches of moderately electron-dense flocculent material somewhat similar to the material of the undercoating in the initial segment are present, and that the subaxolemmal undercoating in the initial segment is linked to peripherally situated microtubules by regularly spaced cross bridges to produce a ladder-like appearance. Ribosomes (r.) and small elements of smooth reticulum (arrows) in the initial segment and protrusion, and granular endoplasmic reticulum (g.e.r.) and glial filaments (f.) in the astrocyte are indicated. Figure 15*a* and inset, magn. ×4950; figure 15*b* magn. ×40950.

Figure 16. A transversely sectioned initial axon segment, with a prominent subaxolemmal undercoating and well defined microtubule fascicles, partly enclosed within astrocyte processes (a.). An F-bouton establishes a Gray type 2 synaptic contact with the initial segment (arrow). Magn. ×45000.

Description of plate 6

Figures 17–20. Electron microscopy. Cell bodies and dendrites of class II cells.

Figure 17. Parts of three class I cells (I); a small class II cell (II), an astrocyte (as.) and a microglial cell (m.) at the edge of an extensive area of glomerular neuropil (asterisks). The largest of the class I cells emits two dendrites, one of which passes adjacent to the astrocyte and the class II cell body. This dendrite receives a somatodendritic synapse from the class II cell body (enlarged from a serial section in inset (*a*): note the dense core vesicle among the more numerous irregularly shaped electron-lucent vesicles, and the edge of the nucleus of the class II cell at the left). The class I soma from which the latter dendrite emerges receives a synaptic contact from the dendrite of another class II cell (dendrosomatic synapse) at the arrow (enlarged from a serial section in inset (*b*): note the ribosomes (r.) in the presynaptic dendrite, the pleomorphic synaptic vesicles, the prominent presynaptic densities and the relatively narrow postsynaptic density). Magn. ×2700; inset (*a*) magn. ×79650; inset (*b*) magn. ×49950.

Figures 18–20. Three class II cell perikarya (nuclei at N) and the proximal parts of presynaptic dendrites emerging from them, all of which contain granular reticulum or free polyribosomes, or both. A lateral extension of the emerging dendrite in figure 18 establishes synaptic contact with a P-bouton (P): the contact site is enlarged from a serial section in the inset. The dendrite in figure 19, parts of which are shown in three sections from a series, is postsynaptic to an F-bouton (arrow in figure 19*b*), and presynaptic to a small dendritic spine (arrow in figure 19*c*). The emerging dendrite in figure 20 is extremely irregular in shape, gives off a pleomorphic vesicle-containing process (large arrow), and establishes presynaptic contacts with a conventional dendrite (D1) (at small arrow) and probably also with D2 (contact not evident at this level). Figure 18 magn. ×6300; inset ×41400; figure 19*a* magn. ×13500; figures 19*b*, *c* magn. ×19350; figure 20 magn. ×20700.

Description of plate 7

Figure 21. Electron microscopy. Variations in the size and shape of class II cell bodies. Outlines of 11 class II cells traced from electron micrographs of single sections. All the cells depicted had a presynaptic dendrite or cell body, or both. They derive from several different animals, are randomly oriented in the drawing with respect to one another and to the axes of OPN, but are all reproduced to the same scale. Note the considerable range in cell body and nuclear sizes and shapes, in the cytoplasm to nucleus ratio (which is very low for some cells), and in the extent of nuclear infolding. The positions and polarities of the synaptic contacts made by these cell bodies, their dendrites and appendages are indicated by small arrows. The dotted line at the end of the dendrite of cell 4 represents an obscuring grid bar. Parts of several of these cells are illustrated in other figures: cell 2 in figure 21; cell 6 in figure 18; cell 10 in figure 20. Magn. ×4060.

Description of plate 8

Figures 22–25. Electron microscopy. Somatodendritic synapses and presynaptic dendrites of class II cells.

Figure 22. Somatodendritic synapses of three neurons. Figures 22*a* and *b* are from an unclassified neuron with a mixture of characteristics (see description of figure 24 in which this cell is further illustrated), whereas two typical class II cells are shown in figures 22*c* and 22*d* and *e*. Note how similar the synaptic specializations are and how comparatively few and focal are the synaptic vesicles. In two examples a round dense core vesicle is present among the pleomorphic lucent vesicles (small arrows in figures 22*b* and *c*; see also inset (*a*) of figure 17). The synaptic contacts illustrated in figures 22*d* and *e* were between the same presynaptic and postsynaptic elements and were approximately 3 μm apart. N, nucleus; D, postsynaptic dendrite. Figures 22*a* magn. ×49500; figure 22*b* magn. ×41400; figure 22*c* magn. ×49950; figures 22*d*, *e* magn. ×40050.

Figure 23. Somatosomatic synaptic contact (arrow; figure 23*a*) between a presynaptic class II cell soma with dark cytoplasm and nucleus (NII) and a larger class I cell with paler cytoplasm and nucleus (NI). The synaptic specialization is enlarged in figure 23*b*. Note the variety of vesicle profile shapes. r., Ribosomes. Figure 23*a* magn. ×14400; figure 23*b* magn. ×96750.

Figure 24. Tracing from one section of an unclassified neuron, in the size range of, and with the nuclear characteristics of, a class I cell, but with cell body, dendrite and dendritic appendages all exhibiting typical class II cell presynaptic characteristics. Three vesicle-containing dendritic appendages are indicated by asterisks. They and the stretch of dendritic shaft from which they arise are further illustrated in the inset e.m. in which the origins of the protrusions are marked by small arrows. Although difficult to resolve at this low magnification the two more proximally located appendages contain polyribosome clusters in addition to pleomorphic synaptic vesicles. Two somatodendritic synapses established by this cell (arrows a and b) are illustrated in figures 22*a* and *b*. Magn. ×2700; inset magn. ×9900.

Figure 25. Tracing of a presynaptic dendrite with an extremely irregular contour indented by various adjacent neural elements and giving rise to numerous irregularly shaped protrusions (for example, marked by asterisk), some of which contain synaptic vesicles. The sites of synaptic contacts onto two small dendrites are indicated by the arrows. Magn. ×15300.

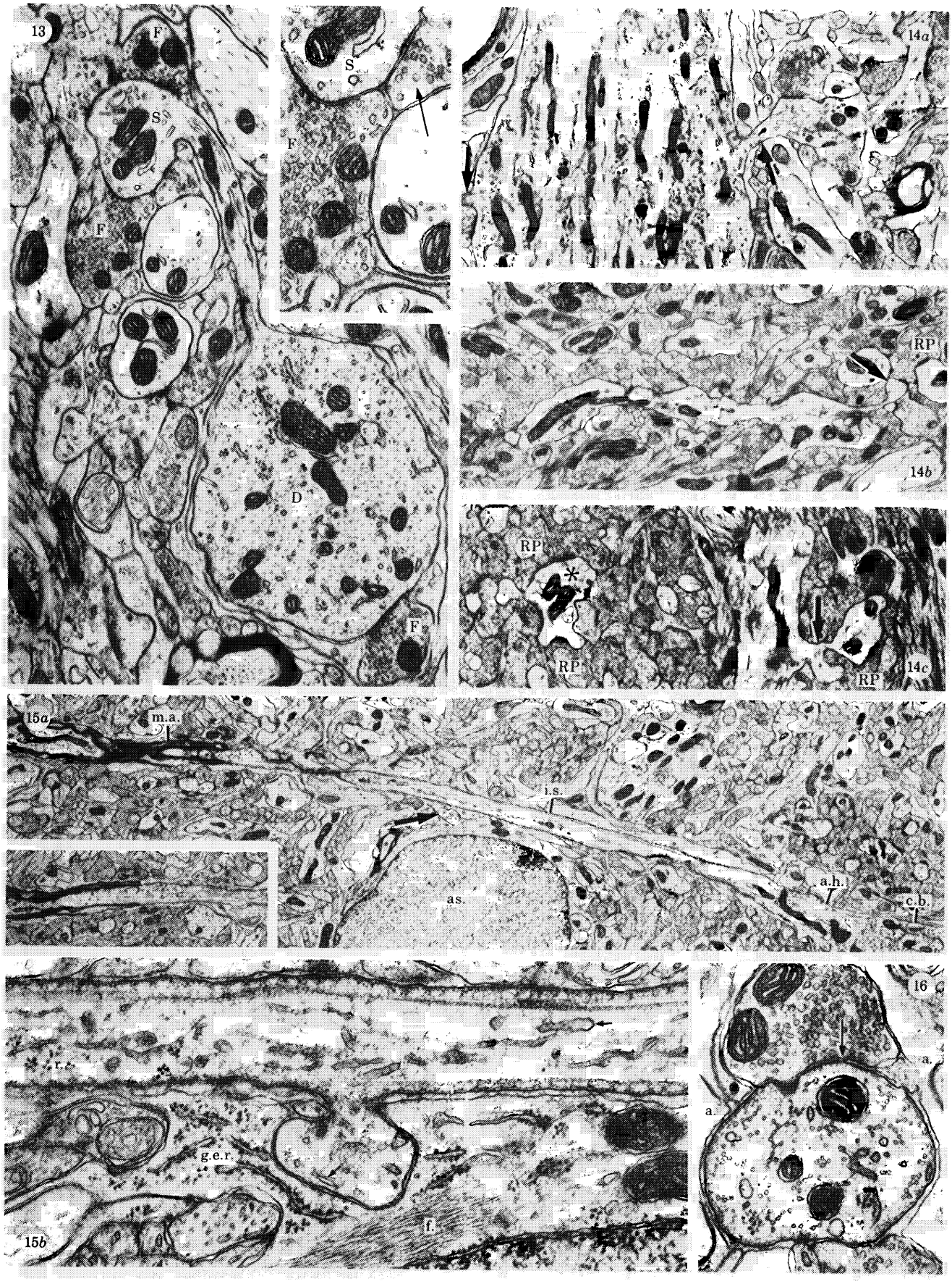

FIGURES 13–16. For description see facing plate 4.

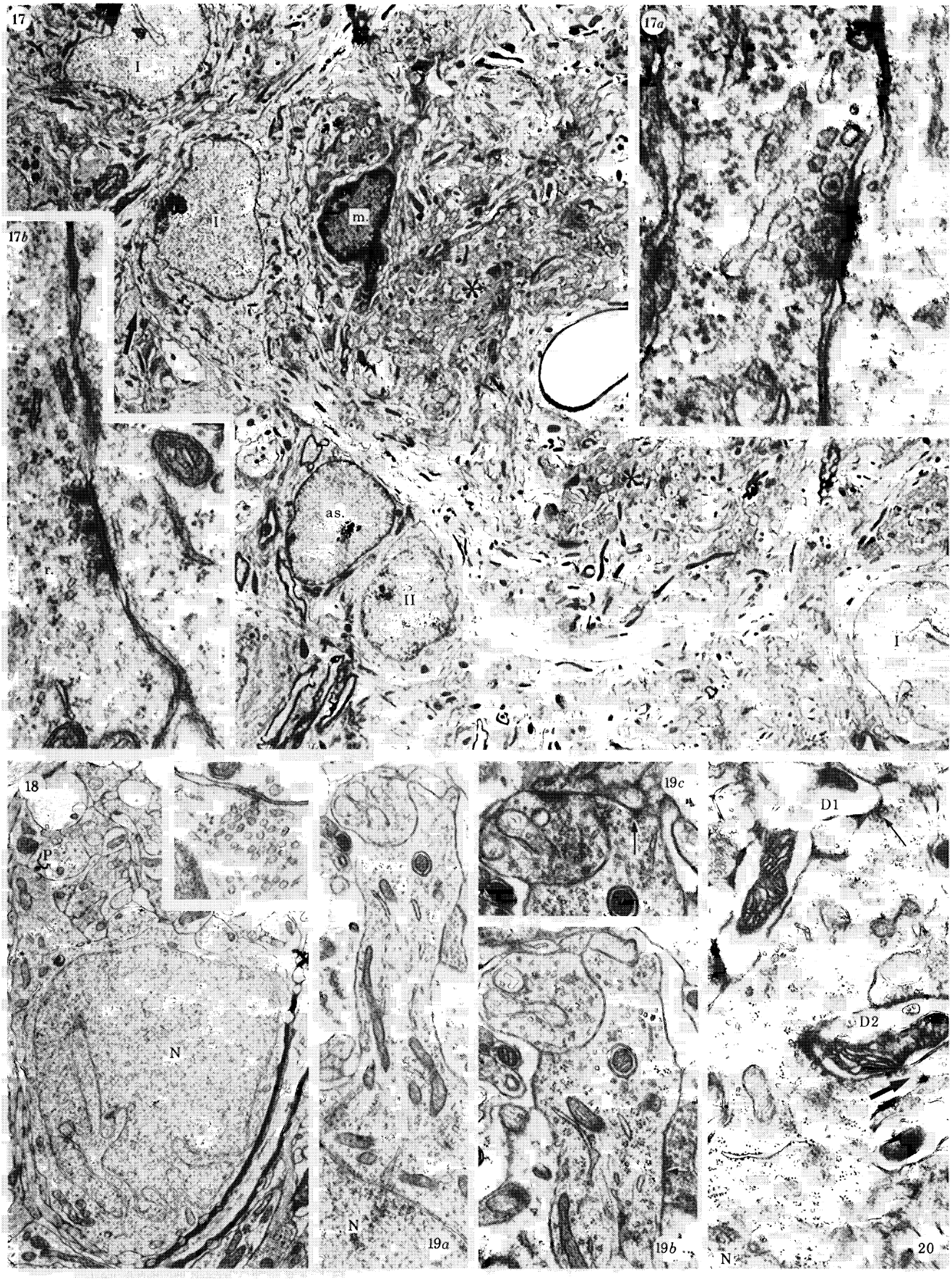

FIGURES 17–20. For description see facing plate 4.

21

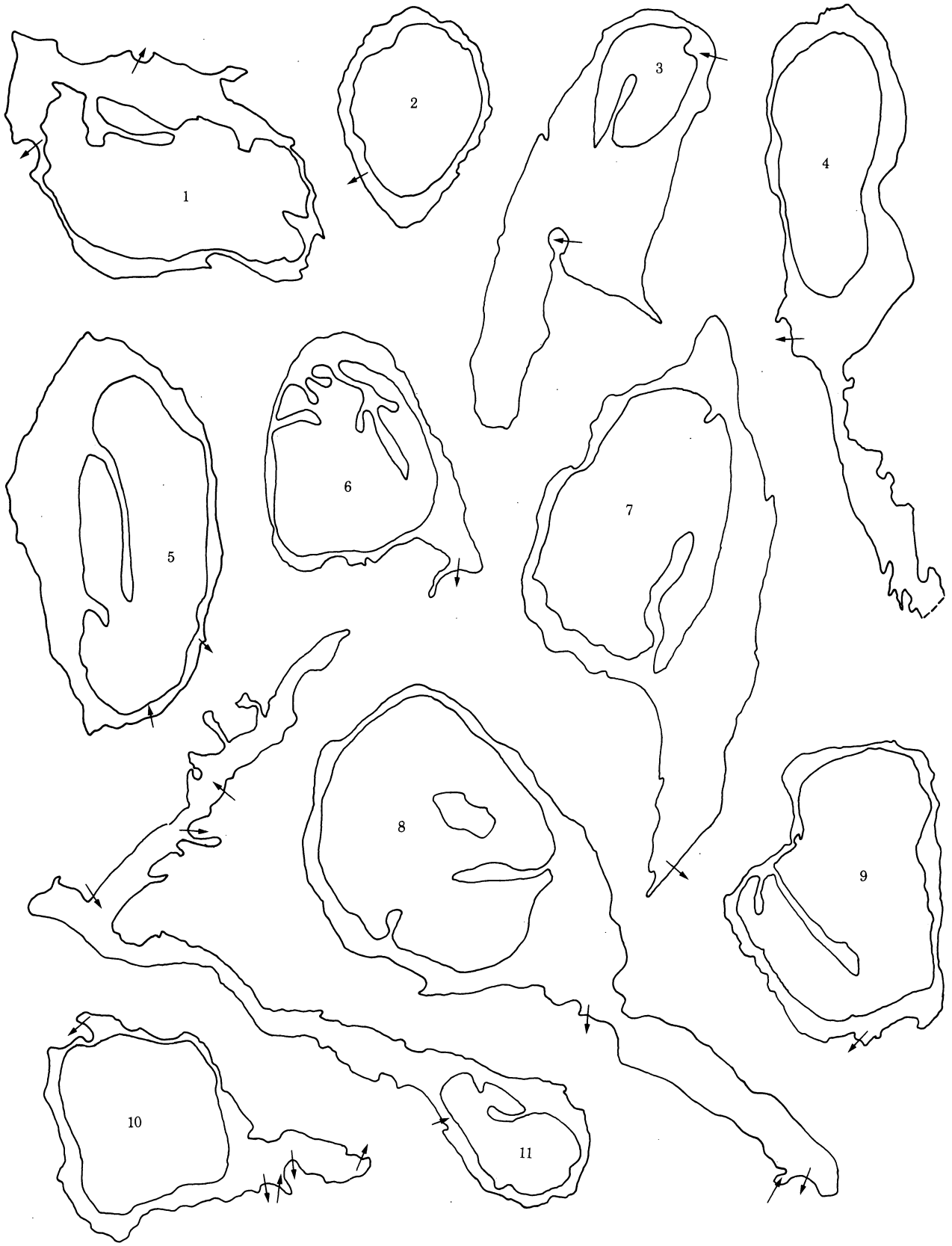

FIGURE 21. For description see facing plate 5.

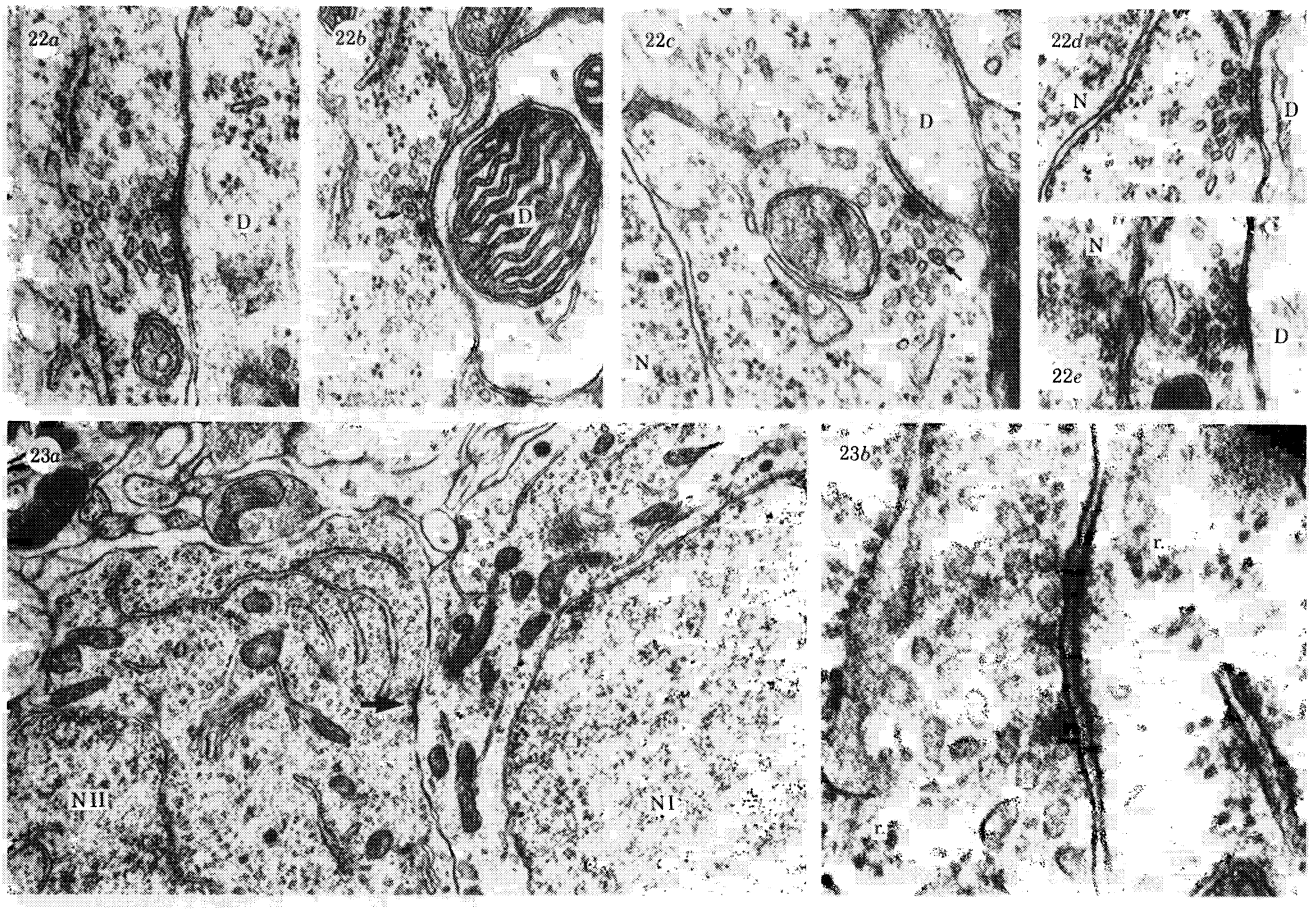

24

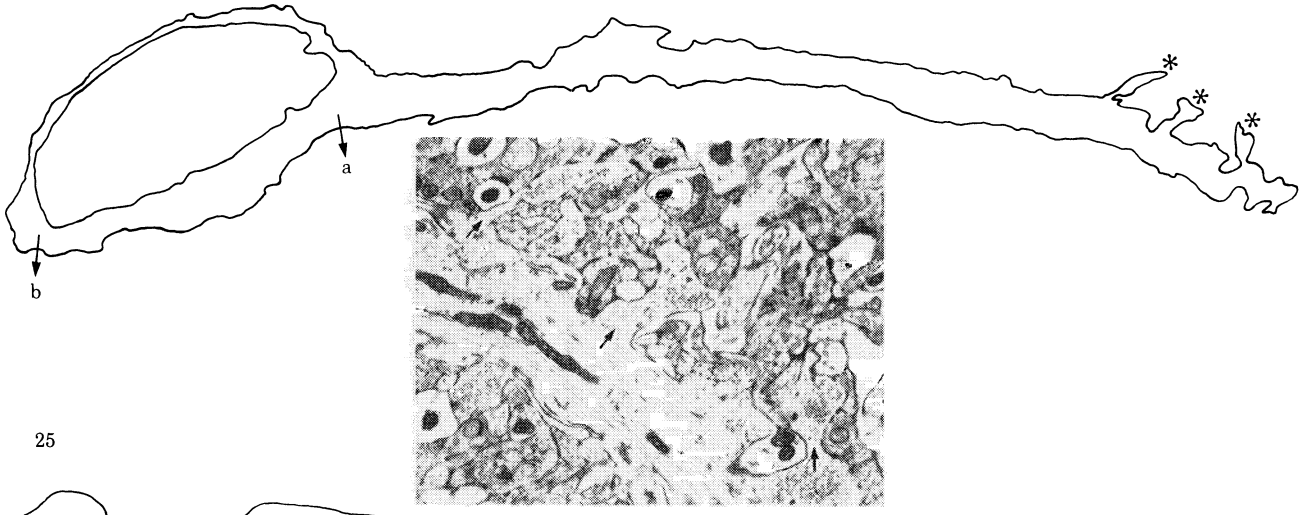

25

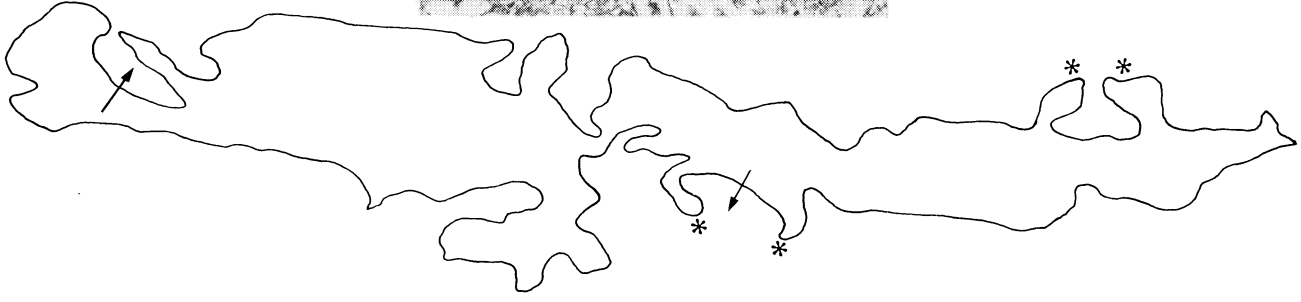

FIGURES 22–25. For description see facing plate 5.

approximately 400 μm in the mediolateral and 300 μm in the dorsoventral axis. It is situated at the level of the posterior commissure and the caudal portion of the lateral geniculate body, and lies immediately below the most medial portion of the brachium of the superior colliculus (see figure 1).

The OPN is distinctive in cell- and myelin-stained preparations, for as first mentioned by Fuse (1916, 1936) and subsequently emphasized by Scalia (1972), the virtual absence of myelinated fibres endows the nucleus with a characteristic pale and gelatinous appearance, an appearance accentuated by the contrast between OPN neuropil and the overlying, densely stained myelinated fibres of the collicular brachium and the sparser myelinated fibres around most of the rest of the periphery of the nucleus (see figures 1, 2*a*, *c*). More correctly, these features characterize the most rostral and dorsal portion of OPN (*pars oralis* of Scalia 1972): the laterally directed caudal portion of the nucleus is cytoarchitecturally less distinct. In the present study, attention was focused on the *pars oralis* of OPN which is referred to here simply as OPN.

In coronal sections, OPN displays two poorly demarcated zones; a peripheral annulus or 'shell' of closely packed, medium-sized cell bodies some one to three cells thick, and a central core of neuropil within which nerve cell bodies are less densely packed (figure 2*a*, *b*, *d*). The latter are scattered throughout the core region and are occasionally apparently clustered at its centre (figure 2*b*). Single myelinated fibres, or small myelinated fibre bundles often appear to radiate from (or into) this central cluster of cells towards the peripheral shell, rather like the spokes of a wheel (figure 2*b*). Nuclei of glial cells (predominantly astrocytes) are scattered throughout OPN and blood vessels are generally rather prominent, the largest ones displaying a dorsolateral to ventromedial course through the OPN (figure 2*a*).

(b) *Golgi studies.* The rapid Golgi procedure (Valverde 1970) was the method of choice. In addition to providing satisfactory impregnation of cells, axons and dendrites (figures 3 and 4) it also allowed the boundaries of OPN to be delineated with greater certainty than was possible in Kopsch or Cox preparations, because the staining by osmium tetroxide of the myelinated fibre bundles around OPN served to distinguish the latter from adjacent pretectal areas. The incidence of successfully impregnated OPN neurons in this material was not high (compared, for example, with dorsal thalamic nuclei and other regions in the same sections), perhaps in part because of the small size of OPN and the high density of myelin surrounding the nucleus. Another problem was that many well impregnated neurons were partly obscured by the dense impregnation centred on and just below the brachium of the superior colliculus, or by crystalline deposits in this area. Finally, well impregnated neurons were sometimes partly obscured by extensive, dense, axonal plexuses which were commonly impregnated in rapid Golgi material. Such plexuses occasionally filled the entire cross-sectional area of OPN and were extremely complex, comprising extensively arborized and intertwined beaded preterminal and terminal axons. Some of the preterminal axons generating such terminal plexuses were traced from fibres in the brachium of the superior colliculus suggesting that they represent axons of retinal origin. Such an interpretation is in keeping with that of Viktorov (1969) in a previous Golgi study of OPN, and with our experimental findings that retinal terminal fields are found throughout the entire extent of OPN (see §3*b*ia).

Most of the impregnated neurons could be assigned to one of two major classes (class I and class II, see below) but some neurons displayed a combination of features which made it difficult to classify them with confidence.

Class I cells. The cell bodies of class I cells were approximately spherical and 15–30 μm in

diameter, commonly with three, but with up to six primary dendrites which displayed no apparent preferential orientation (figures 3*a* and 5, plate 2), and which branched, usually dichotomously some 20–30 μm from the cell body. Secondary dendrites did not branch extensively and tertiary dendrites branched only very rarely. The dendrites were long, relatively smooth-surfaced and generally followed a straight path from their origin. They were sparsely and irregularly spined (figures 3*b*, 5). Some dendrites were apparently devoid of spines, whereas others, sometimes originating from the same perikaryon, bore spines evenly distributed over their length. Most spines were short and simple with a thin shaft and bulbous head: others were more complex and some were double-headed (figure 3*b*).

Class I cells appeared to be concentrated within the peripheral shell of OPN as reported in a previous Golgi study by Verbitskaya *et al.* (1977). Their dendrites either ramified among other peripherally located cells or passed into the central core of neuropil. Only rarely did their dendrites leave the confines of OPN and enter surrounding regions, such as the medial pretectal area (figures 3*a*, 5).

The axons of class I cells took origin either from a proximal dendritic shaft, usually about 10 μm from the cell body (figure 3*c*, *d*) or directly from the cell body (figure 3*b*). In both cases the axon displayed a distinctive wide axon hillock which gave rise to a smooth, spineless and thin initial segment, the latter often displaying one or more 'kinks'. These axons were never observed to branch or to emit recurrent collaterals and could not be followed further than 20–40 μm beyond their origin, almost certainly due to failure of axonal impregnation distal to the commencement of the myelin sheath.

Class II cells. Class II cells were characterized by small- to medium-sized cell bodies, often oval or elongate, with approximate dimensions of 7–10 μm × 10–18 μm (figures 4*a*, *b*, *d* and 6). They were commonly bipolar in form with two main dendrites originating from opposite poles of an elongate soma. Dendrites were minimally branched and could be distinguished from the dendrites of class I cells by the complex nature of their spines and abundant irregular protrusions, which are described below. Class II cells could be divided into two subpopulations: class IIa (figure 6*a*) and class IIb (figure 6*b*).

The class IIa cell was characterized by some or all of the following features: medium-sized elliptical cell body; a predominantly bipolar configuration; usually a dorsomedial–ventrolateral orientation; and long dendrites with a relatively straight course, branching rarely, chiefly distally, and at acute angles (figure 6*a*). A putative axon was observed originating from only one class IIa cell. This axon arose, without a distinct hillock, from a proximal dendrite, had a beaded appearance, and could be traced for 150 μm (figure 4*b*).

Class IIb cells had similar collections of irregular and complex dendritic protrusions but differed from class IIa cells in the following way. Their somata were small and almost spherical and gave rise either to two main dendrites in a bipolar configuration or to three dendrites (figure 6*b*). Dendrites branched more frequently than was the case for class IIa cells and sometimes at obtuse angles. Some dendrites maintained a curved course around the parent perikaryon and generated a rather small dendritic domain, only 100 μm or so in diameter. Putative axons were found to originate from the soma or proximal dendrite of three class IIb cells. Two had a smooth outline and characteristic axon hillock, the other was beaded without a recognizable hillock and neither could be traced more than 30–50 μm from their point of origin. Class II cells were generally located within the central neuropil of OPN with dendritic arborizations confined within the boundaries of the nucleus (see figure 6). Those within the

peripheral shell of OPN gave rise to dendrites that either protruded into the central core or ramified within the neuronal shell (figure 4*a*).

The complex dendritic appendages of class II cells. The complex dendritic appendages arising from class II cells were of variable form and were commonly concentrated in the distal dendritic region or around the most proximal part of the dendritic shaft. Some, perhaps more accurately termed axon-like dendritic processes, were thin, long, and often branched and beaded, occasionally giving rise to small end-knobs (figure 4*c*). Some of these processes may have been axonal although they did not arise from distinct axon hillocks. Other types of dendritic appendage were thicker and shorter, often highly branched and of considerable complexity and varied shape (figure 4*c–f*). Some had multilobed protuberances, others long stalks that gave rise to numerous small branchlets or to large bulbous heads. Simple blunt evaginations and spines of a more conventional nature were also present. It was sometimes difficult to distinguish between what might be a single, large irregularly shaped blunt protrusion and a collection of smaller, adjacent dendritic appendages impregnated as a group.

A few cells could not be classified into one of the above groups because they possessed some features common to more than one class. Two neurons displayed characteristics of both class IIa and IIb cells and three neurons had perikarya and dendrites of class I form but gave rise to a small number of complex dendritic appendages characteristic of class II cells.

(ii) *Electron microscopy*

(a) *Neurons.* Most of the neurons of OPN could be classified into one of two broad categories on the basis of their fine structure: medium-sized cells with relatively electron-lucent cytoplasm and exclusively postsynaptic cell bodies and dendrites (class I neurons); and smaller, more electron-dense cells, with perikarya, dendrites and dendritic appendages which were both postsynaptic and presynaptic (class II neurons). The choice of nomenclature identical to that used for the two main cell classes recognized in OPN by l.m. in Golgi preparations is deliberate and reflects a conclusion, albeit one based on indirect evidence, that the class I and II cells of the e.m. classification correspond to the class I and II cells of l.m. It has not been possible to distinguish ultrastructurally between the class IIa and IIb cells of the light microscope-based classification.

Class I neurons. Class I neurons were the predominant neuronal cell type (figures 7–10, plates 3 and 4). They were found both in the central core and in the peripheral shell where they were more numerous. Their cell bodies were generally circular in profile and contained a pale nucleus often with a prominent nucleolus (figures 8–10) and with evenly dispersed chromatin and a few patches of heterochromatin. The nuclear envelope was commonly thrown into folds which were most prominent in the region of the nucleus facing the origin of a major dendrite (figure 10*a*). Their cytoplasm was relatively abundant, electron-lucent and rich in those organelles generally found in neurons of the central nervous system (Peters *et al.* 1976). Granular endoplasmic reticulum (g.e.r.) frequently in the form of Nissl bodies (figure 7), free ribosomes and polyribosomes were abundant, Golgi complexes were well developed (figures 8 and 9) and mitochondria were numerous, evenly distributed, of small diameter and variable length with an electron dense matrix and evenly spaced cristae. Smooth endoplasmic reticulum (s.e.r.) and microtubules were not abundant and neurofilaments and subsurface cisternae (Rosenbluth 1962) were only occasionally observed. Multivesicular bodies, lysosome-like dense bodies, lipofuscin granules, and basal bodies, sometimes associated with cilia were all common

constituents of class I cells. The cell surface was relatively smooth, with indentations occupied chiefly by astrocytic processes (figure 9) and less commonly by dendritic or axonal profiles (figure 9 inset; figures 10*b*, *c*, and 11*a*, *b*). In addition to dendrites, and occasionally an axon, these cell bodies also gave rise to spine-like appendages of variable shape and size (figure 12), which contained flocculent cytoplasmic material characteristic of dendritic spines and were invariably associated with regions of complex neuropil (figure 12*b*, *c*) within which their synaptic relationships were identical to those of dendritic shafts and dendritic spines (see below).

The dendrites of class I neurons were commonly traced from or into continuity with their parent perikarya (figures 10*a* and 12*a*). The dendritic surface was smooth except for intermittent spines and the cytoplasmic matrix was pale. In distal dendrites, evenly spaced parallel microtubules and long mitochondria were the principal organelles, but a progressively richer organelle content was present closer to the cell body, where mitochondria, microtubules, g.e.r., free ribosomes, s.e.r. and elements of the Golgi apparatus were present. Dendritic spines were variable in size and shape (figures 13 and 14, plate 5) and included simple bulbous and drumstick-like forms and more complex spines with irregularly shaped or branched heads (figures 14*a*, *c*).

Axon hillocks and initial segments, identified by using established criteria (Peters *et al.* 1976), arose from perikarya or from proximal dendritic shafts. One initial segment, which arose from a cell body, was traced, through serial sections, for 20 μm to the start of the myelin sheath (figure 15*a*, *b*). This initial segment also gave rise to an unusual bulbous protrusion invaginated into an astrocyte process (figure 15*b*). Axon terminals containing densely packed flattened vesicles (F-boutons or terminals; see §3*a*iic) established synaptic contacts with axon hillocks and occasionally with initial segments (figure 16).

Class II neurons. Although class II cell bodies spanned a considerable range of diameters (figures 17–21, plates 6 and 7) they were generally smaller than class I cells and were of variable and irregular shape with an indented outline (figure 21). Most characteristic of all, these cells often contained synaptic vesicles and established presynaptic contacts (see below). Their nuclei were generally ovoid in form and appeared darker than the nuclei of class I cells due to a more densely packed matrix of uncondensed chromatin. Heterochromatin was relatively more prominent than in class I cell nuclei. The nuclear envelope was occasionally folded (figures 18 and 21), but generally not as markedly as in the case of class I cells: nuclear indentations were generally located opposite the origin of a dendrite (figure 21, cells 3, 7, 8 and 11). The nucleus occupied a relatively larger proportion of the cross sectional area of the soma than was the case for class I cells, a feature of the interneurons within thalamic relay nuclei previously described by several authors (LeVay 1971; Lieberman 1973; Pasik *et al.* 1973).

The cytoplasm of class II cells was in the form of a thin perinuclear rim and contained closely packed ribosomes, polyribosomes and large amounts of floccular, presumably proteinaceous material which imparted an overall electron-dense appearance to the cytoplasm (figures 17–20). Cisterns of g.e.r. were sparse and rarely aggregated to form Nissl bodies, whereas Golgi complexes were well defined and comparable in size and extent to those in class I cells and were particularly prominent close to the origin of large dendrites. Subsurface cisterns were uncommon and s.e.r. not abundant. Mitochondria were of uniform diameter and variable length, with slightly swollen irregular cristae. They appeared to be intermediate with respect to matrical electron density and the shape of their cristae, between the mitochondria of optic nerve terminals (RP-boutons, see §3*a*iic) and those of class I cells and dendrites. Neurofilaments

were never observed in these cells, and although the frequency of microtubules was similar to that found in class I cells the microtubules were more haphazardly arranged in the class II cell bodies. Myelin bodies and lysosome-like (but not lipofuscin-like) dense bodies were encountered with approximately the same frequency as in class I cells. Pleomorphic synaptic vesicles, generally in clusters near the plasma membrane were occasionally encountered and were associated with an active zone at a synaptic contact with a neural element abutting the cell body (figures 17, inset *a*, 22*a–e*, 23, plate 8). Only a small proportion of sections through the cell body of class II cells revealed the presence of synaptic vesicles, suggesting that the efferent synapses of these somata are sparse and very focal. The cell membrane was often deeply indented by the dendritic shafts and spines of class I cells, upon many of which efferent synaptic contacts were established (figures 22*b*, *c*), whereas axon terminals making axosomatic contacts on these cells were generally apposed to the plasma membrane without invaginating it. Class II cell bodies rarely gave rise to spine-like processes.

The dendrites of class II cells (figures 25–29, plate 9, and see also figure 24) differed from those of class I cells in many ways: they were generally narrower, particularly at their origin, had a relatively electron-dense cytoplasmic matrix due chiefly to the presence of large amounts of floccular material, some of which was associated with the surface of microtubules, and to large numbers of ribosomes; and sometimes a very irregular outline due to rather complex undulations, folds and surface protrusions (figures 20, 21 (cells 4 and 11), 24, 25, 27). But the greatest difference between the dendrites of class I and II cells was the presence of presynaptic specializations in class II cell dendrites (see §3*a*ii c). Other organelles within proximal dendrites of class II cells were mitochondria similar to those within the perikaryon, small saccules of g.e.r. and s.e.r. and small Golgi complexes. Microtubules were abundant and in distal dendrites were the predominant organelle together with a few ribosomes, elements of s.e.r., and synaptic vesicle clusters. The complex and varied protrusions of class II cell dendrites (figures 21 (cell 11), 24, 25, 28, 29), large numbers of which have been traced through serial sections into continuity with their parent dendritic shafts and cell bodies, are referred to as P-profiles or boutons in keeping with the terminology proposed by Lieberman & Webster (1972). Small class II cell dendritic profiles (as opposed to profiles of dendritic appendages) whose general cytoplasmic characteristics and more importantly whose synaptic relationships were similar to those of the dendritic appendages, are also designated as P-profiles in the following account, principally to avoid excessive complication in relation to the quantitative observations.

No structures identifiable as axonal initial segments were observed originating from class II cells or their dendrites in the e.m. study. Since class II cells in Golgi preparations appeared to give rise to axons, there would appear to be a discrepancy between l.m. and e.m. results on the question of whether or not class II cells have axons. This problem will be further considered in §4*a*ii.

Very occasionally, cells were encountered with a mixture of class I and class II cell features. The most striking example is illustrated in figure 24. This cell was much larger than most class II cells and had the cytoplasmic and nuclear electron density usually associated with class I cells, but in all other respects was a typical type II cell, with a presynaptic soma and a presynaptic dendrite from which typical P-boutons were traced (inset to figure 24).

(b) *The neuropil.* The organization of the neuropil appeared to be identical in albino and pigmented rats and the following description is based on material from both strains. The cells of OPN are set in a complex neuropil which contains very few myelinated fibres (figures 17

and 30) and which is dominated by extensive regions of densely packed neuronal profiles engaged in complex synaptic relationships. These areas of complex neuropil (figure 30, plate 10) are somewhat similar to the glomerular neuropil of thalamic relay nuclei (Jones & Powell 1969*a*; Guillery 1971; Lieberman & Webster 1974) although, in OPN, they are larger, less well defined and less well circumscribed by astrocytic laminae than is the case for much of the glomerular neuropil of the dorsal lateral geniculate nucleus (LGd) and other dorsal thalamic nuclei. A detailed account of the synaptic relationships within OPN neuropil is given in §3*a*ii. Between areas of glomerular-type neuropil are areas of a much simpler neuropil consisting chiefly of axodendritic contacts enclosed or partly enclosed in glial cell processes.

Astrocytes, oligodendrocytes and microglia were all recognized within OPN. Astrocytes were the most abundant, readily identified by their filament bundles and complex, irregular processes, which penetrate and infiltrate the smallest regions of extracellular space and intermingle with and separate neuronal elements (see, for example, figures 9 and 30). Microglia were the least common in normal material but both microglia and astrocytes appeared more active and numerous in deafferented material (see §3*b*iia). A few specialized contacts were recognized between glial elements, and between glial elements and neuronal profiles. Close membrane appositions, probably gap junctions, were common, and adherens-like contacts were occasionally seen between astrocytic processes. An example of an adherens-like junction between an astrocyte process and a class I cell soma plasma membrane was also observed (figure 11*a*). One example of an oligodendrocyte process apposed to a dendrite opposite a

Description of plate 9

Figures 26–29. Electron microscopy. Dendrites and dendritic appendages of class II cells.

Figure 26. Transversely sectioned presynaptic dendrite (pD) packed with granular endoplasmic reticulum, ribosomes, microtubules and synaptic vesicles. A synaptic contact is made onto a small dendrite (D). Two adjacent RP-profiles (RP) are connected by an adherens-like contact. Magn. ×44100.

Figure 27. Five finger-like protrusions (1–5) from a longitudinally sectioned presynaptic dendrite (which enters the picture at bottom right). The protrusions contain synaptic vesicles or ribosomes. A synaptic contact is established with a spine-like dendritic profile (S) embraced by protrusions 2 and 3. Magn. ×24300.

Figure 28. Longitudinally sectioned presynaptic dendrite (pD) establishing a synaptic contact with a conventional dendrite at the arrow, and giving rise to a spine-like P-bouton (P). The P-bouton is presynaptic in its neck region to a small dendritic spine (S) and its expanded head is postsynaptic to another P-bouton. These two synaptic contacts are arrowed and better seen in the inset which is taken from a serial section. Magn. ×38250; inset magn. ×50850.

Figure 29. Three sections of a series through a longitudinally sectioned presynaptic dendrite (pD) from which arise two P-boutons, P1 in figure 29*a* and P2 in figures 29*b* and *c*, (figures 29*b* and *c* are oriented at approximately 75° (anticlockwise) to figure 29*a*: the region of pD from which P2 originates is marked by an asterisk). P1 is postsynaptic to an RP-bouton (RP1). Close to the point at which P2 emerges from it, pD establishes synaptic contact with a dendritic spine (S) which is also postsynaptic to another RP-bouton (RP2). Figure 29*c* was tilted to clarify the synaptic specialization between pD and S. Magn. ×26550.

Description of plate 10

Figure 30. Electron microscopy. Neuropil of OPN. Survey of neuropil, mostly of the complex glomerular variety, dominated by RP-boutons, a few of which are marked by asterisks, and containing also numerous spines (S) and larger dendritic elements (D), P-boutons (P) and a few F-boutons (F). Two P-boutons are postsynaptic to RP-boutons (short arrows) and one is seen as an outpushing (double arrow) of a presynaptic dendritic shaft (pD). The profiles labelled P_1 and P_2 are continuous in serial sections and are parts of a large complex P-bouton. One of the F-boutons makes synaptic contact with a class II cell soma (II). An RD-bouton (RD) is present in an area of simpler neuropil to the left of the figure. Part of an astrocyte (as.) appears at the bottom of the figure. Magn ×12150.

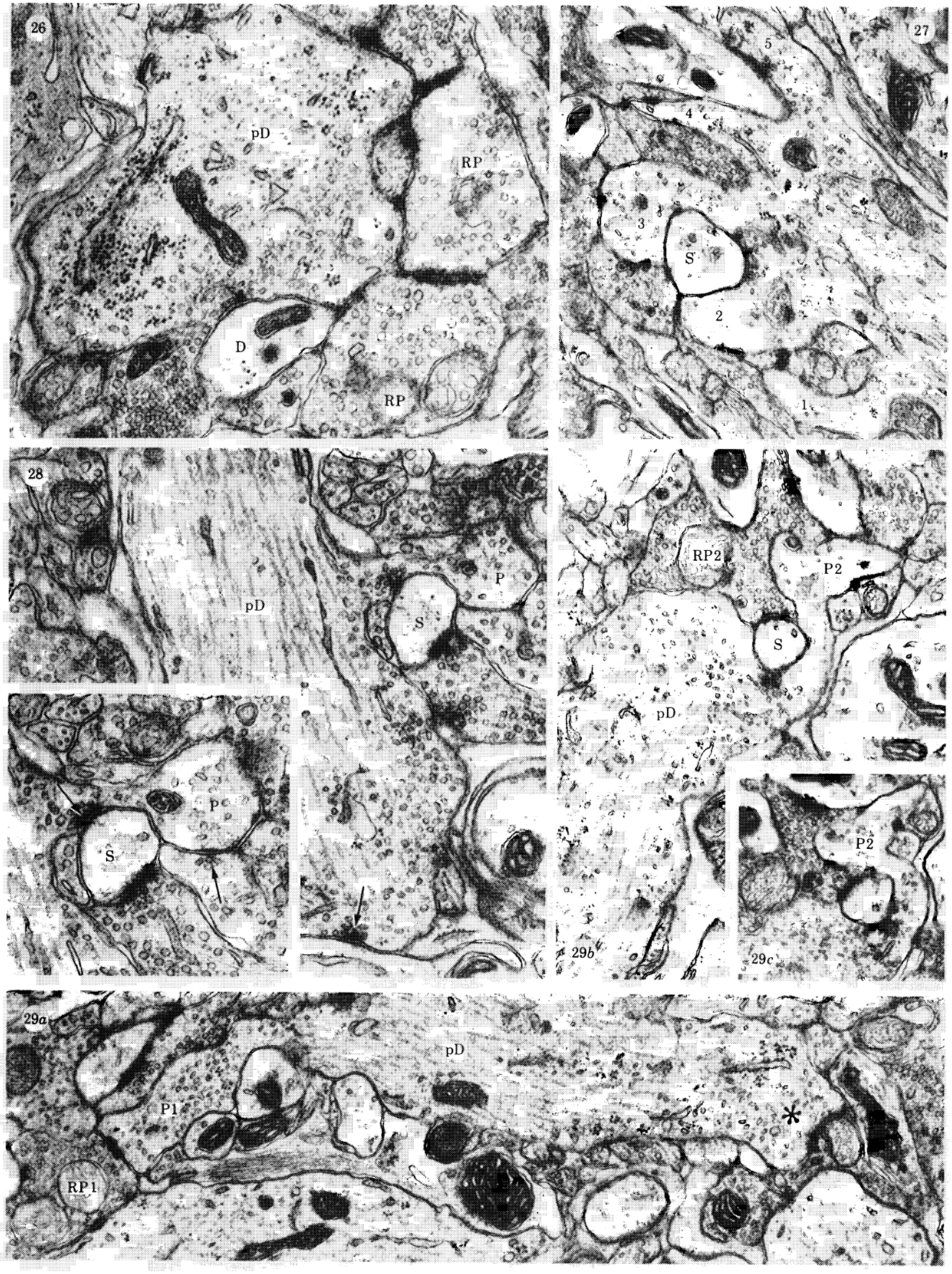

FIGURES 26–29. For description see opposite.

(*Facing p.* 586)

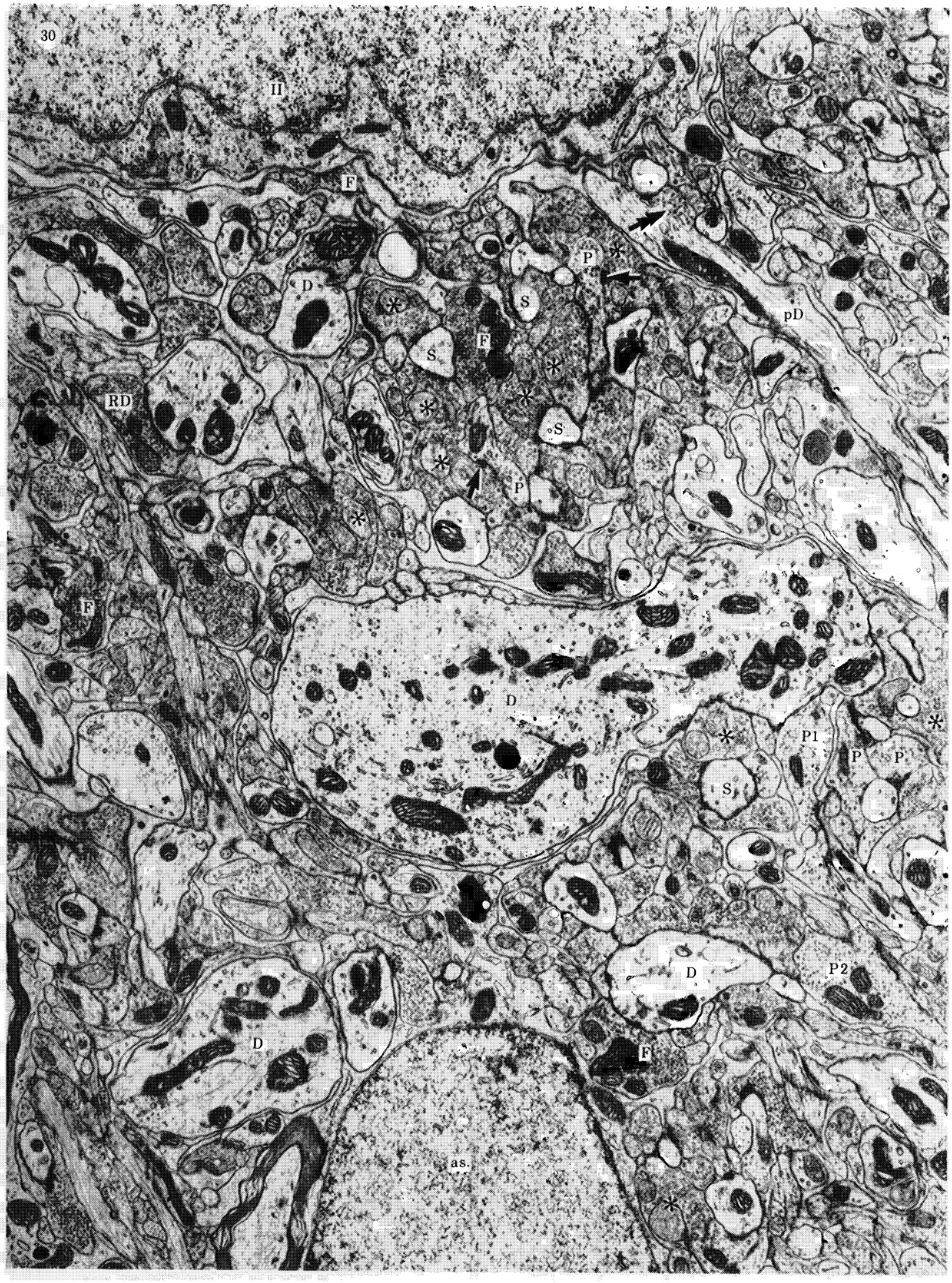

FIGURE 30. For description see p. 586.

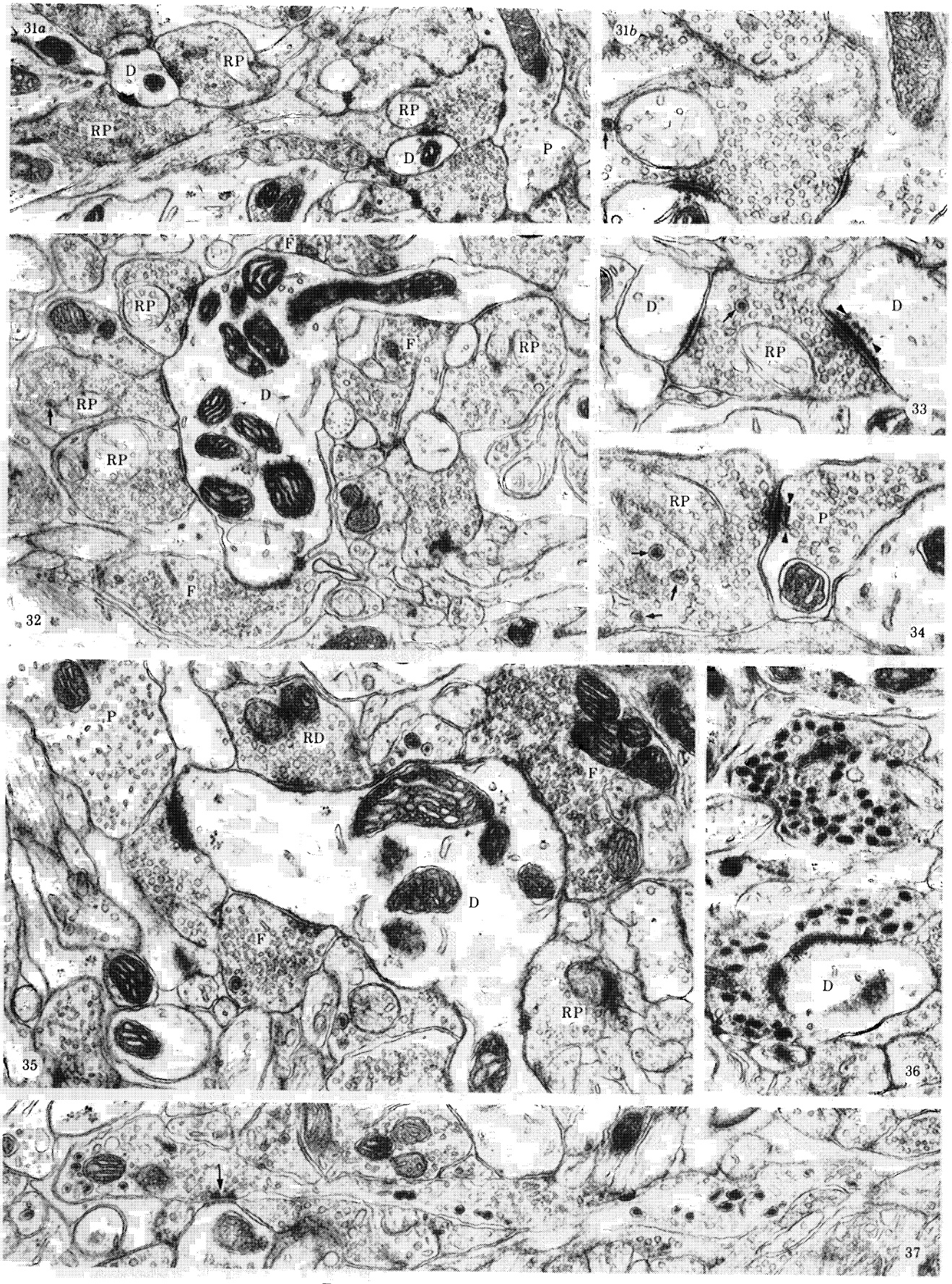

FIGURES 31–37. For description see p. 587.

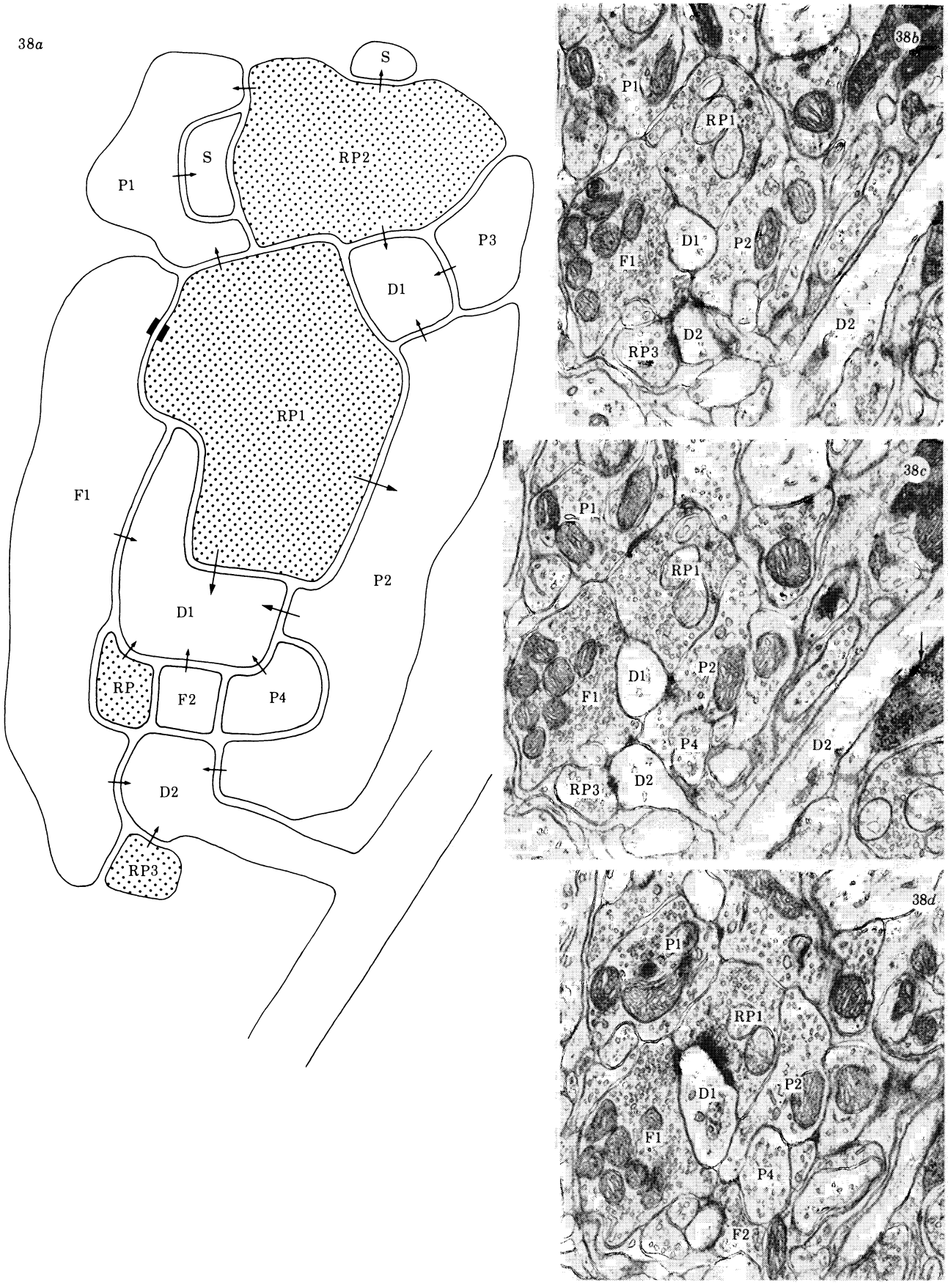

FIGURE 38. For description see opposite.

submembranous density resembling a Gray type 1 postsynaptic density, complete with subsynaptic bar, was also observed (figure 38*c*).

(c) *Presynaptic elements*. Three classes of axonal presynaptic elements (RP-, RD- and F-profiles) and one class of dendritic presynaptic element (P-profiles) were identified. The relative percentages of each class in the neuropil as a whole are summarized in table 1. The percentage figures are lower than previously published estimates (Campbell & Lieberman 1982) because in the earlier study, unclassified profiles were not taken into account, whereas in the present paper, two additional groups of profiles are included, comprising those with predominantly round vesicles but no mitochondria (UR profiles) and those containing flattened vesicles but no mitochondria (UF profiles).

RP-profiles. These axon terminal profiles contained rounded (hence R) synaptic vesicles and pale (hence P) mitochondria (compare with the RLP profiles of Guillery (1969)). They were of variable size (see table 1) and occasionally irregular shape (figures 31–34, plate 11) and were the most common presynaptic components of the neuropil, constituting 36% of all vesicle-

Description of plate 11

Figures 31–37. Electron microscopy. Presynaptic components of OPN neuropil.

Figures 31–34. RP-boutons (RP) establishing synaptic contacts with conventional dendrites (D) (figures 31, 32, 33) and with P-profiles (P) (figures 31, 34). The spherical synaptic vesicles and large, pale mitochondria with irregular and dilated cristae of the RP-boutons are evident, as are the prominent postsynaptic densities at their Gray type 1 synaptic contacts. Subsynaptic bars (arrowheads) are present at one of the RP→D contacts in figure 33 and at the RP→P contact in figure 34. Dense core vesicles are present in several of the RP-boutons (small arrows in figure 31*b*, 32, 33 and 34). In figure 31*a* the RP-bouton towards the right of the figure expands from a narrow pre- or interterminal axon containing microtubules and a few scattered vesicles: the enlargement from a serial section in figure 31*b* shows the synaptic contacts made with a D-profile and a P-profile. Of the two other RP-boutons labelled in figure 31*a* both of which are presynaptic to the same dendrite, the lower one appears to be a varicosity en passant. In figure 32, the dendrite is postsynaptic to four RP-boutons (RP) and to three F-terminals (F). Figure 31*a* magn. ×17100; figure 31*b* magn. ×44550; figure 32 magn. ×19350; figure 33 magn. ×44550; figure 34 magn. ×40050.

Figure 35. Two F-terminals (F), an RD-terminal (RD) and an RP-terminal (RP) in synaptic contact with the same dendrite (D). Part of a P-profile (P) is also seen. Magn. ×27000.

Figure 36. Two bouton-like structures packed with pleomorphic large dense core vesicles. Also present, especially in the lower bouton are smaller lucent spherical vesicles. The latter bouton makes a Gray type 1 synaptic contact onto a dendrite (D). Such boutons were uncommon and were ignored in the quantitative analyses. Magn. ×25200.

Figure 37. Elongate, varicose axon with predominantly flattened vesicles but with large numbers of pleomorphic dense core vesicles. A synaptic contact with a small dendrite is arrowed. Magn. ×27000.

Description of plate 12

Figure 38. Electron microscopy. Synaptic organization of OPN neuropil. Schematic drawing (figure 38*a*), based on a series of approximately 30 sections, of a region of glomerular neuropil. Figures 38*b*, *c* and *d* show parts of selected sections in the series. Four RP-boutons (RP, RP1, RP2 and RP3; shown in stipple), four P-boutons (P1, P2, P3, P4), two F-boutons (F1, F2) and several conventional dendritic elements (D1, D2, S) engage in synaptic relationships as depicted by the arrows in figure 38*a*. The profile labelled D2 in figure 38*a* is a spine head, as clearly shown in figure 38*c*. The two profiles labelled D1 are continuous around RP1, but are drawn as separate profiles to avoid confusion. A triplet synapse involving RP1, P2 and D1 is represented by the larger arrows in figure 38*a*, and one component of each of its constituent synaptic contacts is shown in each of the micrographs (RP1→P2 in figure 38*b*; P2→D1 in figure 38*c*; RP1→D1 in figure 38*d*). An unusual paramembranous density (arrow in figure 38*c*) resembling a postsynaptic density and apposed to an oligodendrocytic process lies in the thin dendritic shaft which gives rise to the small protrusion D2. With the exception of RP2 and P3 all neural elements which are both labelled and numbered in figure 38*a* appear in figures 38*b–d*. Neural structures unlabelled in figures 38*b–d* are not included in the drawing. (Figure 38*b–d* magn. ×25200).

containing profiles. They contained spherical synaptic vesicles with a mean maximum diameter of approximately 50 nm (see table 1) and large, rounded mitochondria with irregular, dilated and widely spaced cristae and a characteristically pale, flocculent matrix (figure 31*b*, 32 and 33). Small tubules of s.e.r., microtubules and occasionally dense core vesicles (diameter 80–100 nm; figures 33 and 34) were also present. These terminals appeared in both simple and glomerular neuropil where they established Gray type 1 synaptic contacts, often associated with a subsynaptic bar (figures 33 and 34), with both D- and P-profiles, and formed puncta adherentia with other RP-profiles, and with D- and F-profiles. Evidence that at least most RP-boutons are of retinal origin is presented below (§3*b*ii).

RD-profiles. These axon terminal profiles contained round (hence R) synaptic vesicles and dark (hence D) mitochondria (figure 35). They were smaller than RP-profiles (table 1) and less irregular in shape. They accounted for approximately 3% of vesicle-filled profiles in the neuropil as a whole and were only rarely seen in regions of glomerular neuropil. Their synaptic vesicles were spherical and slightly smaller than those within RP-profiles (mean maximum diameter approximately 46 nm; see table 1). Their mitochondria were small with regular sized and evenly spaced cristae and a dark matrix. Other organelles present were small s.e.r. elements and occasionally large dense core vesicles (diameter 80–100 nm) and large clear vesicles of similar diameter. RD-terminals made Gray type 1 synaptic contacts chiefly with D-profiles, less commonly with P-profiles, and rarely with class I somata with which they also occasionally formed puncta adherentia: they were never postsynaptic.

P-profiles. These dendrite-derived profiles contained loosely packed pleomorphic synaptic vesicles and were presynaptic (hence P). They were variable in size (table 1) and shape (figures 27–31, 34 and 35) and accounted for approximately 18% of all vesicle-filled neuropil elements. The profiles of their synaptic vesicles (mean maximum diameter approximately 51 nm; see table 1) varied from circular to elliptical (more than 50% displayed an ellipticity ratio of 1.3 or more; Campbell (1982)). Although it is possible that the vesicle population was heterogeneous, most vesicles were disc-like in form (cf. Lieberman & Webster 1972), the appearance of individual vesicle profiles depending on their orientation with respect to the electron beam (Dennison 1971). Mitochondria of P-profiles were similar in appearance to those within F- and RD-profiles, with smooth and rarely dilated cristae and a matrix of an electron density intermediate between that of the mitochondria of RP-profiles and that of the mitochondria within class I dendrites. Also present were small elements of s.e.r., some microtubules, occasionally dense core vesicles and generally a sparsely distributed floccular matrix giving the P-profiles a paler appearance than that of most axonal elements (for example, compare P with the axon terminals in figure 35). Other characteristics of P-profiles, were the presence of ribosomes and polyribosomes, which, however, were not commonly encountered (figures 29*a* and 31*a*) and the postsynaptic relationship to various classes of presynaptic element (figures 29*a*, 31*b* and 34). The presynaptic contacts established by P-boutons resembled Gray type 2 synapses, but with a slightly thicker postsynaptic density. Their active zones often displayed prominent presynaptic densities. P-boutons were presynaptic to D-profiles (figures 19*c*, 26–28) and less commonly to other P-profiles (figures 18 (inset) and 28 (inset)) and to class I somata and somatic spines and were postsynaptic to RP-, RD-, F-, and less frequently to other P-profiles: their synaptic relationships will be further considered in §3*a*iid. Puncta adherentia were occasionally established between P-profiles and D-profiles. The P-boutons were very similar to those found in LGd (Lieberman & Webster 1972, 1974) and

like the latter could be traced through serial sections into continuity with presynaptic dendritic shafts (figures 19, 24, 27 and 29) and somata some of which were themselves presynaptic (figures 28 and 29).

TABLE 1. RELATIVE FREQUENCY AND SIZE, AND SYNAPTIC VESICLE DIAMETERS OF PRESYNAPTIC COMPONENTS OF OPN NEUROPIL

terminal type	number of terminals counted	relative percentage	terminal area / μm^2	vesicle diameters / nm
RP	662	36.0	0.65 (0.09–3.24)†	50.52 (27.01–78.59)†
RD	55	3.0	0.50 (0.14–1.37)	46.45 (31.64–63.85)
P	324	17.5	0.48 (0.06–2.30)	51.27 (34.81–83.19)
F	156	8.5	0.51 (0.12–1.95)	53.47 (22.15–71.22)
UR	415	22.5	0.40 (0.07–1.50)	—
UF	227	12.5	0.34 (0.02–1.30)	—

† Range.

F-profiles. These profiles of axon terminals were of variable size (table 1) and shape, and contained flattened (hence F) synaptic vesicles (figures 9 (inset), 10*b*, 11, 12*b*, *c*, 13, 16, 19, 32 and 35). They were present in both simple and complex neuropil, constituting approximately 8% of all vesicle-containing profiles. Their synaptic vesicles were closely packed and individual vesicles (mean maximum diameter approximately 53 nm; see table 1) appeared to be more flattened than those in P-boutons (more than 84% of the vesicles had an ellipticity ratio of 1.3 or more; Campbell (1982)). Their mitochondria were small and dark and similar to those within RD-profiles. Other organelles included small amounts of s.e.r. and infrequent large dense core vesicles (approximately 100 nm in diameter) (figure 35). A few examples were found of F-profiles emerging from myelinated axons at nodes or distal to the termination of the myelin sheath. F-boutons established Gray type 2 synaptic contacts with class I somata (figures 9–11), class I somatic spines (figure 12*b*), axon hillocks, initial segments (figure 16) and dendrites (D-profiles) (figures 13, 35) and with class II somata (figure 30) their dendrites (figure 19*b*) and their dendritic appendages. They formed puncta adherentia with P-, RP-, and D-profiles, and with the perikarya of class I cells (figures 11*b*) and class II cells. They were never postsynaptic. There were indications that more than one class of F-terminals might be present in OPN, but differences were not sufficiently clearcut to make subclassification feasible.

Unclassified profiles. A few profiles containing large numbers of dense core vesicles, in addition to either rounded (figure 36) or flattened (figure 37) synaptic vesicles were occasionally observed. The nature of these terminals is unknown but they may represent monoamine (see, for example, Lindvall *et al.* 1974; Parent *et al.* 1981; Steinbusch 1981), or possibly peptide inputs (see, for example, Ljungdahl *et al.* 1978). Such terminals were not included in the quantitative analysis.

Of the two categories of unclassified profiles taken into account for the statistical analysis, those with predominantly round vesicles (UR) represented almost 23 % of all vesicle-containing elements and those with predominantly flattened vesicles (UF) represented 12 %.

Postsynaptic elements. The postsynaptic targets of the aforementioned presynaptic components were, in approximate order of frequency of occurrence: the dendrites of class I cells (D-profiles) and the dendrites and dendritic appendages of class II cells (P-profiles), the somata of class I and II cells, and the axon hillocks and initial segments of class I cells.

(d) *Synaptic relationships.* We arbitrarily refer to synaptic relationships involving a single presynaptic and a single postsynaptic element as simple: they comprise the following categories: *axoaxonic*, between F-terminals and the initial segment of the axons of class I cells (figure 16); *axodendritic*, these are the most numerous simple synaptic contacts and may be represented thus:

$$RP \rightarrow D \quad RD \rightarrow D \quad F \rightarrow D$$

$$RP \rightarrow P \quad RD \rightarrow P \quad F \rightarrow P$$

(see previous section for definitions); *axosomatic*, mostly between F-terminals and the cell bodies of class I cells and to a lesser extent of class II cells. In addition, RD-profiles occasionally made synaptic contact with class I cell bodies. The somatic spines of class I cells were postsynaptic to F-terminals and to a lesser extent to RP- and P-profiles and the rare somatic spines of class II cells to RP- and RD-profiles. *Dendrodendritic*, P-boutons and their parent dendritic shafts were presynaptic to the dendrites and dendritic appendages of both class I and class II cells, the frequency of the former (P→D) being greater than that of the latter (P→P). *Dendrosomatic*, comparatively rare, involving P-boutons or presynaptic dendrites in contact with class I cell somata (figure 17 *b*) or somatic spines. *Somatodendritic*, between the cell bodies of class II neurons and dendritic elements of class I cells (figures 17 and 22). *Somatosomatic*, very rarely seen and only between a presynaptic class II cell soma and the soma of a class I cell (figure 23).

More complex synaptic relationships, based predominantly upon the dual synaptic polarities of P-boutons were characteristic of the glomerular neuropil. Such complex synaptic arrangements were occasionally glimpsed in individual sections, but were properly revealed only by the analysis of serial sections (figures 38 and 39). The most common serial arrangement may be schematically represented thus: RP→P→D. But built around this comparatively simple linear series were many other and more complex relationships involving surprisingly large numbers of individual neuronal elements within any area of glomerular neuropil. For example, part of the series illustrated in figures 38*a–d*, plate 12, revealed the following relationships between glomerular components:

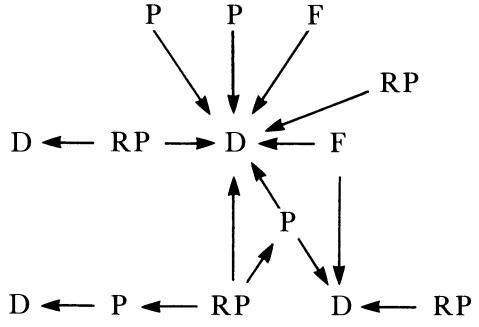

The synaptic relationships depicted in figure 39, plate 13, are more complex still. For example this area of neuropil contained several class I cell dendrites and several RP-boutons, some of which made synaptic contacts with two or more of the dendrites, for example,

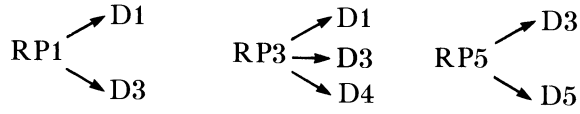

Although it is possible that some of the dendritic elements may have been continuous with one another outside the small volume of neuropil analysed, class I cell dendrites branch so minimally (see §3*a*ib) that most of the dendrites, particularly the larger ones, almost certainly derive from different cells. It would appear, therefore, that individual retinal terminals may innervate more than one OPN projection cell.

The arrangements considered above and illustrated in figures 38 and 39 (see also the descriptions of these figures) may be taken as typical of the many other regions of glomerular neuropil which have been analysed in serial sections by the same method (see Campbell 1982); also the microcircuits represented above depict only *part* of the connectivity pattern in a single region of glomerular neuropil. It would be possible to show amplified schematics representing more of the connections established between the depicted elements and other neural elements in the same region of neuropil and to include the connections of many additional adjacent glomerular components, but not only would the presentation of such additional detail be difficult (because of the constraints involved in the two-dimensional representation of such synaptic relationships) but it would serve more to emphasize the current state of ignorance concerning the functional significance of this complex synaptic organization than to provide any deeper insights into it.

We would however draw attention to the fact that the RP→P→D series is very commonly part of a more complex array in which the RP and D components of the series are also directly linked:

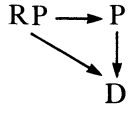

This arrangement, which we refer to as a triplet synapse (Campbell & Lieberman 1982) and which resembles triplet synapses (sometimes called triadic synapses) in thalamic nuclei (Lieberman & Webster 1972, 1974; Hámori *et al.* 1974), is illustrated in figures 38 and 39 (and see also figure 60). A substantial proportion of all RP-boutons in regions of complex neuropil is involved in the formation of such triplet synapses.

A single example was found of a close reciprocal synapse between contiguous P-boutons (not illustrated).

(*b*) *Experimental material*

(i) *Light microscopy*

(a) *Direct retinal input to OPN.* Retinal input to the pretectum was analysed only in animals in which the superior colliculus contralateral to the eye injected with HRP or radio-isotopes was uniformly labelled over its entire medial to lateral and rostral to caudal extents (Scalia & Arango 1979).

Retinal input to OPN in the rat is predominantly contralateral, as previously shown by Scalia & Arango (1979). The retinal fibres reach OPN chiefly via the brachium of the superior colliculus although some reach it via a deeper route after traversing the LGd, lateral posterior and anterior pretectal nuclei. In HRP-preparations of coronally sectioned brains (figure 40, plate 14) the retinal fibres penetrate the contralateral OPN along its dorsal and dorsolateral aspects and give rise to a fine granular terminal field of high density that appear to fill the cross-sectional area of the nucleus uniformly. In addition, a small patch of labelled fibres and possibly terminals was present immediately ventral to, and at rostral levels ventromedial to the main terminal field (best seen in figure 42*a*, *b*, plate 15). In sagittally sectioned brains the terminal label is less uniformly distributed (figures 41 and 43). In both HRP (figure 41) and radioautographic preparations (figure 43) the medial part of the terminal field in sagittally sectioned material resembles that seen in coronal sections of rostral OPN (figures 40, 42 and 44). More laterally, however, in sagittal sections, three distinct patches of terminal label are apparent, arranged in a rostrodorsal to caudoventral direction (figure 41). These three patches are continuous with one another ventrally thus giving rise to a W-shaped terminal field, the mediolateral extent of which is approximately 250 μm. In these preparations the OPN retinal terminal fields appear to have a laminar distribution similar to that demonstrated for the retinal input to squirrel monkey OPN (Weber *et al.* 1981).

Ipsilateral terminal fields in OPN were distinct but much smaller than the contralateral fields. Although the shape and size of the terminal field varied from animal to animal, it was normally confined to the lateral part of the neuronal shell of *pars oralis* and appeared to comprise a single patch (figures 42*c*, 44*c*). Although there appeared to be some signs of separation of ipsilateral and contralateral terminal fields, there was clearly considerable overlap between ipsilateral and contralateral fields at their borders (see figures 44*a–c*). A similar overlap of ipsilateral and contralateral retinal terminal fields has recently been described in the pretectum of the cat (Hoffmann *et al.* 1984). As previously reported by Scalia & Arango (1979) ipsilateral terminal fields were larger and denser in pigmented than in albino rats. It is also noteworthy that the retinal terminal fields in OPN, both ipsilateral and contralateral, were more deeply situated in pigmented than in albino rats (compare figure 42*a* (albino) with figure 44*a*, *b* (pigmented)), and the more superficial position of OPN in albino animals was a consistent observation in all types of preparation. The basis for the more superficial location of OPN in albinos appears to be that the brachium of the superior colliculus is thinner in albino than in pigmented rats, a finding that correlates well with evidence that the diameter of the optic nerve in adult albino rats is 30% smaller than the diameter in mass-matched pigmented rats (Sugimoto *et al.* 1984).

(b) *Transneuronal labelling studies.* Primary retinorecipient regions were well labelled in all the preparations analysed. In addition, areas known to receive second order visual projections, such as the visual cortex (Grafstein 1971), the parabigeminal nucleus (Watanabe & Kawana 1979) and the thalamic reticular nucleus (Webster *et al.* 1981), were also labelled, confirming that transneuronal labelling of efferents from primary retinorecipient regions had been achieved. In this material, a prominent tract of heavily labelled fibres emerged from the ventromedial surface of almost the entire rostrocaudal extent of OPN (figure 45*a*). These fibres coursed ventromedially through the medial pretectal area towards the posterior commissure where they became sparser and turned ventrally, perpendicular to the dorsomedially coursing fibres of the commissure (figure 45*b*). In several preparations, the labelled fibres could be traced into the periaqueductal gray close to the wall of the cerebral aqueduct (figure 45*c*) and in some cases

as far caudal as the Edinger–Westphal nucleus, where they appeared to terminate (figure 45*d*). No fibres were traced across the posterior commissure. However, a similar but very much sparser contingent of transneuronally labelled fibres was traced from the OPN on the side ipsilateral to the injected eye.

(ii) *Electron microscopy*

(a) *Unilateral eye enucleation or optic nerve section.* The following account deals with observations on the OPN contralateral to the enucleated eye. Terminal degeneration was also studied in the dorsolateral part of the OPN ipsilateral to the enucleated eye but no significant differences were noted between the cytology or time course of degeneration on the two sides of the brain.

Only RP-terminals, characterized by spherical synaptic vesicles, large pale mitochondria and Gray type 1 synaptic contacts with D- and P-profiles underwent degeneration (figures 46–60, plates 16–18). The following were all considered to be degenerative changes: enlargement of synaptic vesicles; accumulation of neurofilaments ('neurofilamentous hyperplasia'); accumulation of a flocculent, moderately electron-opaque cytoplasmic material; presence of an electron-opaque cytoplasmic matrix (dense or dark degeneration); shrinkage of terminal and distortion of terminal outline. Some degenerating terminals displayed only one of these characteristics; others a combination of two or more. In general, the presence of swollen synaptic vesicles was most common after short postoperative survivals (one to three days); neurofilamentous hyperplasia, usually associated with swollen vesicles at four to six days; and dark degeneration thereafter. Thus, enlargement of synaptic vesicles and accumulation of neurofilaments appear to represent early stages of the degenerative response and accumulation of electron-dense material and the formation of an electron-dense terminal matrix, a later stage (cf. Raisman & Matthews 1972). This interpretation is strengthened by the observation that degenerating terminals partly or wholly 'engulfed' by glial cell processes were always of the dark type. In addition, a relatively small number of possibly swollen terminals with very electron-lucent matrices and, usually, clumped synaptic vesicles, were also seen, chiefly at early postoperative survivals. The relationship, if any, between this appearance and the other appearances taken as indicative of a degenerative response, was not clear.

Temporal sequence of degenerative changes: 1-*day*, 2-*day and* 3-*day survivals* (10 *animals*). Very few recognizably degenerating terminals were apparent in 1-day and 2-day material. At 3 days numerous terminals with swollen vesicles and abnormal numbers of neurofilaments were apparent (figures 46 and 47). The neurofilament accumulations were in the form of orderly, loose bundles which occupied a variable and occasionally the major part of the terminal profile. Accumulations of neurofilaments were also very striking in some preterminal axons, which sometimes also appeared to be swollen. Some terminals containing either or both swollen vesicles and neurofilaments also contained patches or clumps of flocculent, moderately electron-dense material (figures 46 and 47).

Terminals undergoing the electron-lucent type of degenerative change were first seen at 3 days. They contained very few synaptic vesicles (which were often clumped), or other organelles, and displayed a pale matrix with a sparse evenly distributed and homogeneous flocculent material (see figure 49 from 4-day material). Dark degeneration (figure 48) was rare at this stage.

4-*day and* 5-*day survivals* (9 *animals*). The general appearance of the neuropil was similar to that of neuropil in 3-day animals, but the proportion of degenerating terminals was now much

Description of plate 13

Figure 39. Electron microscopy. Synaptic organization of OPN neuropil. Schematic drawing (figure 39*a*) based on a series of 30 serial sections, of synaptic relationships within an area of glomerular neuropil. Figures 39*b*, *c* and *d* show parts of selected sections from the series. RP-boutons (RP and RP1–7; stippled), P-boutons (P and P1–P4) conventional dendritic elements (D, D1–5, S, *) and an unusually large number of F-boutons (F, F1–7) interact in this area of neuropil but no RD-boutons are involved. Neural elements labelled but not numbered in figure 39*a* are not illustrated in figures 39*b*, *c* and *d*: all others appear in the micrographs, with the exception of F6 of which only a tiny part is seen below RP6 at the bottom left of figure 39*b*. Neural structures not labelled in the micrographs are not included in the drawing. Puncta adherentia are represented by thick dashes and synaptic contacts (and their polarity) by arrows. It is striking how many individual synaptic contacts are in fact components of serial synapses, for example: F3→P1→D3 (note that F3 also synapses directly onto a spine of D3 (marked by an asterisk); RP3→P1→D3; RP5→P3→D5. The two latter series are also parts of triplet synapses, which are shown by the larger arrows in figure 39*a*. Figures 39*b*, *c* and *d* magn. ×14400.

Description of plate 14

Figure 40. Light microscopy. Retinal input to OPN in albino rat revealed by intravitreal injection of HRP. A series of frontal sections through almost the entire rostral (*a*) to caudal (*f*) extent of the pretectum of an adult albino rat which received an injection of HRP into the contralateral eye 20 h before fixation.

Long arrows denote retinal terminal fields in OPN. Note that in sections (*e*) and (*f*) terminal label in OPN appears in discrete medial (m.) and lateral (l.) patches. The area of OPN in sections (*a*), (*c*) and (*e*) is enlarged in figures 42*a*, *b* and *d*.

Short arrows denote terminal fields in the posterior pretectal nucleus (sections (*d*), (*e*) and (*f*)). Terminal fields of the nucleus of the optic tract (*, sections (*b*), (*c*), (*d*), (*e*) and (*f*)) lie within and just ventral to the brachium of the superior colliculus and have indistinct borders. LGd, dorsal lateral geniculate nucleus; LGv, ventral lateral geniculate nucleus. Vibratome sections, 50 μm thick; TMB method; no counterstain; magn. ×24.3.

Description of plate 15

Figures 41–45. Light microscopy. Retinal input to OPN in albino and pigmented rats demonstrated by HRP and radioactive labelling methods and OPN efferents shown by transneuronal transport of radioactive label.

Figure 41. A series of parasagittal sections passing through almost the entire lateral (*a*) to medial (*f*) extent of the pretectum of an adult albino rat which received a contralateral eye injection of HRP. Retinal terminal fields in OPN (large arrows), in the posterior pretectal nucleus (small arrows) and in the nucleus of the optic tract (*) are seen rostral and ventral to the heavily-labelled superficial stratum of the superior colliculus (s.c.) and its brachium (arrowhead). Note the W-shaped configuration of the terminal field in OPN in section (*c*). Frozen sections 40 μm thick; TMB method; neutral red counterstain; magn. ×24.3.

Figure 42. Frontal sections of retinal terminal fields in OPN contralateral (figures 42*a*, *b*, *d* and *e*) and ipsilateral (figure 42*c*) to the HRP-injected eye. Figures 42*a*, *b*, *d* and *e* are arranged in a rostrocaudal sequence. Figure 42*c* is from the same section as figure 42*b* and is oriented correctly with respect to figure 42*b* (that is, dorsal is towards the top and medial towards the left). Figure 42*a* is an enlargement of section (*a*) in figure 40, figure 42*b* is an enlargement of section (*c*) in figure 40 and figure 42*d* is an enlargement of section (*e*) in figure 40. Magn. ×75.6.

Figure 43. Radioautograph, photographed in dark field, of a parasagittal section of OPN situated approximately half way between its medial and lateral edges, showing the retinal terminal field 24 h after contralateral intravitreal injection of [^{3}H]proline. Note the labelled fibres of the brachium of the superior colliculus (large arrow). Small arrows show label in the posterior pretectal nucleus. Compare the discontinuous character of the terminal field in OPN here with the terminal field in the HRP preparation in figure 41 (especially section (*c*)). Frozen section, 40 μm thick, lightly counterstained with thionine, magn. ×75.6.

Figure 44. Frontal sections showing retinal terminal fields in OPN of an adult pigmented rat after HRP injection into one eye. Figures 44*a* and *b* (of which the former is at the more rostral level) show the contralateral OPN, and figure 44*c* (which is correctly oriented with respect to figures 44*a* and *b*, that is, dorsal is at the top and medial to the left) shows a small patch of label in the dorsal part of the ipsilateral OPN (the dashed line indicates the approximate boundary of *pars oralis*). Note that the OPN appears to be more deeply situated than in albino rats at comparable rostrocaudal levels (for example, figure 42*a*) because the brachium of the superior colliculus (br.) is thicker in pigmented than in albino animals. Parts of the contralateral retinal terminal fields of the nucleus of the optic tract are also seen in figures 44*a* and 44*b* (*). Vibratome sections, 50 μm thick; TMB method; lightly counterstained with neutral red; magn. ×75.6.

Figure 45. OPN efferents visualized by transneuronal transport of radioactive label in autoradiographs of the pretectum and upper mesencephalon of an adult albino rat following injections of [^{3}H]fucose and [^{3}H]proline into the contralateral eye and a postinjection survival time of ten days. A ventromedially directed outflow of labelled fibres is seen in figure 45*a* (large arrow). In figure 45*b* the labelled fibres (arrows) are seen to cross the fibres of the posterior commissure (p.c.) (at a level slightly rostral to that portrayed in figure 45*a*, and at greater magnification). In figure 45*c*, which is from a more caudal level than figure 45*a*, labelled fibres are evident (arrows) in the periaqueductal grey, ventrolateral to the cerebral aqueduct (a.). At a more caudal level still (figure 45*d*) labelled fibres and possibly terminals (arrows) lie within the region of the Edinger–Westphal nucleus ventral to the cerebral aqueduct. It is noteworthy that the transneuronally labelled fibres do not appear to cross the midline. The small arrow in figure 45*a* indicates the retinal terminal field of the posterior pretectal nucleus on the side ipsilateral to the injected eye. Figure 45*a* magn. ×10; figure 45*b* magn. ×61.2; figure 45*c* magn. ×61.2; figure 45*d* magn. ×61.2.

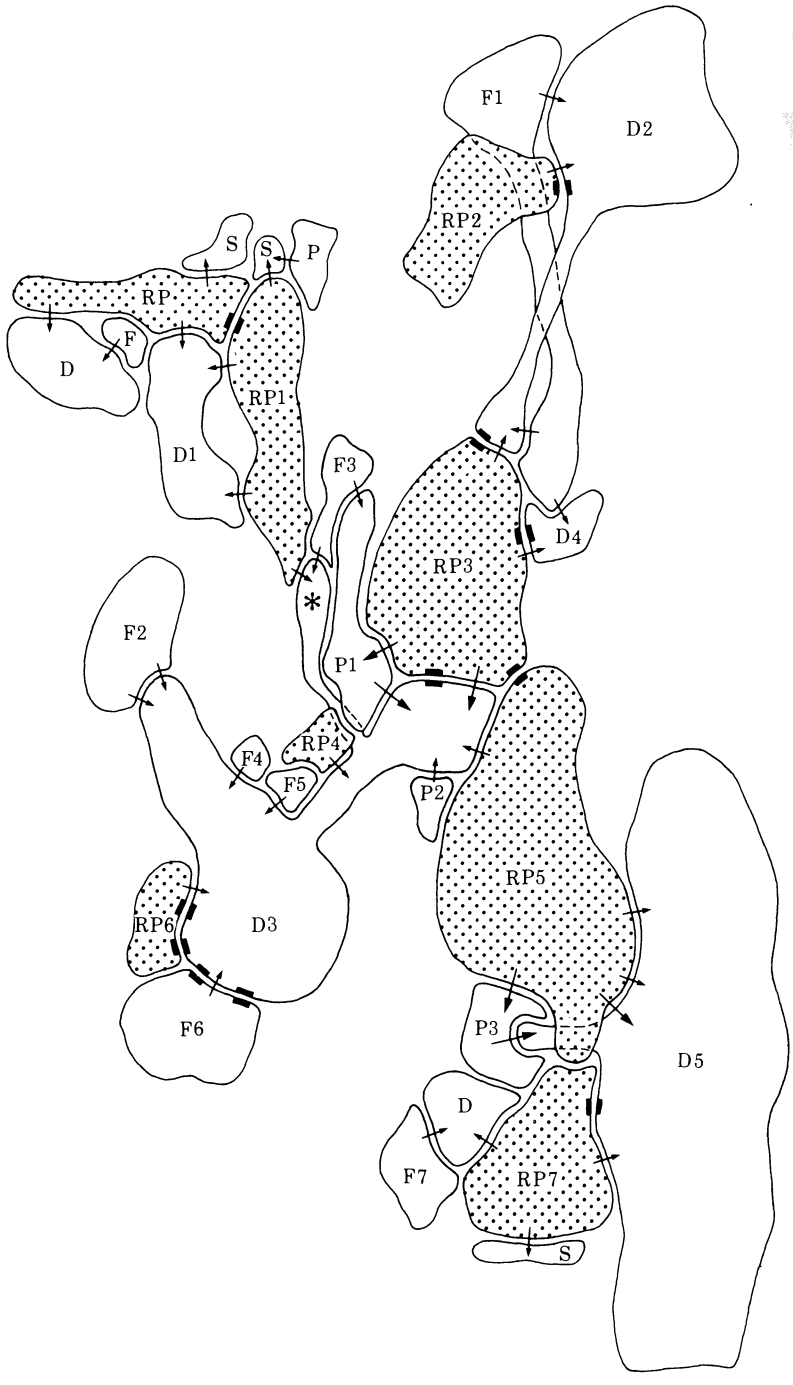

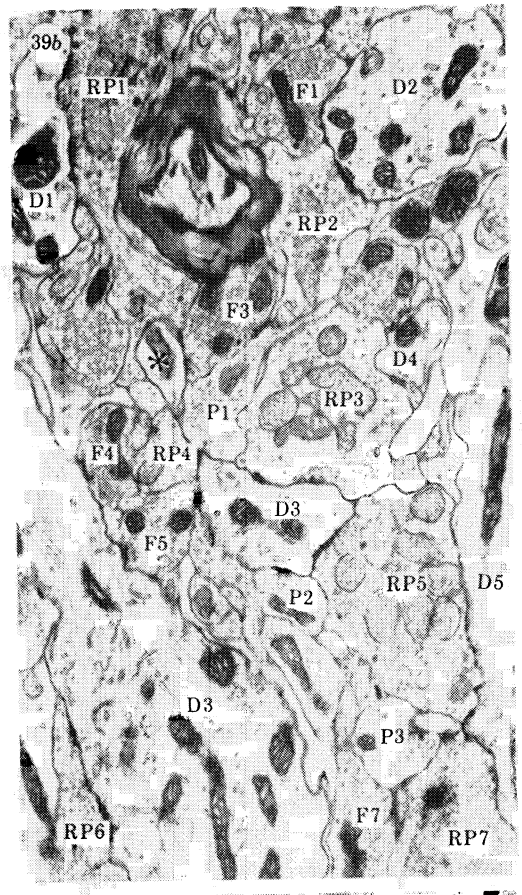

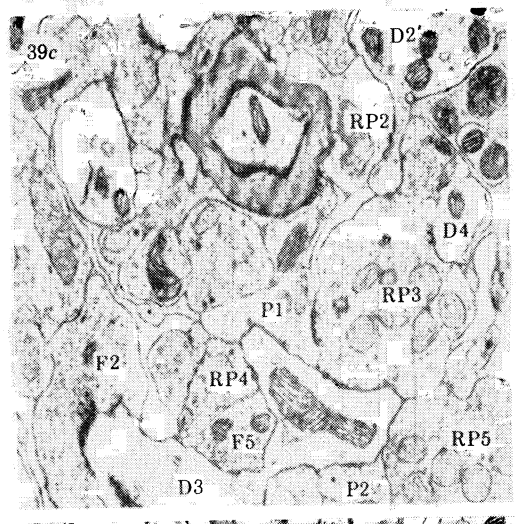

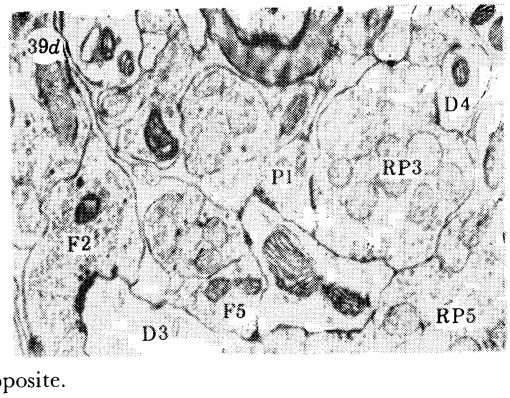

FIGURE 39. For description see opposite.

(*Facing p.* 594)

FIGURE 40. For description see p. 594.

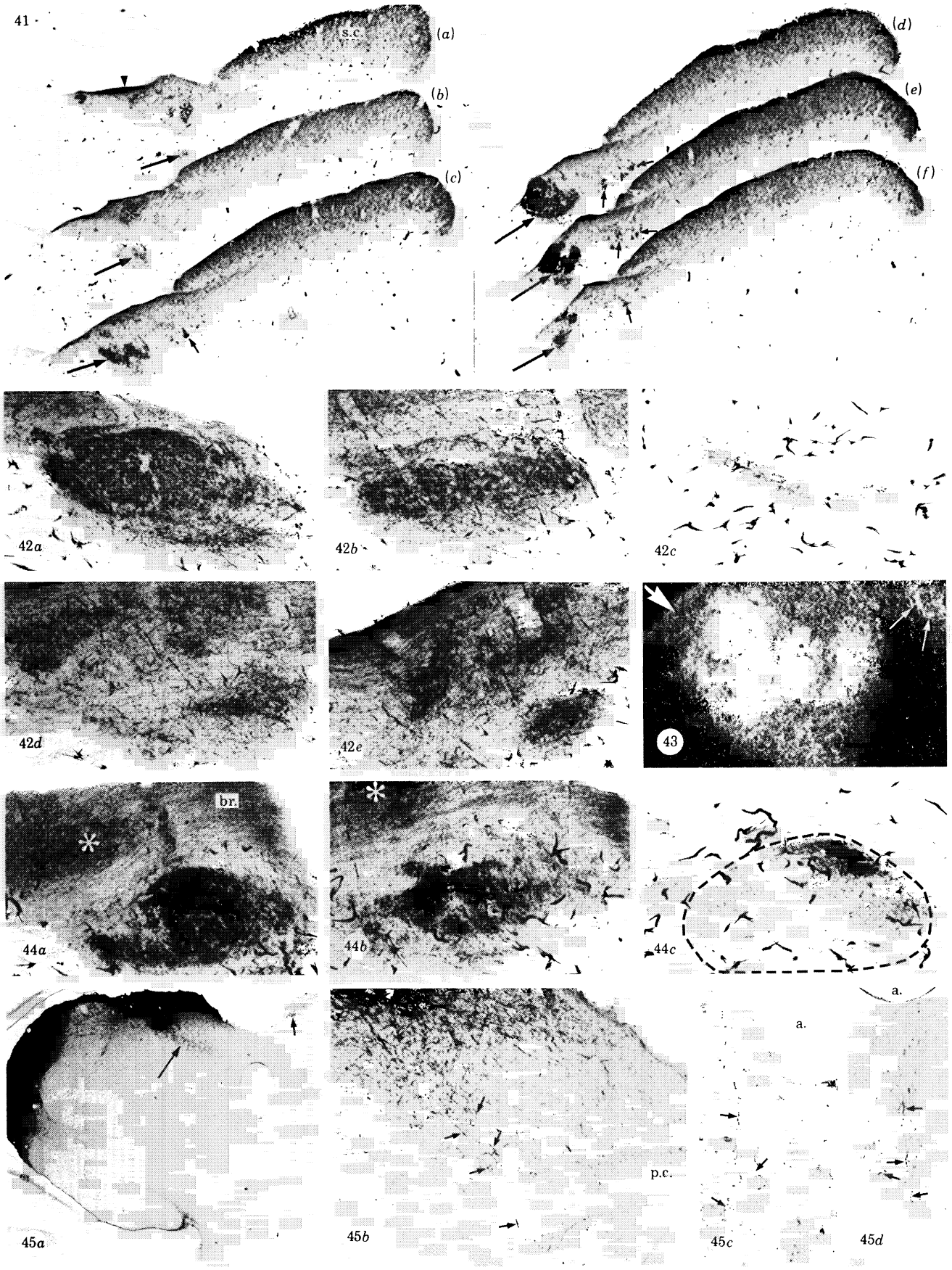

FIGURES 41–45. For description see p. 594.

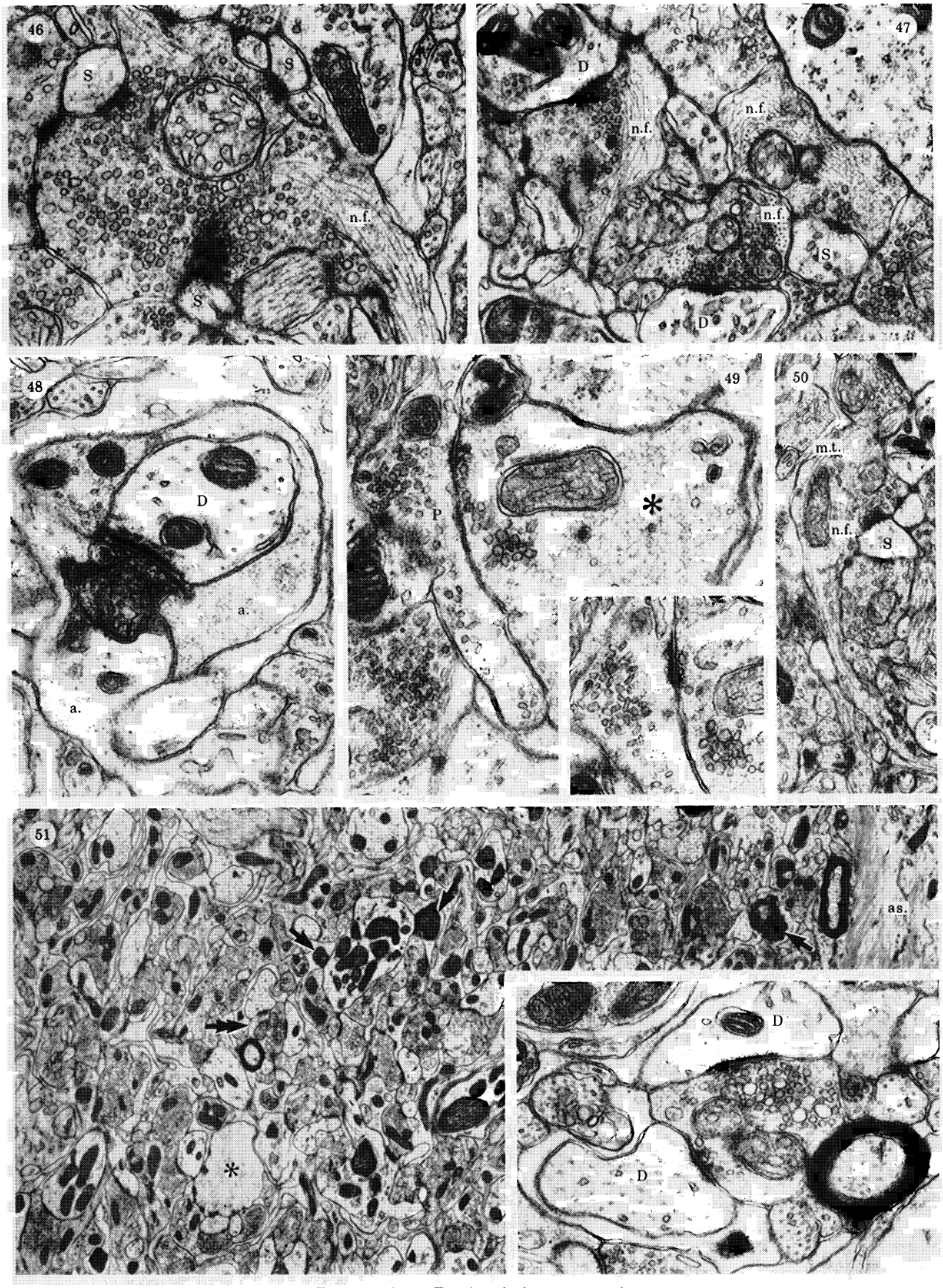

FIGURES 46–51. For description see opposite.

Description of plate 16

Figures 46–51. Electron microscopy. Terminal degeneration three to six days after enucleation.

Figures 46 and 47. Retinal terminals in OPN three days after contralateral eye enucleation. The *en passant* varicosity in figure 46 and the several boutonal profiles in figure 47 display abnormally large numbers of neurofilaments (n.f.). There are also signs of vesicle swelling in figure 46 and of vesicle clumping in figure 47. The degenerating terminals are presynaptic to dendritic spines (S) or larger dendritic elements (D). Figure 46 magn. × 44 550; figure 47 magn. × 44 550.

Figure 48. A shrunken, electron dense degenerating terminal making synaptic contact with a dendrite (D) and surrounded by swollen astrocytic processes (a.). Such appearances were very rare at this stage (three days after enucleation). Magn. × 40 050.

Figure 49. Electron lucent degeneration of a terminal (*) four days after enucleation. The terminal contains flocculent material. A small cluster of distorted synaptic vesicles is associated with a synaptic contact onto a P-profile (P) which is more clearly seen in a serial section in the inset. Magn. × 40 050.

Figure 50. Degenerating terminal expanding from a narrow pre- or interterminal axon, six days after enucleation. Both the axon and the bouton contain microtubules (m.t.) and abnormally large numbers of neurofilaments (n.f.) are present in the bouton. Apparently unswollen vesicles are clustered at a synaptic contact with a dendritic spine (S). Magn. × 21 600.

Figure 51. An area of OPN neuropil six days after enucleation. Several degenerating terminals are present (arrows) including some that are electron dense. A terminal containing swollen vesicles and making synaptic contacts with two dendritic profiles (D) is marked with a double arrow and shown enlarged (and rotated through 90°) in the inset. An unusual degenerating profile, marked with an asterisk, is distended with flocculent material and establishes membrane specializations with several spines, although no vesicles are associated with the contact zones. Astrocyte processes are more prominent than in control material and a large process of a reactive astrocyte, packed with glial filaments is seen at the right (as.). Magn. × 7650; inset × 32 850.

Description of plate 17

Figures 52–57. Electron microscopy. Terminal degeneration 8–12 days after enucleation.

Figures 52–54. Synaptic vesicle swelling and neurofilamentous hyperplasia in degenerating terminals 8 days (figure 52), 11 days (figure 53) and 12 days (figure 54*a*, *b*, *c*) after enucleation. The degenerating terminals (*) establish synaptic contacts with conventional dendritic elements (D) (in every illustration) and with P-boutons (P), (in figures 53 and 54*a*). In figure 54*a* the arrow indicates a punctum adherens between two degenerating terminals. Note also the network of branching and anastomosing agranular tubules or cisterns in two of the degenerating profiles in this figure. The massive increase in neurofilaments in the degenerating terminals associated with some loss of vesicles, results in a compartmentalization of some terminals, with vesicle clumps separated by, or surrounded by, large bundles of neurofilaments. Figure 52 magn. × 38 700; figure 53 magn. × 45 000; figure 54*a* magn. × 11 700; figure 54*b* magn. × 36 450; figure 54*c* magn. × 33 300.

Figure 55. An apparently normal RP-bouton (RP) presynaptic to a dendritic profile (D) and a dark degenerating terminal in synaptic contact with a P-bouton (P), 12 days after enucleation. Magn. × 40 050.

Figure 56. Degenerating terminals 12 days after enucleation displaying a range of electron densities. The two marked with asterisks display swollen vesicles and a slightly darkened matrix containing flocculent material. The arrowed terminal is electron dense, but vesicles and mitochondria are still discernible within the darkened matrix. The terminal marked with the double arrow is distorted and more electron dense and internal substructure is difficult to discern. D, conventional dendritic elements. Magn. × 44 550.

Figure 57. Almost homogeneously electron dense degenerating terminal, 12 days after enucleation, in synaptic contact with a P-bouton (P) and elsewhere surrounded by, and penetrated by, swollen astrocyte processes (a.) two of which appear to be linked by a gap junction (arrowheads). Magn. × 55 350.

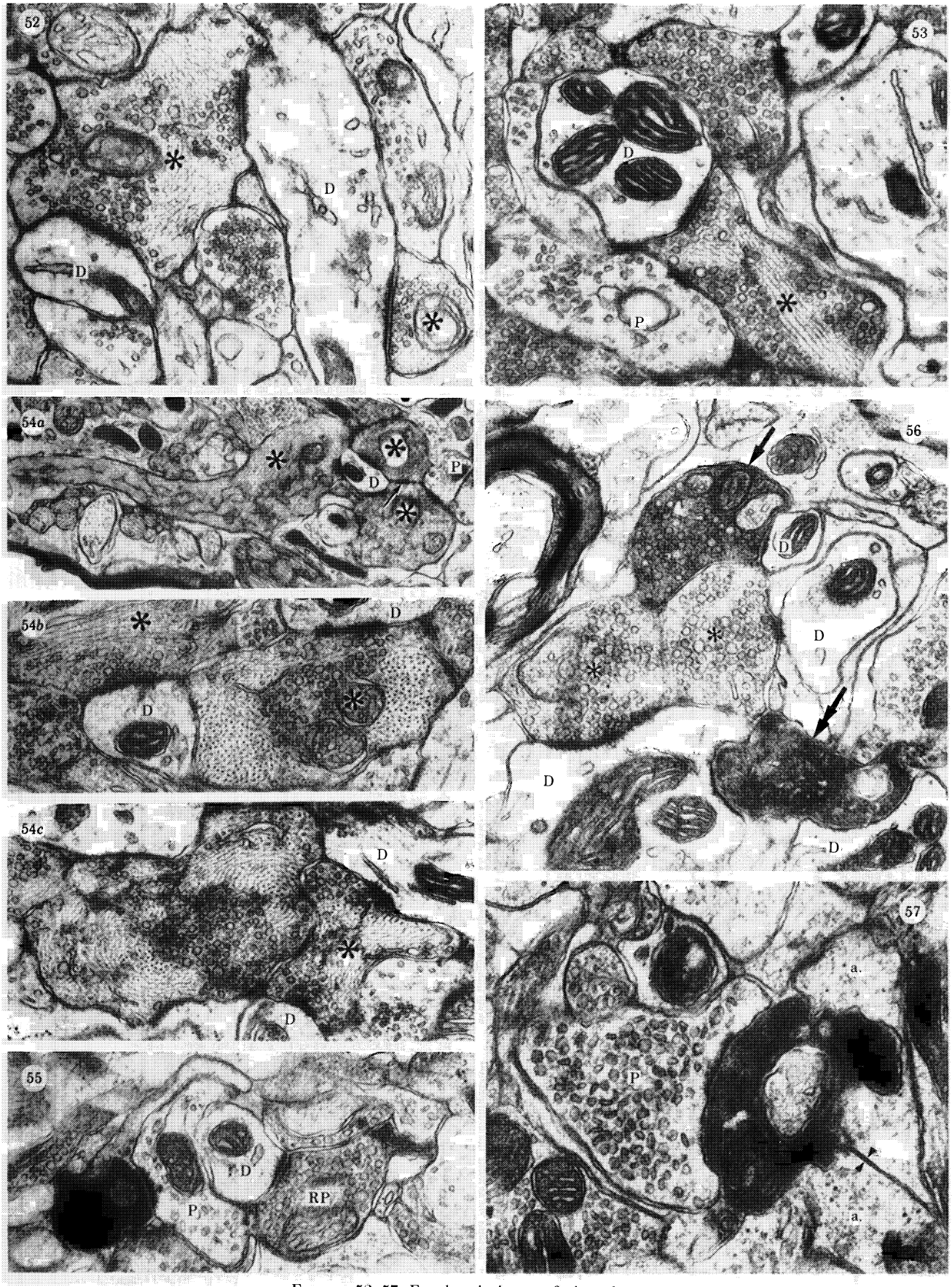

FIGURES 52–57. For description see facing plate 16.

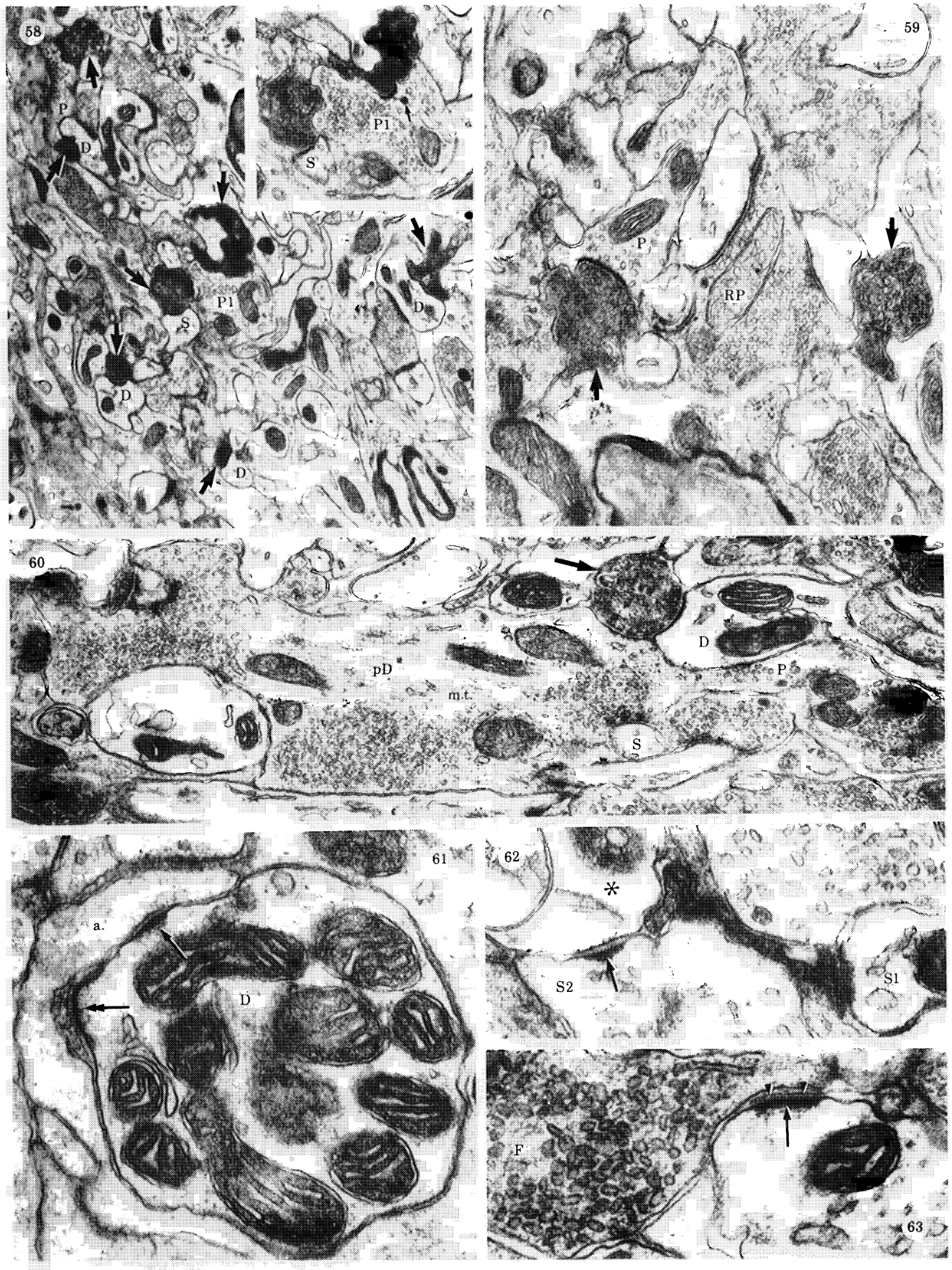

FIGURES 58–63. For description see p. 595.

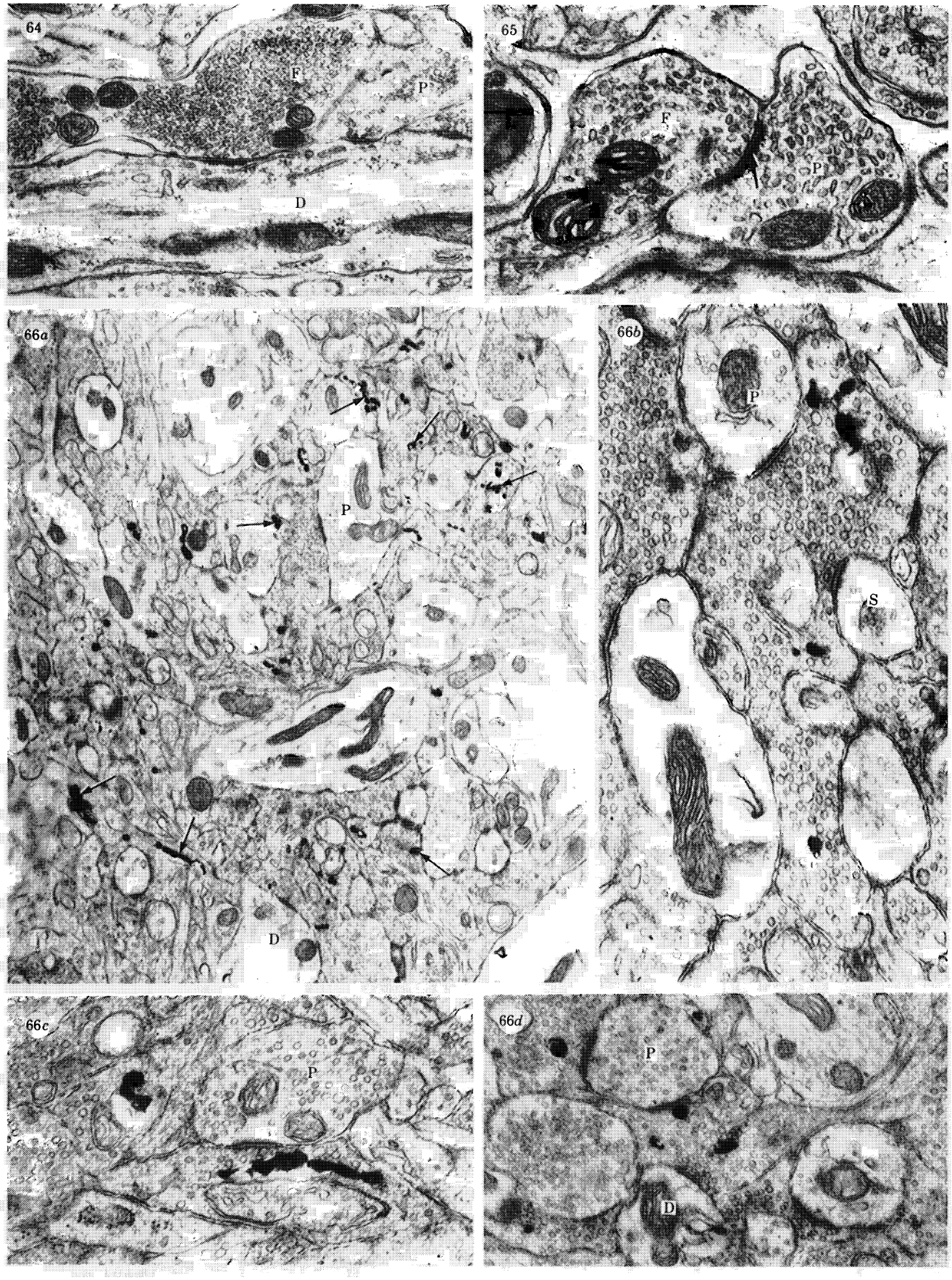

FIGURES 64–66. For description see p. 595.

higher. Most of the latter were characterized by swollen vesicles, large accumulations of neurofilaments and patches or extensive amounts of flocculent dense material. Dark terminals were more common than at 3 days but were still a minority of all degenerating terminals. Terminals displaying lucent degeneration (figure 49) were no more frequent than at day 3.

6-day, 7-day 8-day and 9-day survivals (*11 animals*). Many degenerating terminals (figures 50–52) were electron-dense and similar to the dark terminals of earlier stages but they were more commonly engulfed or partly engulfed by glial cytoplasm at these stages. Terminals containing swollen vesicles or displaying neurofilamentous hyperplasia, sometimes with flocculent dense material, but without an electron opaque matrix were still numerous (figures 50, 51 (inset) and 52). Some terminals with a cytoplasmic matrix intermediate in density between the latter and dark terminals were also present and probably represent an intermediate stage in the evolution of dense degeneration.

Description of plate 18

Figures 58–63. Electron microscopy. Degenerating terminals 15 days after enucleation; 'vacated' densities.

Figure 58. An area of neuropil, 15 days after enucleation, containing several electron dense degenerating boutons (arrows) most of which have synaptic contacts with dendritic elements (D, S) and with P-boutons (P). One such P-bouton (P1) is postsynaptic to two degenerating terminals and one of the contacts is shown, enlarged from a serial section, in the inset. The postsynaptic density of this contact appears to be connected by a strand of material to a ball-like subsynaptic inclusion (arrow). Magn. 9450; inset magn. × 27900.

Figure 59. An apparently normal RP-bouton (RP) in close proximity to two electron dense profiles (arrows) one of which is a degenerate terminal with a synaptic contact onto a P-bouton (P). 15 days after enucleation; magn. × 33300.

Figure 60. A large presynaptic dendrite (pD) containing microtubules (m.t.) and numerous pleomorphic synaptic vesicles, postsynaptic to a dense degenerating terminal (arrow) 15 days after enucleation. The presynaptic dendrite establishes synaptic contact with a small spine (S) and via a small protrusion (P) with a dendrite (D) which is also postsynaptic to the degenerating terminal. Thus the degenerating terminal and the presynaptic dendrite engage in a serial synapse and a triplet synapse at this level. Magn. × 24750.

Figures 61–63. 'Vacated' postsynaptic densities 12 days after enucleation. In figure 61 the dendrite (D) has two postsynaptic densities, one apposed to the remnant of a degenerate terminal (double arrow) embraced by a stout astrocyte process (a.), and the other directly apposed to the same astrocyte process (arrow). It is possible that both postsynaptic densities were originally related to the same retinal terminal. In figure 62, a remnant of a degenerate terminal retains synaptic contact with one spine S1, but may have lost contact with a second spine (S2) which contains a postsynaptic density (arrow) apposed to an unidentified profile (*). In figure 63, the vacated density (arrow) is separated from an F-terminal (F) by an extremely thin slip of glial cytoplasm or a remnant of a degenerate bouton (arrowheads). It may be that the F-terminal was about to 'reoccupy' the vacated density (compare with figure 64). Figure 61 magn. × 59850; figure 62 magn. × 69750; figure 63 magn. × 66600.

Description of plate 19

Figures 64–66. Electron microscopy. Abnormal synaptic arrangements following deafferentation; e.m.-HRP labelling of retinal terminals.

Figures 64 and 65. Abnormal synaptic configurations in OPN 15 days after enucleation. In figure 64 a large F-terminal (F) in contact with a dendritic shaft (D) is associated with a thick postsynaptic density (compare with the postsynaptic density at the contact between an adjacent P-bouton (P) and the same dendritic shaft). In figure 65 a postsynaptic density of similar width (arrow) is seen at a contact between a P-bouton (P) and a 'presynaptic' profile that is probably an F-terminal (F). In both cases the postsynaptic density may have previously been associated with a retinal terminal. Figure 64 magn. × 40050; figure 65 magn. × 55350.

Figure 66. Terminals labelled with electron dense HRP reaction product (some indicated by arrows in figure 66*a*) made visible by the DAB–cobalt chloride method following injection of HRP into the contralateral eye. The labelled profiles are clearly RP-terminals: they contain spherical synaptic vesicles and large pale mitochondria, and are presynaptic to conventional dendritic shafts and spines (D, S) (see especially at S in figure 66*b*) and to P-boutons (P, figures 66*a*, *b*, *c* and *d*). Figure 66*a* magn. × 13500; figure 66*b* magn. × 35550; figure 66*c* magn. × 35550; figure 66*d* magn. × 28800.

11-day and 12-day survivals (*4 animals*). At this stage most degenerating terminals (figures 53–57) displayed either massive neurofilamentous hyperplasia (figures 53, 54), commonly extending into (or from) neurofilament-packed preterminal axons (figure 54*a*), or dark degeneration (figures 55–57). The latter were for the most part small, shrunken, and extremely electron-dense with few recognizable organelles. Less electron-dense dark terminals were generally larger (figure 56).

15-day survival (*1 animal*). Although some terminals with swollen vesicles or neurofilamentous hyperplasia were still apparent, most of the degenerating terminals were of the electron-dense type in various stage of engulfment by astrocytes (figures 58–60). The neuropil was loosely packed, showing evidence of terminal loss and glial hyperplasia.

'Vacated' postsynaptic densities and evidence of reoccupation. Paramembranous densities resembling the postsynaptic density of a Gray type 1 synapse but lacking an associated presynaptic element were frequently encountered at day 11 and thereafter and were also seen (but rarely) at earlier survival times (vacated postsynaptic densities; figures 61–63). The vacated densities, usually located within D-profiles but occasionally within P-profiles, were most commonly apposed to thin slips of astrocyte cytoplasm (figure 61) but were also located opposite other dendritic profiles, oligodendrocytes, myelin sheaths, or unidentified profiles. At day 11 and thereafter, several examples were also observed of P- and F-profiles presynaptic to D-profiles or P-profiles at synaptic specializations with thick postsynaptic densities resembling those of Gray type 1 synapses (figures 64 and 65).

(b) *Intravitreal injection of HRP.* Labelled terminals displayed a variable number of small electron-dense vacuoles and saccules approximately 100 nm in diameter and often up to 1 μm long, with very poorly defined limiting membranes (figures 66*a–d*, plate 19). These vacuoles and saccules occurred singly, in pairs, or in small clusters, and closely resembled inclusions identified as HRP-containing structures in previous studies in which a similar methodology was used (LaVail & LaVail 1974; Repérant 1975; Colman *et al.* 1976). The HRP-containing inclusions were found exclusively in RP-profiles (see especially figure 66*b*) and in myelinated axons containing mitochondria similar to those of RP-profiles (not illustrated).

4. Discussion

(*a*) *Neuron types*

(i) *The class I cells*

There are a number of similarities between the class I cells of OPN and thalamocortical projection cells in the dorsal lateral geniculate nucleus (LGd) in various species (for example, human (Hickey & Guillery 1981); monkey (Wong-Riley 1972*a*); cat (Guillery 1966); rat (Grossman *et al.* 1973)) and other thalamic relay nuclei (see review by Jones 1981) and to projection neurons in the superior colliculus (primates (Laemle 1981); cat (Sterling 1971); rat (Langer & Lund 1974); mouse (Valverde 1973)). The similarities include size (they are medium to large cells), radiating, apparently non-specifically oriented dendrites, comparatively simple dendritic appendages, and an axon which takes origin from a prominent hillock, becomes myelinated close to its origin and emits few, if any, intranuclear collaterals. However, the dendrites of OPN class I cells do not display the prominent clusters of excrescences seen at the branch points of some projection cells in LGd of rat (Grossman *et al.* 1973) or cat (Guillery 1966; Peters & Palay 1966). Nor is their pattern of branching closely similar to that of

geniculocortical projection cells, for in the rat and mouse (Grossman *et al.* 1973; Rafols & Valverde 1973) the latter have relatively short primary dendrites which commonly branch into multiple secondary dendrites whereas the primary dendrites of OPN class I cells branched much further from the cell body and for the most part sparsely and dichotomously.

In their ultrastructural features too, particularly with respect to the relatively voluminous, organelle-rich cytoplasm (including large mitochondria, abundant g.e.r. and a prominent Golgi apparatus), the relatively high frequency of synaptic contacts on the soma, the possession of exclusively postsynaptic dendrites stemming from broad, organelle-rich bases, and well differentiated axon hillocks and axonal initial segments, the class I cells were similar to thalamic projection cells (for example, Colonnier & Guillery 1964; Wong-Riley 1972*a*; Lieberman 1973), although specialized membranous organelles such as those found in relay cells in LGd of rat (Lieberman 1973) and cat (LeVay & Ferster 1977) were not present in these cells. Thus, although we do not have direct evidence at present, such as could be obtained, for example, by retrograde labelling of the cells with HRP from a nucleus to which OPN projects, the indirect evidence of the Golgi and e.m. data suggests that cells of this class are, or at least include, the projection cells of OPN.

(ii) *The class II cells*

Class II cells are markedly different from class I cells. They are smaller, have fewer dendrites, different dendritic trees and give rise to strikingly complex dendritic appendages. In general the class II cells show similarities to the intrinsic neurons (interneurons) of LGd and other thalamic relay nuclei. Although the number of successfully impregnated cells was small, making more detailed classification necessarily tentative, two subclasses of type II cell were recognized in the Golgi material. Cells of class IIa, with their oval or fusiform cell bodies, long, straight and minimally branched dendrites are very similar to the class B cells of the LGd in the same species (Grossman *et al.* 1973), and like the latter, appeared to be preferentially oriented. The class IIa cells are also similar to the pseudoamacrine cells of mouse LGd (Rafols & Valverde 1973) to the fusiform cells of cat LGd and ventrobasal nucleus (Tömböl 1966/1967) and mouse medial terminal nucleus of the accessory optic tract (Iwahori *et al.* 1981), to the horizontal cells of rat superior colliculus (Langer & Lund 1974) and the spiny neurons of the rat suprachiasmatic nucleus (Van den Pol 1980). Class IIb cells, with their branching dendrites arborizing close to, and never extending far from the cell body are more similar to the Golgi type II cells of the cat ventrobasal nucleus (Tömböl 1966/1967; Ralston 1971), the type III cells of the monkey LGd (Wong-Riley 1972*a*), the small pyriform cells of the cat superior colliculus (Sterling 1971) and the axoniform-dendrite bearing cells of human LGd (Hickey & Guillery 1981).

The complex dendritic appendages of OPN class II cells are also very similar to those of Golgi type II cells and other types of interneuron in thalamic relay nuclei and superior colliculus. The long, thin filiform and occasionally beaded appendages with bulbous end knobs have been noted previously on such cells in rat (Grossman *et al.* 1973), cat (Famiglietti & Peters 1972), monkey (Saini & Garey 1981) and human LGd (Hickey & Guillery 1981). Likewise, the shorter stalked, pleomorphic appendages, sometimes branching to form a cluster of closely adjacent varicosities have their counterparts in various thalamic relay nuclei (Morest 1971; Wong-Riley 1972*a*; Famiglietti & Peters 1972; Grossman *et al.* 1973), the superior colliculus (Langer & Lund 1974) and the suprachiasmatic nucleus (Van den Pol 1980). Finally the comparatively simple, drumstick-like spines, which we also observed on OPN class II cell dendrites, have also

been described in Golgi studies of interneurons in other sites (see, for example, Guillery 1966; Ralston 1971; Wong-Riley 1972*a*; Famiglietti & Peters 1972; Grossman *et al.* 1973; Langer & Lund 1974; Van den Pol 1980).

We found no unequivocal axons stemming from class IIa cells in Golgi preparations and only a few and not fully convincing examples, in the case of class IIb cells. Nor were axons traced from the cells interpreted as the counterparts of class II cells in thin sections. The interpretation of such negative observations is problematic. In the extensive literature on interneurons in the LGd, several authors have discussed the possibility that some or all such cells are anaxonal (Le Vay 1971; Scheibel *et al.* 1972; Grossman *et al.* 1973; Shepherd 1979) but Golgi findings on such cells in at least some studies reveal very clear axons (for example, cat (Guillery 1966; Famiglietti & Peters 1972)) and initial segments of presynaptic dendrite-bearing cells in monkey LGd have been described by Hámori *et al.* (1978). Recently P. T. Ohara (personal communication) has identified a typical axon initial segment of an intracellularly recorded interneuron-like cell in rat LGd filled with HRP and subsequently analysed by e.m.

In the electron microscope, the differences between cells thought to correspond to class I cells and those thought to correspond to class II cells, were usually clear. The presumptive class II cell bodies were smaller, their perinuclear cytoplasm and their organelle content comparatively scanty, their nuclei less irregular in outline, more electron dense, and with more clumped heterochromatin masses, and most distinctive of all, was the presence in many cell bodies or in dendrites issuing from them, of clusters of pleomorphic synaptic vesicles, occasionally associated with efferent synaptic specializations. Furthermore, the dendrites and occasionally the perikarya of these cells gave rise to appendages, containing pleomorphic synaptic vesicles and both making and receiving synaptic contacts, which matched the complex dendritic appendages of class II cells in Golgi preparations. Thus, although based on indirect evidence the case for equating the class I and II cells of Golgi preparations with the class I and II cells of e.m. is a strong one, although there were no clear indications in the e.m. material for the subclasses of class II cells defined on the basis of Golgi material.

The question of whether class I cells are projection neurons and class II cells interneurons is altogether more difficult to answer. Clear cut anatomical differences between presumptive projection cells and presumptive interneurons, corresponding in almost every respect to the differences found in OPN, are also found in thalamic relay nuclei (see Jones 1981, 1983) where the results of chronic cortical lesions (including retrograde degeneration of projection cells) (for example, Pasik *et al.* 1973), retrograde labelling from the cortex of projection cells with HRP (Le Vay & Ferster 1979; Weber & Kalil 1983) and immunohistochemical evidence (for example, Ohara *et al.* 1983; Hendrickson *et al.* 1983; Spreafico *et al.* 1983; Penny *et al.* 1983) all point to the conclusion that the cells identified as interneurons do not in fact project to the cortex. Although this dichotomy has recently come under attack as a result of work on the cat, in which HRP-filled neurons that could be driven antidromically from visual cortex were found to include some with the morphology of Guillery's class III cells (Friedlander *et al.* 1981) the bulk of the evidence continues to favour the classical view of a dichotomy between projection cells with axons passing to the cerebral cortex and interneurons without cortically projecting axons, and it would seem reasonable to suppose that this basic pattern holds for the OPN as well and that class I cells are subcortically projecting neurons and class II cells local interneurons.

(*b*) *Synaptic organization*

(i) *Presynaptic elements*

P-boutons. P-boutons almost certainly account for more than the 18% of all presynaptic elements reported in §3*a*iic, since at least half of the profiles containing flattened synaptic vesicles which could not be classified with certainty, were likely to have been sections of P-boutons. Thus a figure of around 27% would probably be more realistic. The P-boutons of OPN are similar in all major respects to the P-boutons of rat LGd (Lieberman & Webster 1972, 1974; Lieberman 1973). Like the latter, they are irregular and variable in form, contain pleomorphic synaptic vesicles, cisterns and tubules of smooth endoplasmic reticulum and occasionally ribosome clusters, and arise from presynaptic dendritic shafts of small, commonly presynaptic cell bodies just as in rat LGd. They are similar also in the fine structure of the efferent synaptic contacts they establish, which are small, with prominent presynaptic densities and a postsynaptic density intermediate in thickness between that of typical Gray type 1 and type 2 contacts. Finally, their synaptic relationships are also similar, namely, they are presynaptic to presumptive projection cell dendrites and to other P-boutons, and postsynaptic (in decreasing order of frequency) to RP-, F-, P- and RD-profiles. Most of these features have also been noted for presynaptic dendrites and the bouton-like structures derived from them in the LGd and other thalamic relay nuclei in a variety of species (see Jones (1981) for review) and in other sites containing interneurons with presynaptic dendrites (for example, superior colliculus (Lund 1969; Valverde 1973; hypothalamus (Güldner 1976) and ventral lateral geniculate nucleus (LGv; Lieberman 1973; Stelzner *et al.* 1976)).

However, there were some minor differences between the P-boutons of OPN and similar structures in other sites: the frequency of synaptic contacts between two P-boutons was lower in OPN than in rat LGd (Lieberman 1973), and the non-synaptic membrane specializations between P-profiles and conventional dendritic elements described in the present study do not appear to have been described previously.

RP-terminals. RP-terminals comprise at least 36% of all presynaptic elements (probably closer to 45% after the likely provenance of unidentifiable profiles with spherical synaptic vesicles is taken into account) and are, or are predominantly, the terminals of retinal afferents. This study, in fact, provides the first clear identification at the electron microscope level of retinal terminals in the OPN of any species, although an earlier report by Repérant (1975), concerned chiefly with the technique of anterograde transport of HRP, illustrates HRP-labelled retinal profiles in the OPN of the albino rat (but without describing their fine structure in detail or the organization of OPN neuropil). More recently, Nakamura *et al.* (1981) have demonstrated retinal terminals labelled with radioactive amino acids and HRP in the nucleus of the optic tract of the cat, which resemble the RP-terminals of rat OPN, while a brief report by Spencer *et al.* (1983) describes similar boutons in the OPN and nucleus of the optic tract in the cat after intravitreal injection of peroxidase–lectin conjugate. RP-boutons resemble putative or identified retinal terminals in other retinoreceptive sites in the rat (LGd (Lieberman & Webster 1972, 1974); LGv (Stelzner *et al.* 1976); superior colliculus (Lund 1969); suprachiasmatic nucleus (Güldner 1976); and other species (cat LGd (Szentagothai *et al.* 1966; Guillery 1969; Robson & Mason 1979); monkey LGd (Colonnier & Guillery 1964; Wong-Riley 1972*b*); cat superior colliculus (Sterling 1971); monkey superior colliculus (Lund 1972; Tigges *et al.* 1973)). However, in many of these studies, as in the present study, not all RP- (or RP-like) terminals

were eliminated by optic nerve section. Since it is unlikely that the surviving RP terminals represent retinal axons from the intact eye (except perhaps in the region of and immediately adjacent to the area of ipsilateral termination), the possibility that some other afferent system to OPN has RP-like terminals must be considered.

The various changes in the fine structure of RP-boutons that were interpreted as signs of degeneration (namely, vesicle swelling and clumping, neurofilamentous hyperplasia, electron-lucent change, deposition of floccular material, electron-dense transformation of the terminal matrix, shrinkage and distortion of the terminal) are similar to degenerative changes reported in many other studies of retinal terminals (for example, Lund 1969; Sterling 1971; Wong-Riley 1972*b*; Lieberman & Webster 1974) and of other parts of the central nervous system (for example, Westrum 1969, 1974; Raisman & Matthews 1972). It was clear from our material that the earliest detectable changes were vesicle-swelling and neurofilamentous hyperplasia, that accumulation of electron-dense material followed later and was associated with shrinkage and distortion of the terminal, and that phagocytosis of degenerating terminals by glial cells is associated only with the dense stage of degeneration. We were, however, unable to ascertain the relationship between the swollen, electron-lucent degenerating boutons and other forms of terminal degeneration.

RD-terminals. The RD-terminals of rat OPN are similar to small boutons with spherical synaptic vesicles and dark mitochondria reported to be consistent components of the neuropil in thalamic nuclei and the superior colliculus. For example they resemble the SR-boutons of rat LGd (Lieberman & Webster 1974) the RSD-boutons of cat and monkey LGd (Guillery 1969; Guillery & Colonnier 1970; Robson 1983) and the R1 boutons of monkey superior colliculus (Tigges *et al.* 1973).

In many sites there is experimental evidence to suggest that boutons of this kind arise, at least in part, from the cerebral cortex. This is the case, for example, in the LGd (Szentágothai *et al.* 1966; Jones & Powell 1969*b*; Guillery 1971; Wong-Riley 1972*c*: Lieberman & Webster 1974; Robson 1983), the pulvinar (Ogren & Hendrickson 1979) the ventrobasal nucleus (Jones & Powell 1969*b*), and the superior colliculus (Lund 1969). However, although the existence of cortical input to OPN in the rat is claimed by Martin & Sefton (1981) and by Verbitskaya *et al.* (1977), in neither of these brief reports is the evidence presented compelling and in an extensive series of l.m. and e.m. studies, by using HRP-tracing and experimental degeneration techniques, no evidence was found for an input to OPN from either area 18 or area 17 by Campbell (1982). Nor is there visual cortical input to OPN in other species (rabbit (Giolli *et al.* 1978); cat (Updyke 1977); opossum (Linden & Rocha-Miranda 1981); monkey (Graham *et al.* 1979)), although recent studies by Dineen & Hendrickson (1983) suggest that the OPN of the monkey receives a direct input from the prestriate cortex.

On the other hand, OPN is known to receive input from the superior colliculus in the rat (Perry 1980), rabbit (Holstege & Collewijn 1982), cat (Graham 1977) and monkey (Benevento *et al.* 1977) and these facts suggest that a likely source of RD-terminals in OPN is the superior colliculus. Indeed, we have found, and will be reporting in detail elsewhere, that after injection of HRP into the superior colliculus, labelled terminals in OPN are of the RD-type (Lieberman *et al.* 1985) a finding that accords well with other studies showing that terminals originating from neurons in the superior colliculus are, or are predominantly of this type (pulvinar (Robson & Hall 1977); LGd (Robson & Hall 1977; Torrealba *et al.* 1981; A. R. Lieberman and A. M. Taylor, unpublished); LGv (Taylor & Lieberman 1985)). However, the superior

colliculus may not be the sole source of such terminals, for OPN also receives an input from the LGv in the rat and cat (Swanson *et al.* 1974; Ribak & Peters 1975) and in the monkey (Hendrickson 1973), and there is experimental evidence that, in the rat, some RD-terminals in OPN arise in the LGv (Campbell 1982).

The RD-boutons of OPN in the rat make Gray type 1 synaptic contacts with D-profiles and to a lesser extent with P-profiles. The latter relationship is worthy of special note for contacts between RD-like terminals and P-boutons or presynaptic dendrites are reported to be rare or absent in many sites, including mouse and rat LGd (Lieberman 1973; Lieberman & Webster 1974), cat LGd (Guillery 1969; Famiglietti & Peters 1972), monkey pulvinar (Ogren & Hendrickson 1979), rabbit LGv (Matthews & Mascetti 1975) and rat superior colliculus (Lund 1969; Lund & Lund 1971), but to be present or even relatively common in other sites, including monkey LGd (Guillery & Colonnier 1970; Wong-Riley 1972*c*) cat ventrobasal nucleus (Ralston & Herman 1969), and cat and monkey superior colliculus (Sterling 1971; Tigges *et al.* 1973). Whether these reported differences reflect different sampling strategies or different criteria for axon terminal identification, or genuine site and species differences remain to be clarified.

F-terminals. Although profiles of F-boutons were sometimes difficult to distinguish from P-profiles, hence the relatively large proportion (12%) of unidentified elements containing flattened vesicles (UF), it was clear that the synaptic vesicles of F-boutons were flatter and more densely packed than those in P-boutons as was previously found to be the case for F- and P-boutons in LGd (Lieberman & Webster 1972, 1974).

The origin of F-boutons in OPN is unknown. One possibility is that they represent the axon terminals of class II cells, at least some of which appear to give rise to axons (see §3*a*ib) although the origins of such axons were not identified by e.m. Such a supposition would be in line with a widespread belief about the origin of F-terminals (F1 axons in the terminology of Guillery (1969)) in dorsal thalamic nuclei; indeed some authors have suggested that all such terminals in thalamic nuclei arise from the axons of local interneurons (Morest 1971, 1975; Famiglietti & Peters 1972). There is, however, no direct evidence to support this view either for the OPN or for dorsal thalamic nuclei and in view of the fact that an extrinsic origin for a subpopulation of F-terminals in dorsal thalamic nuclei, from the thalamic reticular nucleus, has now been established (Ohara *et al.* 1980; Montero & Scott 1981), the possibility that F-terminals in OPN have an extrinsic origin should be considered. This possibility is perhaps strengthened by the fact that F-boutons in OPN were occasionally observed to arise from myelinated fibres. But what the extrinsic source or sources of F-terminals may be is unclear, although we can say that they are unlikely to arise from the thalamic reticular nucleus for there appears to be no evidence for an input to OPN from this nucleus in the rat (Campbell 1982).

Whatever their origin, or origins, it seems likely that the synaptic contacts established by F-boutons are inhibitory (see §4*b*ii) and if so, the F-boutons may be involved with mechanisms inhibiting the pupilloconstrictor pathway (for a review see Brodal 1981).

(ii) *Triplet synapses*

The triplet synapse is a repetitive structural motif of the complex glomerular neuropil of OPN, as it is in many thalamic relay nuclei, where the intermediate (duplex) component of the triplet is also a P-bouton or a P-bouton-like dendritic structure derived from an interneuron, or some other part of the interneuron (for example, rat LGd (Lieberman & Webster 1972, 1974); cat

LGd (Famiglietti & Peters 1972; Rapisardi & Miles 1984); monkey (Hámori *et al.* 1974; Wong-Riley 1972*b*); cat ventrobasal nucleus (Ralston 1971)). In a further close parallel with thalamic nuclei, the 'input' elements to triplet synapses in OPN are predominantly retinal terminals, and the 'output' elements are predominantly or exclusively projection cell dendrites, as is the case for the triplet synapses in the LGd in various species (Famiglietti & Peters 1972; Lieberman & Webster 1972, 1974; Hámori *et al.* 1974), and in other thalamic nuclei (Jones 1981, 1983).

The role or roles of triplet synapses in the functional organization of OPN is obscure and the available physiological data are unenlightening. It is, however, very probable, that triplet synapses in OPN function in much the same way as their counterparts in dorsal thalamic nuclei. This assumption is supported not only by the evident anatomical similarities between interneuron-like cells, their dendrites and their dendritic appendages in OPN and in thalamic nuclei, but also by immunohistochemical evidence showing that, in OPN, such cells contain glutamic acid decarboxylase (GAD), the synthetic enzyme for GABA, and GABA itself (mouse and rat (Campbell *et al.* 1984; Ottersen & Storm-Mathisen 1984*b*)) as is the case in the LGd; (mouse (Ottersen & Storm-Mathisen 1984*a*); rat (Ohara *et al.* 1983); monkey (Hendrickson *et al.* 1983)) and in other thalamic nuclei (cat VB (Spreafico *et al.* 1983; Penny *et al.* 1983)). Additional pharmacological, physiological and anatomical evidence (see, for example, Sterling & Davis 1980; Mize *et al.* 1981; Houser *et al.* 1983) clearly establishes that such cells in thalamic nuclei and in superior colliculus are inhibitory (GABAergic) interneurons (although the interneuronal status of these cells is currently under discussion; see §4*a*ii), and the flattened synaptic vesicles and relatively narrow postsynaptic densities associated with the synaptic specializations made by these cells are in keeping with these data. Thus it may be that the triplet synapses are concerned with feed forward inhibition of projection cells in OPN, the inhibition being mediated by the retinally excited intrinsic interneurons as seems to be the case in the thalamus (Singer *et al.* 1972; Dubin & Cleland 1977; Lindström 1982). Such a model for the role of the triplet synapse fits with most of the available electrophysiological and anatomical evidence but is for the moment largely conjectural, and other suggestions for the role of the triplet synapse have been made (Colonnier 1974; Labos 1975; Jones 1981).

(*c*) *Synaptic readjustment after deafferentation*

The presence, following eye removal, of thick postsynaptic densities resembling those of Gray type 1 synapses at synaptic contacts established by F- or P-boutons (which are normally associated with thinner postsynaptic densities), suggests that some synaptic readjustment takes place in deafferented OPN. It would seem likely that such atypical synaptic specializations were formed by F- or P-boutons replacing a retinal bouton lost by degeneration. RP-boutons and RD-boutons may also be involved in such reoccupation but this would be impossible to detect as these two types of bouton normally establish Gray type 1 synapses. Similar observations have been made in several other studies of c.n.s. areas deprived of their major afferent input, for example in the cat spinal trigeminal nucleus (Westrum & Black 1971); the cat ventral cochlear nucleus (Gentschev & Sotelo 1973); and the rat superior colliculus (Lund & Lund 1971; Houser *et al.* 1983). Most pertinent are the recent studies of Houser *et al.* (1983), who used GAD-immunocytochemistry and e.m., in which reoccupation of Gray type 1 postsynaptic thickenings by GABAergic terminals was observed. Thus both in the superior colliculus and in the OPN (where GAD-immunocytochemistry in normal material has shown that P- and

F-boutons are probably both GABAergic (Campbell *et al.* 1984)), it appears that axon terminals that normally have excitatory effects on the cells they innervate, may be replaced by potentially inhibitory presynaptic endings, which give every indication, according to structural and histochemical criteria, of being functional, although whether or not appropriate postsynaptic receptors are present to mediate the effects of released GABA is unknown.

(*d*) *OPN efferents to the Edinger–Westphal region*

The large number of labelled fibres coursing from OPN to the periaqueductal grey and to the Edinger–Westphal region after intravitreal injections of [^{3}H]fucose–[^{3}H]proline mixture strongly indicates that radioactive material is transneuronally transported from retinal terminals to OPN projection neurons. This interpretation is supported by labelling, in the same brains, of areas known to receive second order retinal projections, notably the visual cortex, parabigeminal nucleus and thalamic reticular nucleus. In HRP-eye-injection experiments on adult rats, similar fibres could not be traced from OPN to the Edinger–Westphal nucleus, in keeping with evidence that free HRP (that is, non-lectin-conjugated HRP) is rarely transported transneuronally (Mesulam 1982), although a faint patch of label at the ventromedial border of OPN, containing fibres oriented like those displaying transneuronal radioactive labelling, was consistently seen. (These fibres could never be traced beyond the immediate vicinity of the OPN and we were unable to determine whether or not the label represented transneuronal HRP transport.) In neonatal rats with intravitreal injections of HRP, however, HRP-labelled fibres, probably transneuronally labelled, could be traced as far as the posterior commissure (Campbell 1982). Furthermore, Itaya & Van Hoesen (1982), by using lectin (WGA)–HRP conjugates, which are transneuronally transported to some extent at least, have reported findings very similar to ours with respect to the existence of a pathway between the OPN and the ipsilateral Edinger–Westphal nucleus in the adult rat. Because neither our findings nor those of Itaya & Van Hoesen (1982) provide evidence for a crossed component in the projection from OPN to the Edinger–Westphal nucleus (compare with data for monkey and pigeon reviewed by Gamlin *et al.* (1984)), the pathway for the consensual reflex (which is well developed in the rat (Clarke & Ikeda 1981) must depend on fibre crossing at some other level in the pathway or on the presence of bilateral retinal input to each OPN, or both. These findings with the transneuronal transport methods add to the previous evidence for a direct pathway between OPN and the Edinger–Westphal region (monkey (Pierson & Carpenter 1974; Benevento *et al.* 1977; Steiger & Büttner-Ennever 1979); cat (Breen *et al.* 1983); and see Gamlin *et al.* (1984) for pigeon) thus further strengthening the evidence for involvement of the OPN in the pupillary light reflex. Recently, the existence of a direct projection from OPN to the Edinger–Westphal nucleus in the monkey has been questioned by Tokunaga *et al.* (1981) who failed to detect transneuronal label in the Edinger–Westphal region after intravitreal injection of [^{3}H]fucose–[^{3}H]proline. These authors interpret this surprising failure as reflecting the possible existence of multisynaptic local circuitry intercalated between retinal terminals and OPN projection neurons in the monkey OPN. However, since there is good, albeit indirect, evidence for monosynaptic innervation of projection neurons in the OPN, as is the case in other retinorecipient centres (see, for example, Lund 1972; Wong-Riley 1972*b*; Lieberman & Webster 1974), this seems a somewhat unlikely interpretation. Furthermore, there is electrophysiological evidence that only a single synaptic interposition is present at the level of the pretectum in the pupilloconstrictor pathway of the cat (Hultborn *et al.* 1978).

(*e*) *Concluding remarks*

This study has provided the only detailed account of which we are aware, of the cellular and synaptic organization of a pretectal nucleus in any mammal. We have shown that the neurons of OPN fall into two main categories, larger presumptive projection cells, some of which appear to send axons to the ipsilateral Edinger–Westphal nucleus, and smaller cells with presynaptic cell bodies, dendrites and dendritic appendages, which are presumptive inhibitory (GABAergic) interneurons, and that both cell types are directly (monosynaptically) innervated from the retina in areas of glomerular neuropil in which complex serial synapses and triplet (triadic) synapses are found. These findings provide anatomical correlates for many of the physiological findings reported in recent studies (Hultborn *et al.* 1978; Clarke & Ikeda 1981; Trejo & Cicerone 1984), and strengthen the evidence for the importance of the OPN in the pathway for the pupillary light reflex.

It has recently been suggested that the OPN relays luminance information virtually unchanged (Inoue 1980). This seems to us unlikely. The existence of various non-retinal inputs to the OPN (especially from the superior colliculus and the LGv), the presence of inhibitory interneurons and the general anatomical complexity of the OPN neuropil, which is comparable to that of the LGd and other dorsal thalamic nuclei, suggest that subtle and possibly important processing and modification of luminance information occur within this nucleus. Physiological studies designed to test this possibility are needed.

We are grateful to the Wellcome Trust for partial financial support, to Dr Derek Pegg who participated in the preparation and analysis of the Golgi material and drew figures 5 and 6, to Dr Peter Ohara for help during the early stages of this work, to Albert Meier and Bjarne Krunderup for photographic help, to Karin Wiedemann for help with the drawings and to Shihan Jayasuriya and Susanne Thomsen for secretarial assistance.

References

Adams, J. C. 1977 Technical considerations on the use of horseradish peroxidase as a neuronal marker. *Neuroscience* **2**, 141–145.

Benevento, C. A., Rezak, M. & Santos-Anderson, R. 1977 An autoradiographic study of the projections of the pretectum in the rhesus monkey (*Macaca mulatta*): evidence for sensorimotor links to the thalamus and oculomotor nuclei. *Brain Res.* **127**, 197–218.

Berman, N. 1977 Connections of the pretectum in the cat. *J. comp. Neurol.* **174**, 227–254.

Breen, L. A., Burke, R. M. & Loewy, A. D. 1983 Brainstem connections to the Edinger–Westphal nucleus of the cat: a retrograde tracer study. *Brain Res.* **261**, 303–306.

Brodal, A. 1981 *Neurological anatomy in relation to clinical medicine.* 3rd ed. Oxford University Press.

Campbell, G. 1982 Anatomical studies of the rat pretectum, with special reference to the cellular and synaptic organisation of the olivary pretectal nucleus. Ph.D. Thesis, University of London.

Campbell, G., Hunt, S. P., Lieberman, A. R., Ohara, P. T., Ottersen, O. P., Storm-Mathisen, J. & Wu, J.-Y. 1984 Immunohistochemical identification of GAD- and GABA-containing neurons in the olivary pretectal nucleus (OPN) of rat and mouse. *J. Physiol., Lond.* **353**, 45*P*.

Campbell, G. & Lieberman, A. R. 1979 Presynaptic dendrites in the olivary pretectal nucleus of the albino rat. *J. Anat.* **129**, 863–866. (Abstract.)

Campbell, G. & Lieberman, A. R. 1980 Synaptic relationships and forms of terminal degeneration of retinal afferents to the olivary pretectal nucleus of the rat. *J. Anat.* **130**, 645–646. (Abstract.)

Campbell, G. & Lieberman, A. R. 1982 Synaptic organisation in the olivary pretectal nucleus of the adult rat. *Neurosci. Lett.* **28**, 151–155.

Carpenter, M. B. & Pierson, R. J. 1973 Pretectal region and the pupillary light reflex. An anatomical analysis in the monkey. *J. comp. Neurol.* **149**, 271–300.

Clarke, R. J. & Ikeda, H. 1981 Pupillary response and luminance and darkness detector neurones in the pretectum of the rat. In *Doc. Ophthal. Proc. Series* (ed. by L. Maffei), vol. 3, pp. 53–61. The Hague: Dr W. Junk Publishers.

Collewijn, H. 1975 Direction-selective units in the rabbit's nucleus of the optic tract. *Brain Res.* **100**, 489–508.

Colman, D. R., Scalia, F. & Cabrales, E. 1976 Light and electron microscopic observations on the anterograde transport of horseradish peroxidase in the optic pathway in the mouse and rat. *Brain Res.* **102**, 156–163.

Colonnier, M. 1974 Spatial interrelationships as physiological mechanisms in the central nervous system. In *Essays on the nervous system: a Festschrift for Professor J. Z. Young*, (ed. R. Bellairs & E. G. Gray), pp. 344–366. Oxford: Clarendon Press.

Colonnier, M. & Guillery, R. W. 1964 Synaptic organization in the lateral geniculate nucleus of the monkey. *Z. Zellforsch. mikrosk. Anat.* **62**, 333–355.

Cowan, W. M., Gottlieb, D. I., Hendrickson, A. E., Price, J. L. & Woolsey, T. A. 1972 The autoradiographic demonstration of axonal connections in the central nervous system. *Brain Res.* **37**, 21–51.

Dennison, M. E. 1971 Electron stereoscopy as a means of classifying synaptic vesicles. *J. Cell Sci.* **8**, 525–539.

Dineen, J. T. & Hendrickson, A. 1983 Overlap of retinal and prestriate cortical pathways in the primate pretectum. *Brain Res.* **278**, 250–254.

Dubin, M. W. & Cleland, B. G. 1977 Organisation of the visual inputs to interneurons of lateral geniculate nucleus of the cat. *J. Neurophysiol.* **40**, 410–427.

Famiglietti, E. V., Jr, & Peters, A. 1972 The synaptic glomerulus and the intrinsic neuron in the dorsal lateral geniculate nucleus of the cat. *J. comp. Neurol.* **144**, 285–334.

Friedlander, M. J., Lin, C.-S., Stanford, L. R. & Sherman, S. M. 1981 Morphology of functionally identified neurons in lateral geniculate nucleus of the cat. *J. Neurophysiol.* **46**, 80–129.

Fuse, G. 1916 Uber das germundene Graw in vorderen Zweihügel, den Nucleis olivaris. Corp. quadrigemini anterioris beim Meuschen. *Arbeiten ans dem Hirnanatomischen institut in Zürich.* Heft **X**, 96–112.

Fuse, G. 1936 Das gerundene Graw order der Olivenkern des vooderan Zweihügels, Nucleus olivaris corporis quadrigemini anterioris, bei Meusch und Tier. *Arbeiten ans dem anatomischen Institut der Kaiserlich-Japanischen Universität zer Sendai.* Heft **XIX**, 49–486.

Gamlin, P. D. R., Reiner, A., Erichsen, J. T., Karten, H. J. & Cohen, D. H. 1984 The neural substrate for the pupillary light reflex in the pigeon (*Columba livia*). *J. comp. Neurol.* **226**, 523–543.

Gentschev, T. & Sotelo, C. 1973 Degenerative patterns in the ventral cochlear nucleus of the rat after primary deafferentation. An ultrastructural study. *Brain Res.* **62**, 37–60.

Giolli, R. A. & Guthrie, M. D. 1971 Organisation of subcortical projections of visual areas I & II in the rabbit. An experimental degeneration study. *J. comp. Neurol.* **143**, 351–376.

Giolli, R. A., Towns, L. C., Takahashi, T. T., Karamanlidis, A. N. & Williams, D. D. 1978 An autoradiographic study of the projections of visual cortical area 1 to the thalamus, pretectum and superior colliculus of the rabbit. *J. comp. Neurol.* **180**, 743–752.

Grafstein, B. 1971 Transneuronal transfer of radioactivity in the central nervous system. *Science, Wash.* **172**, 177–179.

Graham, J. 1977 An autoradiographic study of the efferent connections of the superior colliculus in the cat. *J. comp. Neurol.* **173**, 629–654.

Graham, J., Lin, C.-S. & Kaas, J. H. 1979 Subcortical projections of six visual cortical areas in the owl monkey, *Aotus trivirgatus*. *J. comp. Neurol.* **187**, 557–580.

Graham, R. C., Jr. & Karnovsky, M. J. 1966 The early stages of absorption of injected horseradish peroxidase in the proximal tubules of mouse kidney: ultrastructural cytochemistry by a new technique. *J. Histochem. Cytochem.* **14**, 291–302.

Graybiel, A. M. & Berson, D. M. 1980 Autoradiographic evidence for a projection from the pretectal nucleus of the optic tract to the dorsal lateral geniculate nucleus in the cat. *Brain Res.* **195**, 1–12.

Graybiel, A. M. & Hartwieg, E. A. 1974 Some afferent connections of the oculomotor complex in the cat: an experimental study with tracer techniques. *Brain Res.* **81**, 543–551.

Grossman, A., Lieberman, A. R. & Webster, K. E. 1973 A Golgi study of the rat dorsal lateral geniculate nucleus. *J. comp. Neurol.* **150**, 441–466.

Guillery, R. W. 1966 A study of Golgi preparations from the dorsal lateral geniculate nucleus of the adult cat. *J. comp. Neurol.* **128**, 21–50.

Guillery, R. W. 1969 The organization of synaptic interconnections in the laminae of the dorsal lateral geniculate nucleus of the cat. *Z. Zellforsch. mikrosk. Anat.* **96**, 1–38.

Guillery, R. W. 1971 Patterns of synaptic interconnections in the dorsal lateral geniculate nucleus of cat and monkey: a brief review. *Vision Res.* suppl. no. 3, 211–227.

Guillery, R. W. & Colonnier, M. 1970 Synaptic patterns in the dorsal lateral geniculate nucleus of the monkey. *Z. Zellforsch. mikrosk. Anat.* **103**, 90–108.

Güldner, F.-H. 1976 Synaptology of the rat suprachiasmatic nucleus. *Cell Tiss. Res.* **165**, 509–544.

Hámori, J., Pasik, T., Pasik, P. & Szentágothai, J. 1974 Triadic synaptic arrangements and their possible significance in the lateral geniculate nucleus of the monkey. *Brain Res.* **80**, 379–393.

Hámori, J., Pasik, T. & Pasik, P. 1978 Electron-microscopic identification of axonal initial segments belonging to interneurons in the dorsal lateral geniculate nucleus of the monkey. *Neuroscience* **3**, 403–412.

Hendrickson, A. 1973 The pregeniculate nucleus of the monkey. *Anat. Rec.* **175**, 341. (Abstract.)

Hendrickson, A. E., Ogren, M. P., Vaughn, J. E., Barber, R. P. & Wu, J.-Y. 1983 Light and electron microscopic immunocytochemical localisation of glutamic acid decarboxylase in monkey geniculate complex: evidence for GABAergic neurons and synapses. *J. Neurosci.* **3**, 1245–1262.

Hendrickson, A., Wilson, M. E. & Toyne, M. J. 1970 The distribution of optic nerve fibres in *Macaca mulatta*. *Brain Res.* **23**, 425–427.

Hickey, T. L. & Guillery, R. W. 1981 A study of Golgi preparations from the human lateral geniculate nucleus. *J. comp. Neurol.* **200**, 545–577.

Hoffmann, K.-P., Ballas, I. & Wagner, H.-J. 1984 Double labelling of retinofugal projections in the cat. A study using anterograde transport of ^{3}[H]proline and horseradish peroxidase. *Expl Brain Res.* **53**, 420–430.

Holstege, G. & Collewijn, H. 1982 The efferent connections of the nucleus of the optic tract and the superior colliculus in the rabbit. *J. comp. Neurol.* **209**, 139–175.

Houser, C. R., Lee, M. & Vaughn, J. E. 1983 Immunocytochemical localization of glutamic acid decarboxylase in normal and deafferented superior colliculus: evidence for reorganization of γ-aminobutyric acid synapses. *J. Neurosci.* **3**, 2030–2042.

Hultborn, H., Mori, K. & Tsukahara, N. 1978 The neuronal pathway subserving the pupillary light reflex. *Brain Res.* **159**, 255–267.

Inoue, T. 1980 The response of rabbit ciliary nerve to luminance intensity. *Brain Res.* **201**, 206–209.

Itaya, S. K. & Van Hoesen, G. H. 1982 WGA-HRP as a transneuronal marker in the visual pathways of monkey and rat. *Brain Res.* **236**, 199–204.

Itoh, K. 1977 Efferent projections of the pretectum in the cat. *Expl Brain Res.* **30**, 89–105.

Itoh, K., Takada, M., Yasui, Y. & Mizuno, N. 1983 A pretectofacial projection in the cat: a possible link in the visually-triggered blink reflex pathways. *Brain Res.* **274**, 332–335.

Iwahori, N., Uchuda, K. & Mizuno, N. 1981 The dorsal lateral geniculate nucleus in the mouse: A Golgi study. *Neurosci. Lett.* suppl. 6, 112. (Abstract.)

Jones, E. G. 1981 Functional subdivisions and synaptic organization of the mammalian thalamus. In *Neurophysiology IV. International Review of Physiology* (ed. R. Porter), vol. 25, pp. 173–245. Baltimore: University Park Press.

Jones, E. G. 1983 The thalamus: In *Chemical neuroanatomy* (ed. P. C. Emson), pp. 257–293. New York: Raven Press.

Jones, E. G. & Powell, T. P. S. 1969*a* Electron microscopy of synaptic glomeruli in the thalamic relay nuclei of the cat. *Proc. R. Soc. Lond.* B **172**, 153–171.

Jones, E. G. & Powell, T. P. S. 1969*b* An electron microscopic study of the mode of termination of cortico-thalamic fibres within the sensory relay nuclei of the thalamus. *Proc. R. Soc. Lond.* B **172**, 173–185.

Kanaseki, T. & Sprague, J. M. 1974 Anatomical organization of pretectal nuclei and tectal laminae in the cat. *J. comp. Neurol.* **158**, 319–338.

Karnovsky, M. J. 1965 A formaldehyde-glutaraldehyde fixative of high osmolality for use in electron microscopy. *J. Cell Biol.* **27**, 137A. (Abstract.)

Lábos, E. 1975 Enhancement of integrative capacities by coupling synaptic triads in lateral geniculate body. *Expl Brain Res.*, suppl. 1, 116. (Abstract.)

Laemle, L. K. 1981 A Golgi study of cellular morphology in the superficial layers of superior colliculus of man, *Saimiri* and *Macaca*. *J. Hirnforsch.* **22**, 253–263.

Langer, T. P. & Lund, R. D. 1974 The upper layers of the superior colliculus of the rat: A Golgi study. *J. comp. Neurol.* **158**, 405–436.

LaVail, J. H. & LaVail, M. M. 1974 The retrograde intraaxonal transport of horseradish peroxidase in the chick visual system: a light and electron microscopic study. *J. comp. Neurol.* **157**, 303–358.

Le Vay, S. 1971 On the neurons and synapses of the lateral geniculate nucleus of the monkey, and the effects of eye enucleation. *Z. Zellforsch. mikrosk. Anat.* **113**, 396–419.

Le Vay, S. & Ferster, D. 1977 Relay cell classes in the lateral geniculate nucleus of the cat and the effects of visual deprivation. *J. comp. Neurol.* **172**, 563–584.

Le Vay, S. & Ferster, D. 1979 Proportion of interneurons in the cat's lateral geniculate nucleus. *Brain Res.* **164**, 304–308.

Lieberman, A. R. 1973 Neurons with presynaptic perikarya and presynaptic dendrites in the rat lateral geniculate nucleus. *Brain Res.* **59**, 35–59.

Lieberman, A. R. & Webster, K. E. 1972 Presynaptic dendrites and a distinctive class of synaptic vesicle in the rat dorsal lateral geniculate nucleus. *Brain Res.* **42**, 196–200.

Lieberman, A. R. & Webster, K. E. 1974 Aspects of the synaptic organization of intrinsic neurons in the dorsal lateral geniculate nucleus. An ultrastructural study of the normal and of the experimentally deafferented nucleus in the rat. *J. Neurocytol.* **3**, 677–710.

Lieberman, A. R., Taylor, A. M. & Campbell, G. 1985 Axon terminals of the projection from the superior colliculus to the olivary pretectal nucleus in the rat. *Neurosci. Lett.* **56**, 235–239.

Linden, R. & Rocha-Miranda, C. E. 1981 The pretectal complex in the opossum: projections from the striate cortex and correlation with retinal terminal fields. *Brain Res.* **207**, 267–277.

Lindström, S. 1982 Synaptic organisation of inhibitory pathways to principal cells in the lateral geniculate nucleus of the cat. *Brain Res.* **234**, 447–453.

Lindvall, O., Bjorklund, A., Nobin, A. & Stenevi, A. 1974 The adrenergic innervation of the rat thalamus as revealed by the glyoxylic acid fluorescence method. *J. comp. Neurol.* **154**, 317–348.

Ljungdahl, A., Hokfelt, T. & Nilsson, G. 1978 Distribution of substance P-like immunoreactivity in the central nervous system of the rat. 1. Cell bodies and nerve terminals. *Neuroscience* **3**, 861–943.

Loewy, A. D. 1979 Neural regulation of the pupil. In *Integrative functions of the autonomic nervous system.* (ed. C. McC. Brooks, K. Koizumi & A. Sato), pp. 131–141. Tokyo: University of Tokyo Press/Elsevier.

Lund, R. D. 1969 Synaptic patterns in the superficial layers of the superior colliculus of the rat. *J. comp. Neurol.* **135**, 179–208.

Lund, R. D. 1972 Synaptic patterns in the superficial layers of the superior colliculus of the monkey, *Macaca mulatta*. *Expl Brain Res.* **15**, 194–211.

Lund, R. D. & Lund, J. S. 1971 Modifications of synaptic patterns in the superior colliculus of the rat during development and following deafferentation. *Vision Res.*, suppl. 3, 281–298.

Martin, P. R. & Sefton, A. J. 1981 Visual projections to pretectal nuclei of the rat. *Proc. Aust. Physiol. Pharmacol. Soc.* **12**, 98*P*.

Mathers, L. H. & Mascetti, G. G. 1975 Electrophysiological and morphological properties of neurons in the ventral lateral geniculate nucleus of the rabbit. *Expl Neurol.* **46**, 506–520.

Mesulam, M.-M. 1978 Tetramethyl benzidine for horseradish peroxidase neurohistochemistry: A non-carcinogenic blue reaction product with superior sensitivity for visualizing neural afferents and efferents. *J. Histochem. Cytochem.* **26**, 106–117.

Mesulam, M.-M. 1982 Principles of horseradish peroxidase neurohistochemistry and their application for tracing neural pathways – axonal transport, enzyme histochemistry and light microscopic analysis. In *Tracing neural connections with horseradish peroxidase* (ed. M.-M. Mesulam), pp. 1–51. New York: John Wiley and Sons.

Mize, R. R., Spencer, R. F. & Sterling, P. 1981 Neurons and glia in cat superior colliculus accumulate [^{3}H]gamma-aminobutyric acid (GABA). *J. comp. Neurol.* **202**, 385–396.

Montero, V. M. & Scott, G. L. 1981 Synaptic terminals in the dorsal lateral geniculate nucleus from neurons of the thalamic reticular nucleus. A light and electron microscope autoradiographic study. *Neuroscience* **6**, 2561–2577.

Morest, D. K. 1971 Dendro-dendritic synapses of cells that have axons: the fine structure of the Golgi type II cell in the medial geniculate body of the cat. *Z. Anat. EntwGesch.* **133**, 216–246.

Morest, D. K. 1975 Synaptic relationships of Golgi type II cells in the medial geniculate body of the cat. *J. comp. Neurol.* **162**, 157–194.

Nakamura, Y., Mizuno, N. & Konishi, A. 1981 Electron microscope identification of axon terminals of retinopretectal fibres in the cat by a combined horseradish peroxidase and tritiated amino acids tracing method. *Brain Res.* **212**, 127–130.

Nauta, W. J. H. & Van Straaten, J. J. 1947 The primary optic centres of the rat. An experimental study by the 'bouton' method. *J. Anat.* **81**, 127–134.

Ogren, M. P. & Hendrickson, A. E. 1979 The morphology and distribution of striate cortex terminals in the inferior and lateral subdivisions of the Macaca monkey pulvinar. *J. comp. Neurol.* **188**, 179–200.

Ohara, P. T., Lieberman, A. R., Hunt, S. P. & Wu, J.-Y. 1983 Neural elements containing glutamic acid decarboxylase (GAD) in the dorsal lateral geniculate nucleus of the rat; immunohistochemical studies by light and electron microscopy. *Neuroscience* **8**, 189–211.

Ohara, P. T., Sefton, A. J. & Lieberman, A. R. 1980 Mode of termination of afferents from the thalamic reticular nucleus in the dorsal lateral geniculate nucleus of the rat. *Brain Res.* **197**, 503–506.

Ottersen, O. P. & Storm-Mathisen, J. 1984*a* Neurones containing or accumulating transmitter amino acids. In *Handbook of chemical neuroanatomy* (ed. A. Björklund, T. Hökfelt & M. J. Kuhar), vol. 2. (in the press.)

Ottersen, O. P. & Storm-Mathisen, J. 1984*b* GABA-containing neurons in the thalamus and pretectum of the rodent: an immunocytochemical study. *Anat. Embryol.* **170**, 197–207.

Parent, A., Descarries, L. & Beaudet, A. 1981 Organization of ascending serotonin systems in the adult rat brain. A radioautographic study after intraventricular administration of [^{3}H]5-Hydroxytryptamine. *Neuroscience* **6**, 115–138.

Pasik, P., Pasik, T., Hámori, J. & Szentágothai, J. 1973 Golgi Type II interneurons in the neuronal circuit of the monkey lateral geniculate nucleus. *Expl Brain Res.* **17**, 18–34.

Pease, D. C. 1964 *Histological techniques for electron microscopy.* 2nd ed. New York: Academic Press.

Pegg, D. J., Campbell, G. & Lieberman, A. R. 1982 A Golgi study of neurons in the olivary pretectal nucleus (OPN) of the adult rat. *J. Anat.* **135**, 813–815. (Abstract.)

Penny, G. R., Fitzpatrick, D., Schmechel, D. E. & Diamond, I. T. 1983 Glutamic acid decarboxylase-immunoreactive neurons and horseradish peroxidase-labelled projection neurons in the ventral posterior nucleus of the cat and *Galago senegalensis*. *J. Neurosci.* **3**, 1868–1887.

Perry, V. H. 1980 A tectocortical visual pathway in the rat. *Neuroscience* **5**, 915–927.

Perry, V. H. & Cowey, A. 1979 Changes in the retino-fugal pathways following cortical and tectal lesions in neonatal and adult rats. *Expl Brain Res.* **35**, 97–108.

Peters, A. & Palay, S. L. 1966 The morphology of laminae A and A_1 of the dorsal nucleus of the lateral geniculate body of the cat. *J. Anat.* **100**, 451–486.

Peters, A., Palay, S. L. & Webster, H. deF. 1976 *The fine structure of the nervous system: the neurons and supporting cells.* Philadelphia: W. B. Saunders Company.

Pierson, R. J. & Carpenter, M. B. 1974 Anatomical analysis of pupillary reflex pathways in the rhesus monkey. *J. comp. Neurol.* **158**, 121–144.

Rafols, J. A. & Valverde, F. 1973 The structure of the dorsal lateral geniculate nucleus in the mouse. A Golgi and electron microscopic study. *J. comp. Neurol.* **150**, 303–332.

Raisman, G. & Matthews, M. R. 1972 Degeneration and regeneration of synapses. In *The structure and function of nervous tissue* (ed. G. H. Bourne), vol. IV, pp. 61–105. New York and London: Academic Press.

Ralston, H. J. III 1971 Evidence for presynaptic dendrites and a proposal for their mechanism of action. *Nature, Lond.* **230**, 585–587.

Ralston, H. J., III & Herman, M. M. 1969 The fine structure of neurons and synapses in the ventrobasal thalamus of the cat. *Brain Res.* **14**, 77–97.

Rapisardi, S. C. & Miles, T. P. 1984 Synaptology of retinal terminals in the dorsal lateral geniculate nucleus of the cat. *J. comp. Neurol.* **223**, 515–534.

Repérant, J. 1975 The orthograde transport of horseradish peroxidase in the visual system. *Brain Res.* **85**, 307–312.

Reynolds, E. S. 1963 The use of lead citrate at high pH as an electron-opaque stain in electron microscopy. *J. Cell Biol.* **17**, 208–212.

Ribak, C. E. & Peters, A. 1975 An autoradiographic study of projections from the lateral geniculate body of the rat. *Brain Res.* **92**, 341–368.

Robson, J. A. 1983 The morphology of corticofugal axons to the dorsal lateral geniculate nucleus in the cat. *J. comp. Neurol.* **216**, 89–103.

Robson, J. A. & Hall, W. C. 1977 The organization of the pulvinar in the grey squirrel (*Sciurus carolinensis*). II. Synaptic organization and comparisons with the dorsal lateral geniculate nucleus. *J. comp. Neurol.* **173**, 389–416.

Robson, J. A. & Mason, C. A. 1979 The synaptic organization of terminals traced from individual labelled retino-geniculate axons in the cat. *Neuroscience* **4**, 99–111.

Rosenbluth, J. 1962 Subsurface cisterns and their relationship to the neuronal plasma membrane. *J. Cell Biol.* **13**, 405–421.

Saini, K. D. & Garey, L. J. 1981 Morphology of neurons in the lateral geniculate nucleus of the monkey. A Golgi study. *Expl Brain Res.* **42**, 235–248.

Santos-Anderson, R., Rezak, M. & Benevento, L. A. 1976 An autoradiographic study of the projections of the pretectum in Macaque monkey. *Neurosci. Abs.* **2**, 1091.

Scalia, F. 1972 The termination of retinal axons in the pretectal region of mammals. *J. comp. Neurol.* **145**, 223–253.

Scalia, F. & Arango, V. 1979 Topographic organization of the projections of the retina to the pretectal region in the rat. *J. comp. Neurol.* **186**, 271–292.

Scheibel, M. E., Davies, T. L. & Scheibel, A. B. 1972 An unusual axonless cell in the thalamus of the adult cat. *Expl Neurol.* **36**, 512–518.

Shepherd, G. M. 1979 *The synaptic organisation of the brain. An introduction*, 2nd edn. New York: Oxford University Press.

Singer, W., Pöppel, E. & Creutzfeldt, O. 1972 Inhibitory interaction in the cat's lateral geniculate nucleus. *Expl Brain Res.* **14**, 210–226.

Spencer, R. F., Mize, R. R. & Baker, R. 1983 Retinal projections to cat pretectum labelled by anterograde transport of peroxidase-conjugated lectin. *Invest. Ophthalmol.* suppl. to vol. 24, 227. (Abstract.)

Sprague, J. M., Berlucchi, G. & Rizzolatti, G. 1973 The role of the superior colliculus and pretectum in vision and visually guided behaviour. In *Handbook of sensory physiology, vol. 7, part IIIB. Central processing of visual information* (ed. R. Jung), pp. 27–101. Berlin: Springer.

Spreafico, R., Schmechel, D. E., Ellis, L. C. Jr & Rustioni, A. 1983 Cortical relay neurons and interneurons in the n. ventralis posterolataralis of cats: a horseradish peroxidase, electron-microscope, Golgi and immunocytochemical study. *Neuroscience* **9**, 491–509.

Steiger, H.-J. & Büttner-Ennever, J. A. 1979 Oculomotor nucleus afferents in the monkey demonstrated with HRP. *Brain Res.* **160**, 1–15.

Steinbusch, H. W. M. 1981 Distribution of serotonin-immunoreactivity in the central nervous system of the rat – cell bodies and terminals. *Neuroscience* **6**, 557–618.

Stelzner, D. J., Baisden, R. D. & Goodman, D. C. 1976 The ventral lateral geniculate nucleus, pars lateralis of the rat. Synaptic organisation and conditions for axonal sprouting. *Cell Tiss. Res.* **170**, 435–454.

Sterling, P. 1971 Receptive fields and synaptic organisation of the superficial gray layer of the cat superior colliculus. *Vis. Res.*, suppl. **3**, 309–328.

Sterling, P. & Davis, T. L. 1980 Neurons in cat lateral geniculate nucleus that concentrate exogenous [^{3}H]γ-aminobutyric acid (GABA). *J. comp. Neurol.* **192**, 737–749.

Sugimoto, T., Fukuda, Y. & Wakakuwa, K. 1984 Quantitative analysis of a cross-sectional area of the optic nerve: a comparison between albino and pigmented rats. *Expl Brain Res.* **54**, 266–274.

Swanson, L. W., Cowan, W. M. & Jones, E. G. 1974 An autoradiographic study of the efferent connections of the ventral lateral geniculate nucleus in the albino rat and the cat. *J. comp. Neurol.* **156**, 143–164.

Szentágothai, J., Hámori, J. & Tömböl, T. 1966 Degeneration and electron microscope analysis of the synaptic glomeruli in the lateral geniculate body. *Expl Brain Res.* **2**, 283–301.

Taylor, A. M. & Lieberman, A. R. 1985 Identification, ultrastructure, and synaptic relationships of the axon terminals of neurons in the superior colliculus that project to the ventral lateral geniculate nucleus: HRP-EM studies in the adult rat. *J. Anat.* **140**, 515–516. (Abstract.)

Tigges, J. & O'Steen, W. K. 1974 Termination of retinofugal fibres in squirrel monkey: a re-investigation using autoradiographic methods. *Brain Res.* **79**, 489–495.

Tigges, M., Tigges, J., Luttrell, G. L. & Frazier, C. M. 1973 Ultrastructural changes in the superficial layers of the superior colliculus in *Galago crassicandatus* (primates) after eye enucleation. *Z. Zellforsch. mikrosk. Anat.* **140**, 291–307.

Tokunaga, A., Akert, K., Garey, L. J. & Otani, K. 1981 Primary and secondary subcortical projections of the monkey visual system. An autoradiographic study. *Brain Res.* **214**, 137–143.

Tömböl, T. 1966/1967 Short axon neurons and their synaptic relations in the specific thalamic nuclei. *Brain Res.* **3**, 307–326.

Torrealba, F., Partlow, G. D. & Guillery, R. W. 1981 Organisation of the projection from the superior colliculus to the dorsal lateral geniculate nucleus of the cat. *Neuroscience* **6**, 1341–1360.

Trejo, L. J. & Cicerone, C. M. 1984 Cells in the pretectal olivary nucleus are in the pathway for the direct light reflex of the pupil in the rat. *Brain Res.* **300**, 49–62.

Uchizono, K. 1965 Characteristics of excitatory and inhibitory synapses in the central nervous system of the cat. *Nature, Lond.* **207**, 642–643.

Updyke, B. V. 1977 Topographic organization of the projections from cortical areas 17, 18 and 19 onto the thalamus, pretectum and superior colliculus in the cat. *J. comp. Neurol.* **173**, 81–122.

Valverde, F. 1970 The Golgi method. A tool for comparative structural analyses. In *Contemporary research methods in neuroanatomy* (ed. W. J. H. Nauta & S. O. E. Ebbesson), pp. 12–31. New York: Springer-Verlag.

Valverde, F. 1973 The neuropil in superficial layers of the superior colliculus of the mouse. A correlated Golgi and electron microscopic study. *Z. Anat. EntwGesch.* **142**, 117–147.

Van Den Pol, A. N. 1980 The hypothalamic suprachiasmatic nucleus of rat: intrinsic anatomy. *J. comp. Neurol.* **191**, 661–702.

Verbitskaya, L. V., Uranova, N. A. & Viktorov, I. V. 1977 Interaction between retinal and visual cortical fibers in several subcortical visual centers of the rat. *Arkhiv. Anatomii, Gistologii i Embriologii* **72**, 31–38 (In Russian).

Viktorov, I. V. 1969 Termination of the optic fibers in the pretectal region of the rat brain. *Doklady Akademii Nauk SSSR* **188**, 451–453 (In Russian).

Watanabe, K. & Kawana, E. 1979 Efferent projections of the parabigeminal nucleus in rats: A horseradish peroxidase study. *Brain Res.* **168**, 1–11.

Weber, J. T. & Harting, J. K. 1980 The efferent projections of the pretectal complex: An autoradiographic and horseradish peroxidase analysis. *Brain Res.* **194**, 1–28.

Weber, A. J. & Kalil, R. E. 1983 The percentage of interneurons in the dorsal lateral geniculate nucleus of the cat and observations on several variables that affect the sensitivity of horseradish peroxidase as a retrograde marker. *J. comp. Neurol.* **220**, 336–346.

Weber, J. T., Young, R. & Hutchins, B. 1981 Morphologic and autoradiographic evidence for a laminated pretectal olivary nucleus in the squirrel monkey. *Brain Res.* **224**, 153–159.

Webster, K. E., Arzymanow, B. J., Ohara, P. T. & Lieberman, A. R. 1981 Transneuronal labelling of the visual portion of the thalamic reticular nucleus in the rat. *J. Anat.* **133**, 654. (Abstract.)

Westrum, L. E. 1974 Electron microscopy of deafferentation in the spinal trigeminal nucleus. *Adv. Neurol.* **4**, 53–60.

Westrum, L. E. & Black, R. G. 1971 Fine structural aspects of the synaptic organization of the spinal trigeminal nucleus (pars interpolaris) of the cat. *Brain Res.* **25**, 265–287.

Wong-Riley, M. T. T. 1972*a* Neuronal and synaptic organization of the normal dorsal lateral geniculate nucleus of the squirrel monkey, *Saimiri sciureus*. *J. comp. Neurol.* **144**, 25–60.

Wong-Riley, M. T. T. 1972*b* Terminal degeneration and glial reactions in the lateral geniculate nucleus of the squirrel monkey after eye removal. *J. comp. Neurol.* **144**, 61–92.

Wong-Riley, M. T. T. 1972*c* Changes in the dorsal lateral geniculate nucleus of the squirrel monkey after unilateral ablation of the visual cortex. *J. comp. Neurol.* **146**, 519–548.

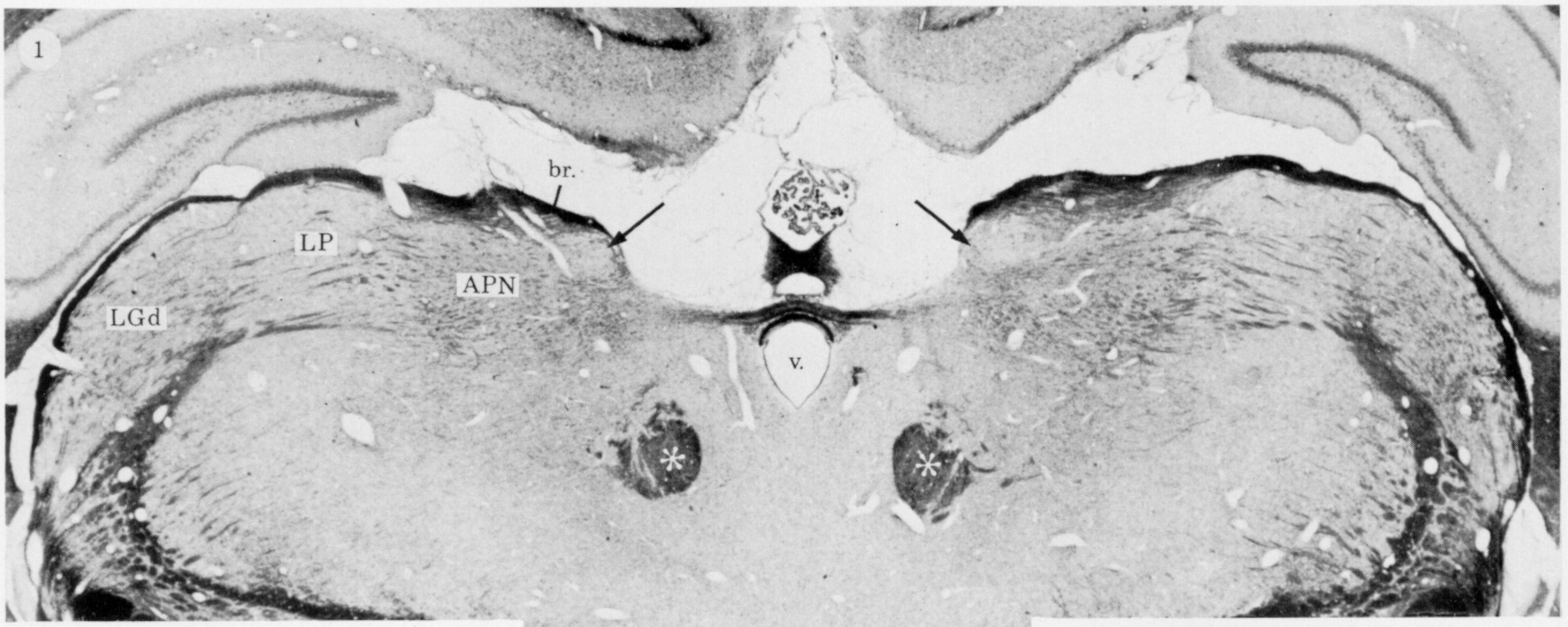

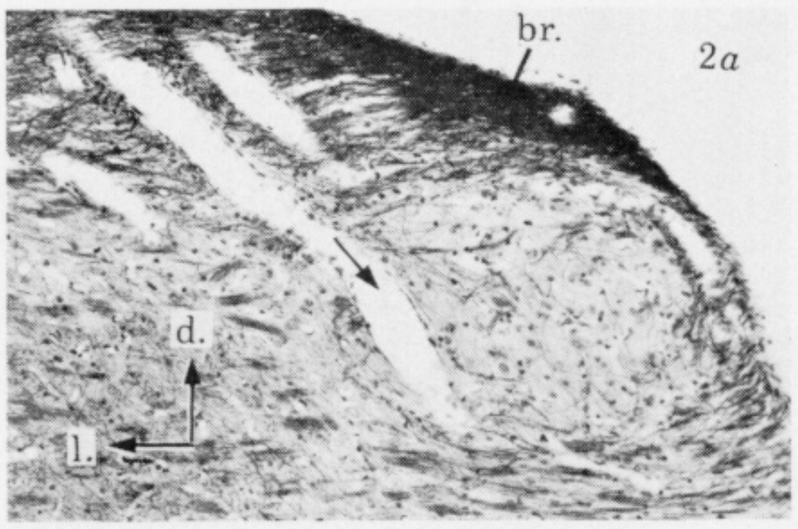

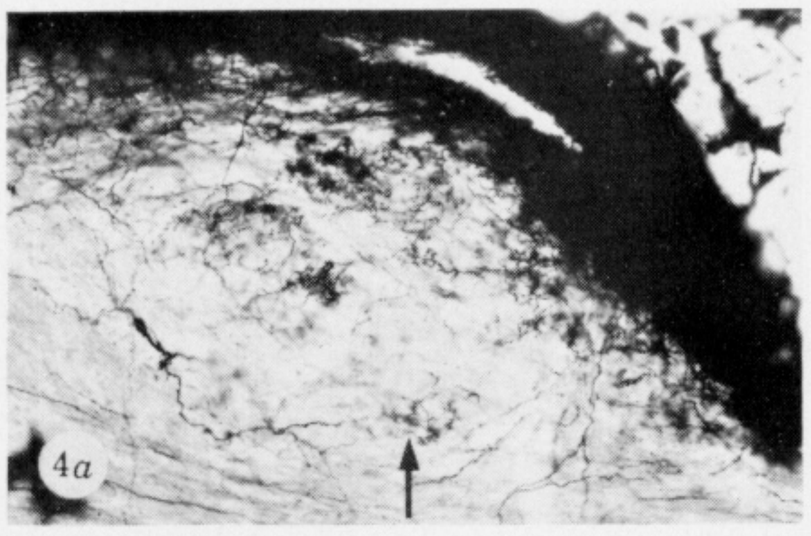

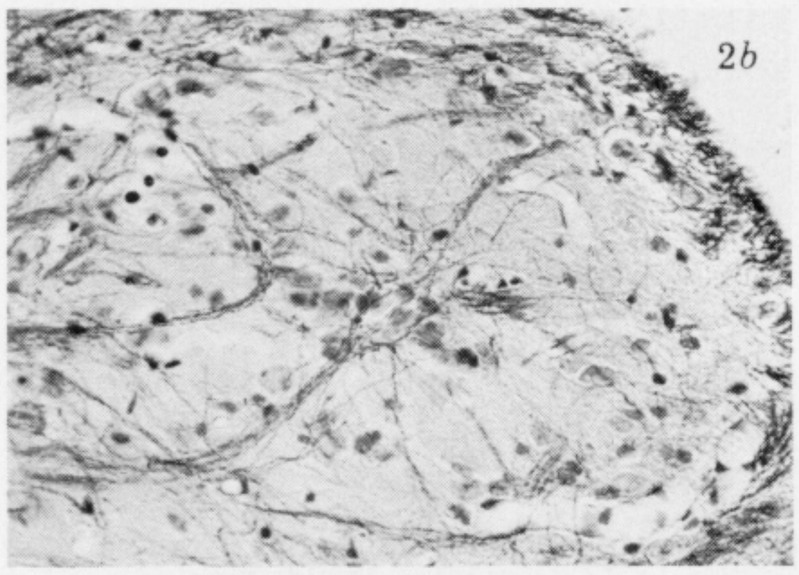

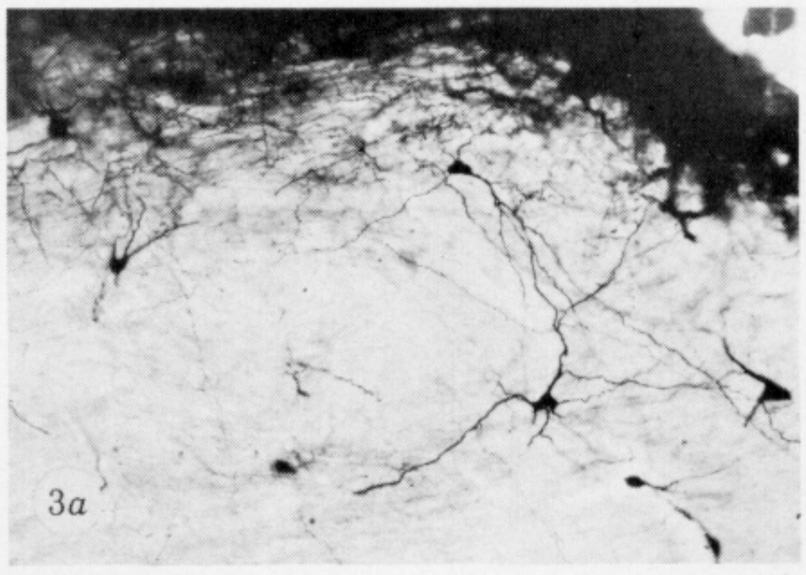

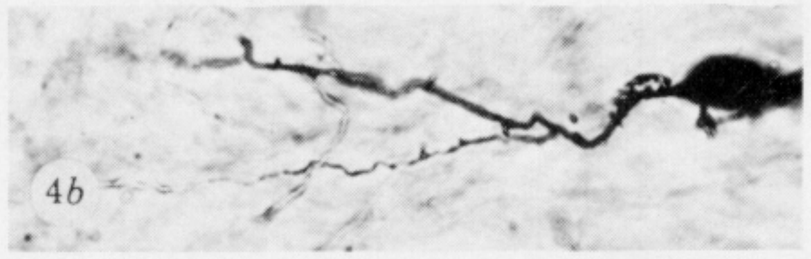

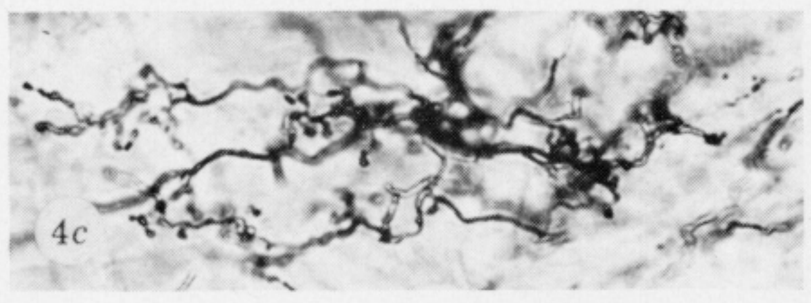

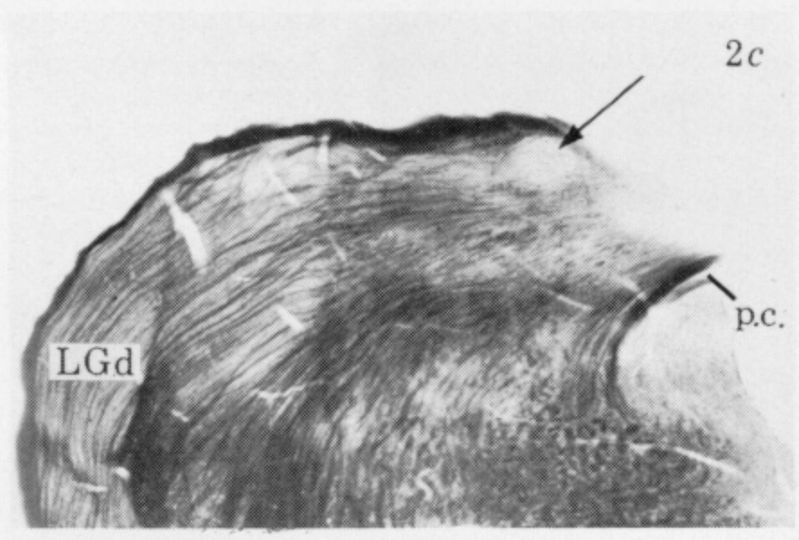

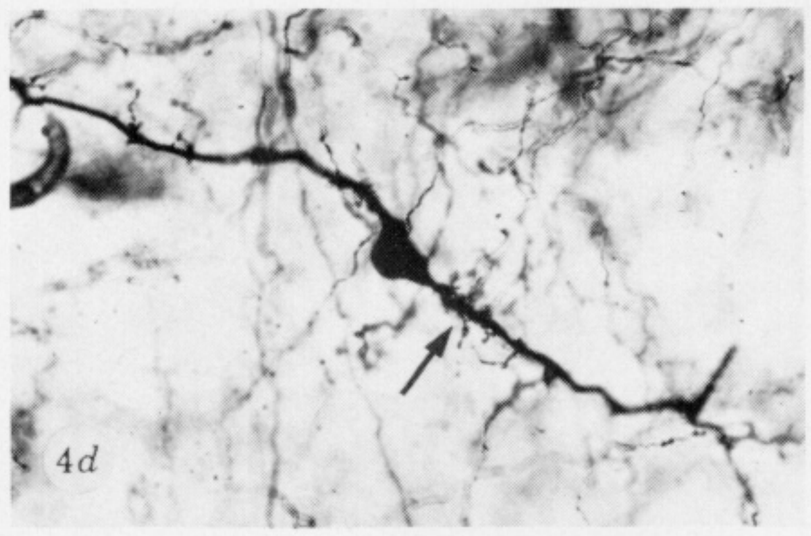

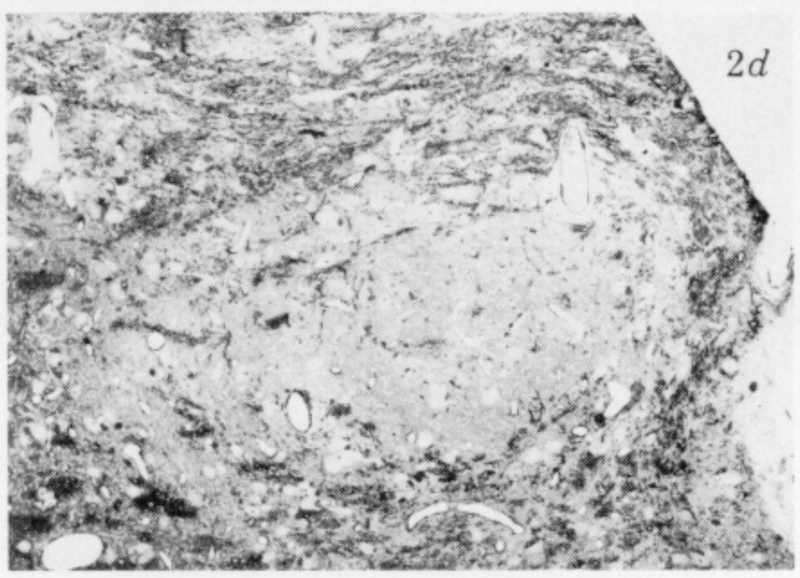

FIGURES 1–4. For description see facing p. 580.

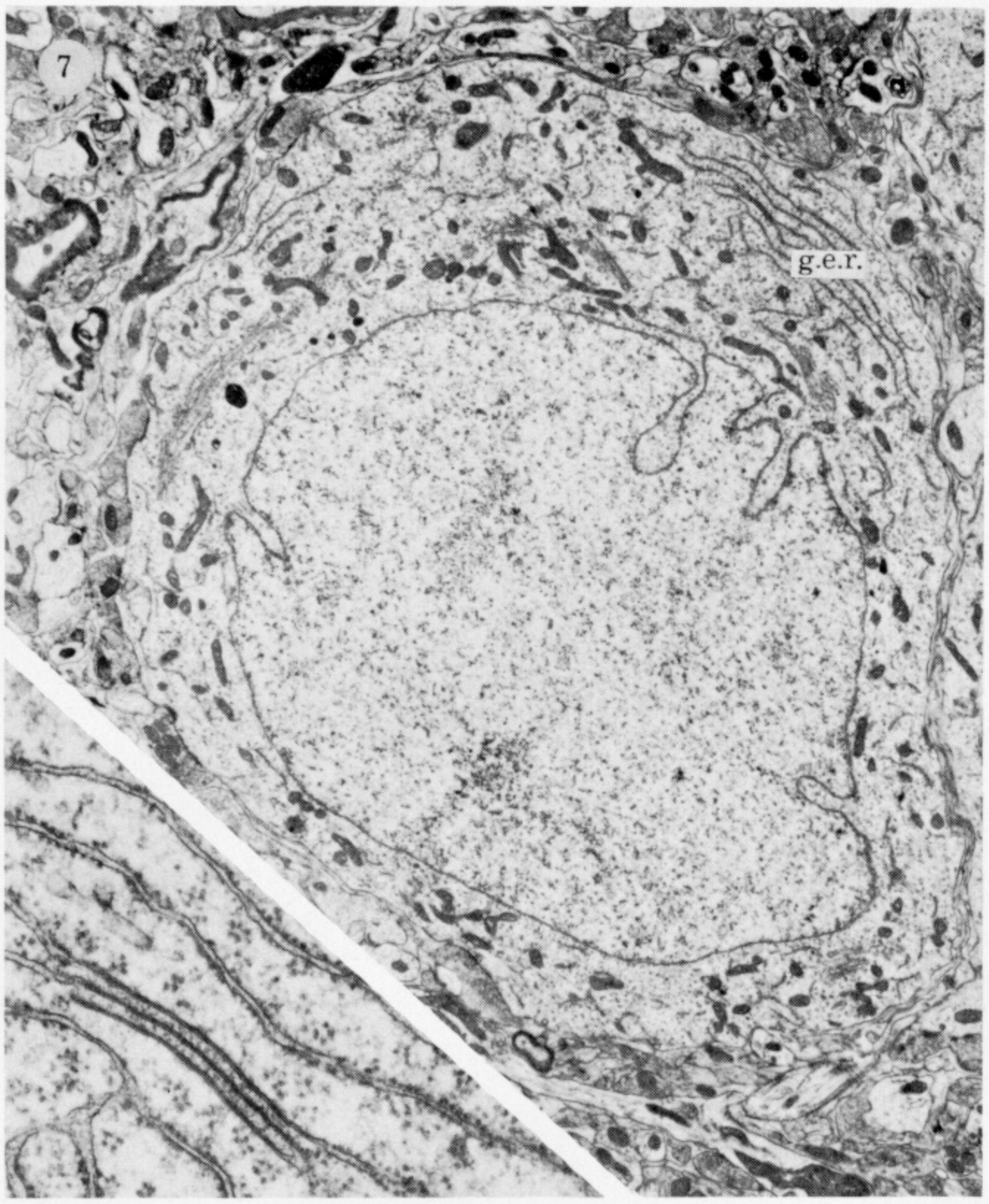

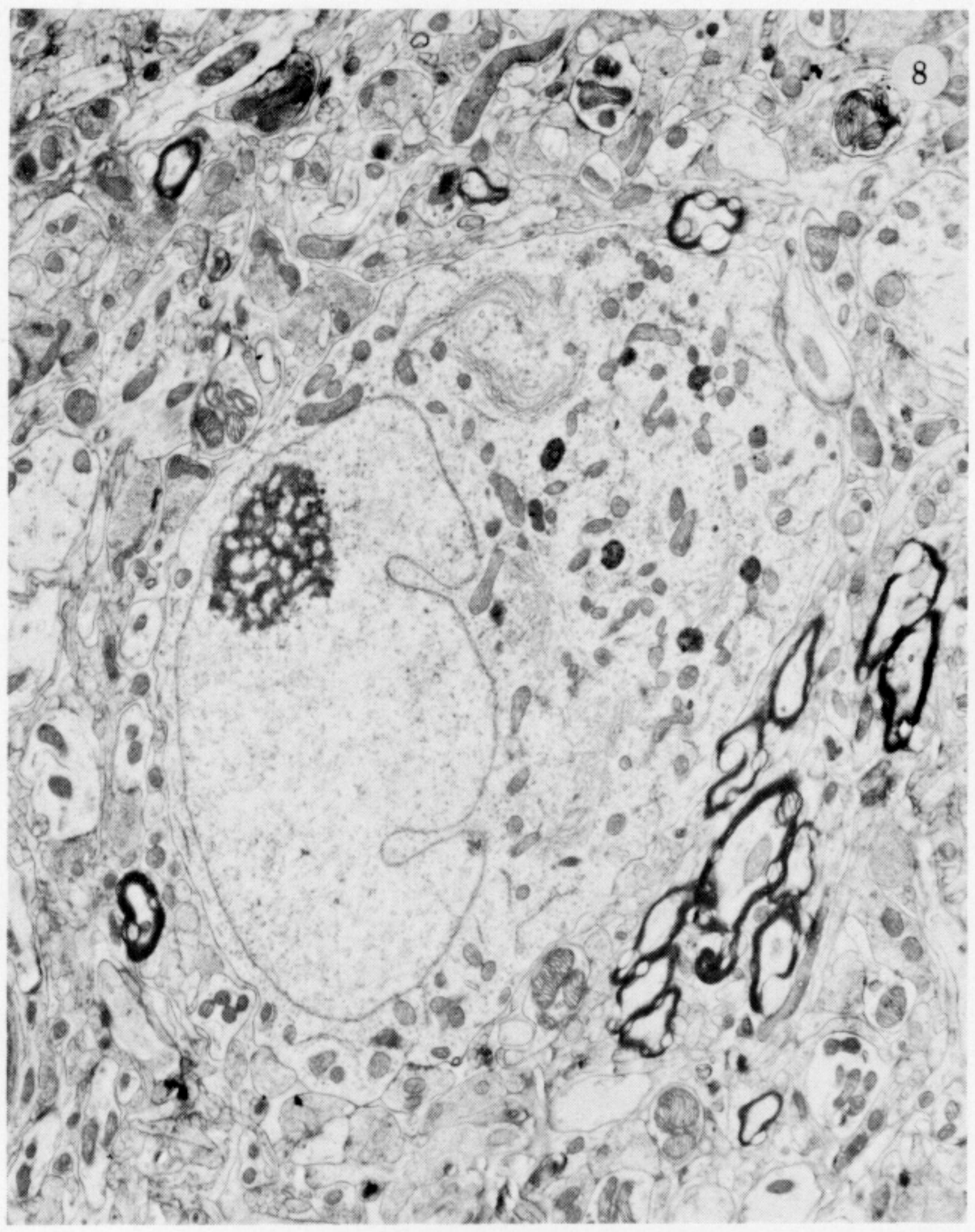

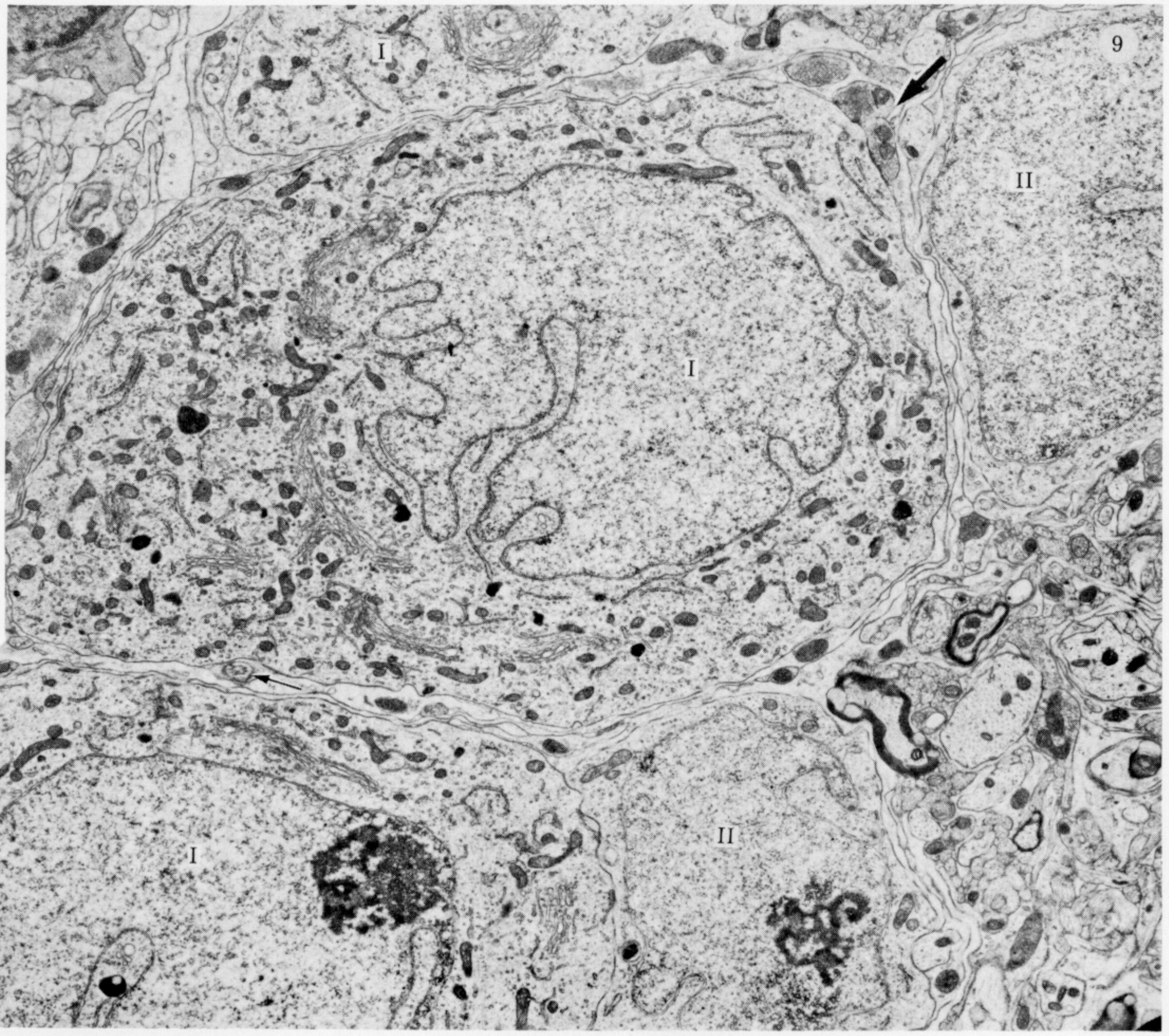

FIGURES 7–9. For description see facing plate 1.

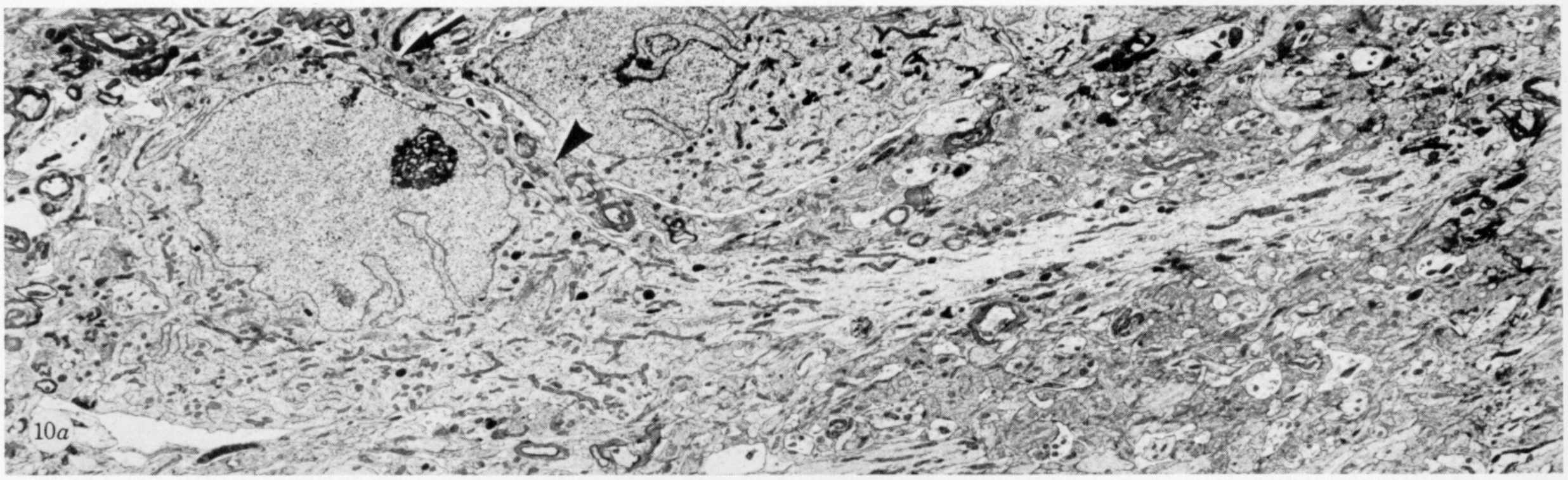

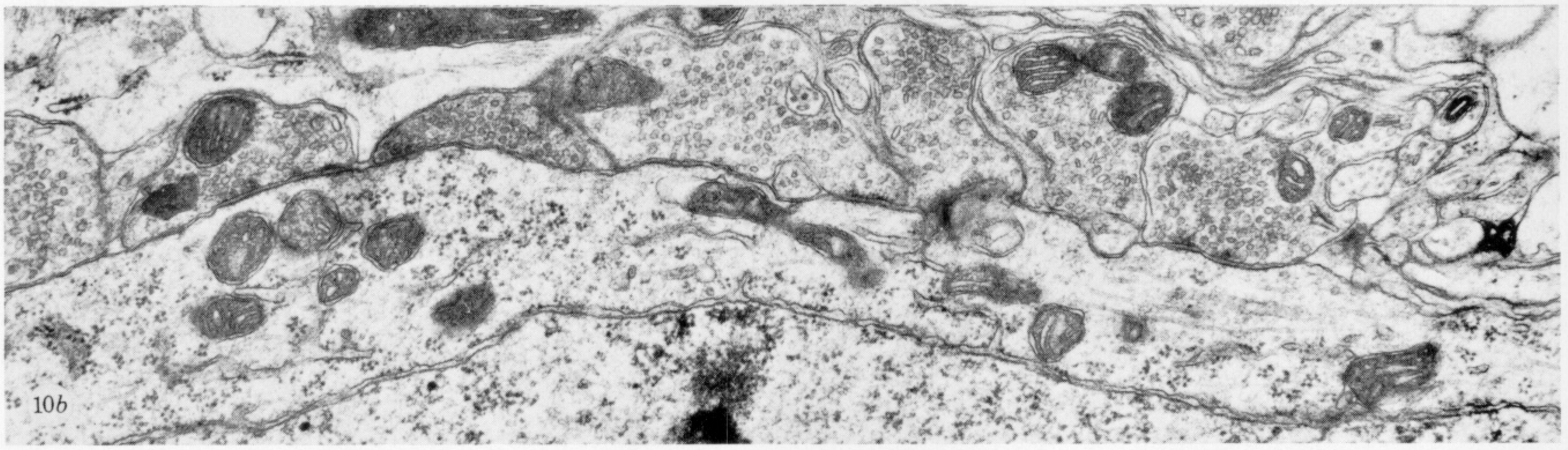

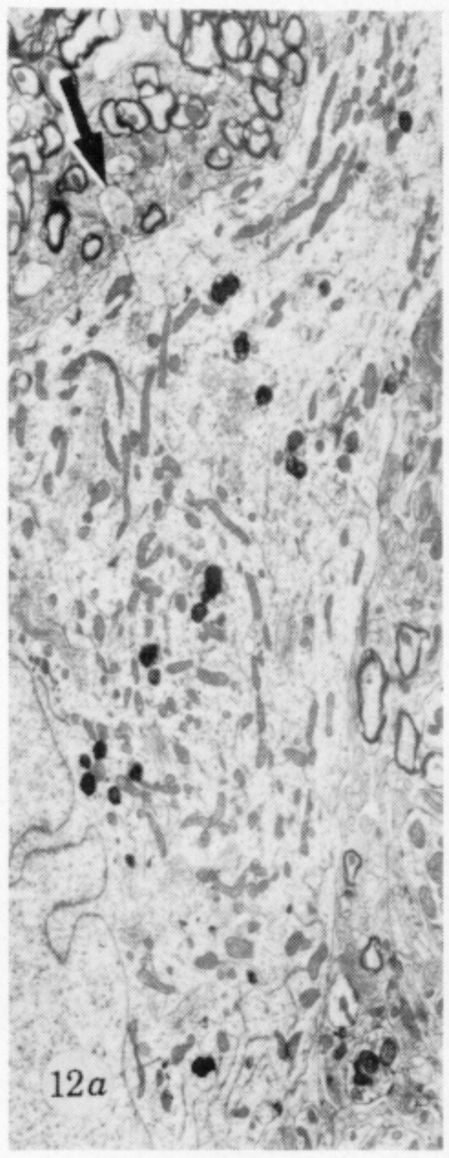

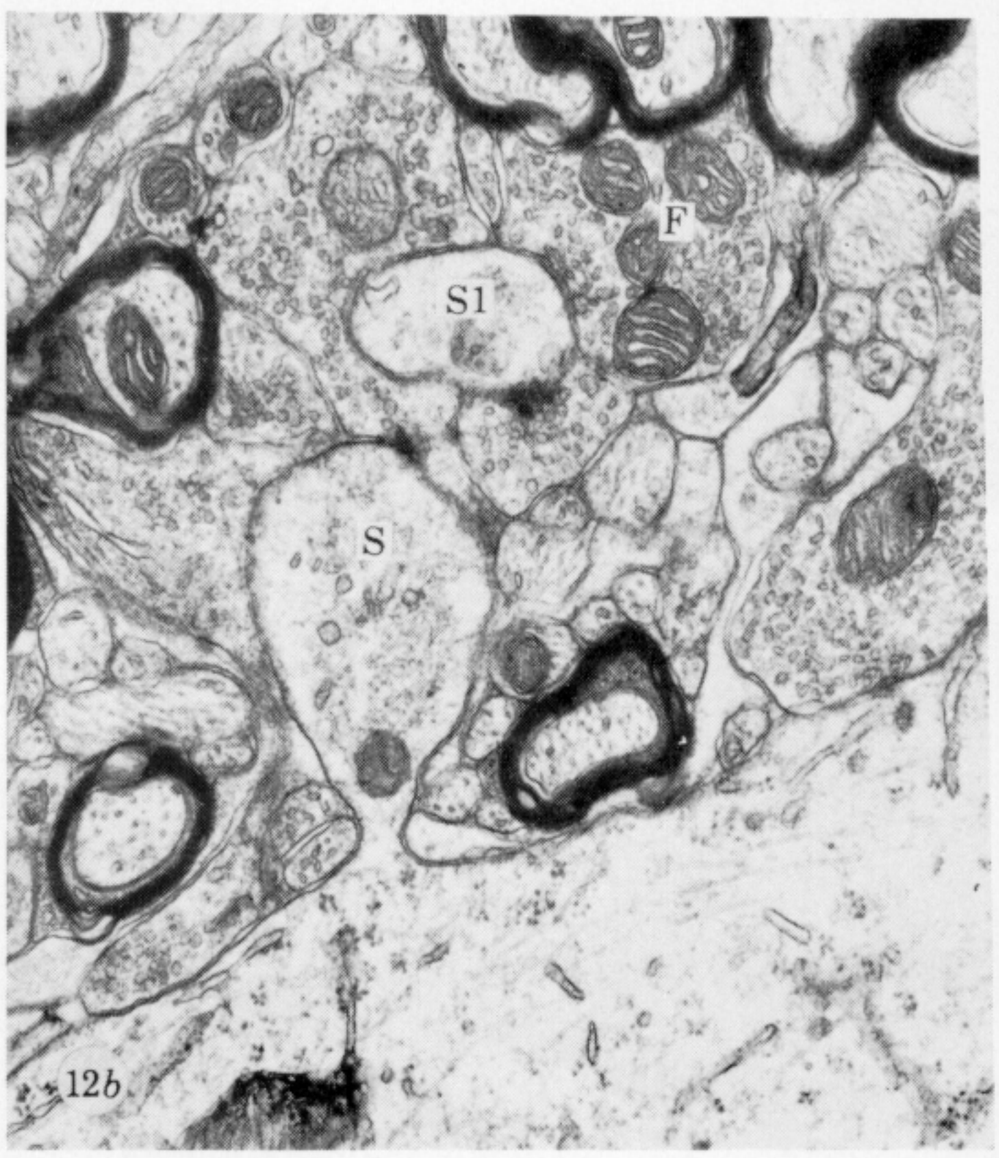

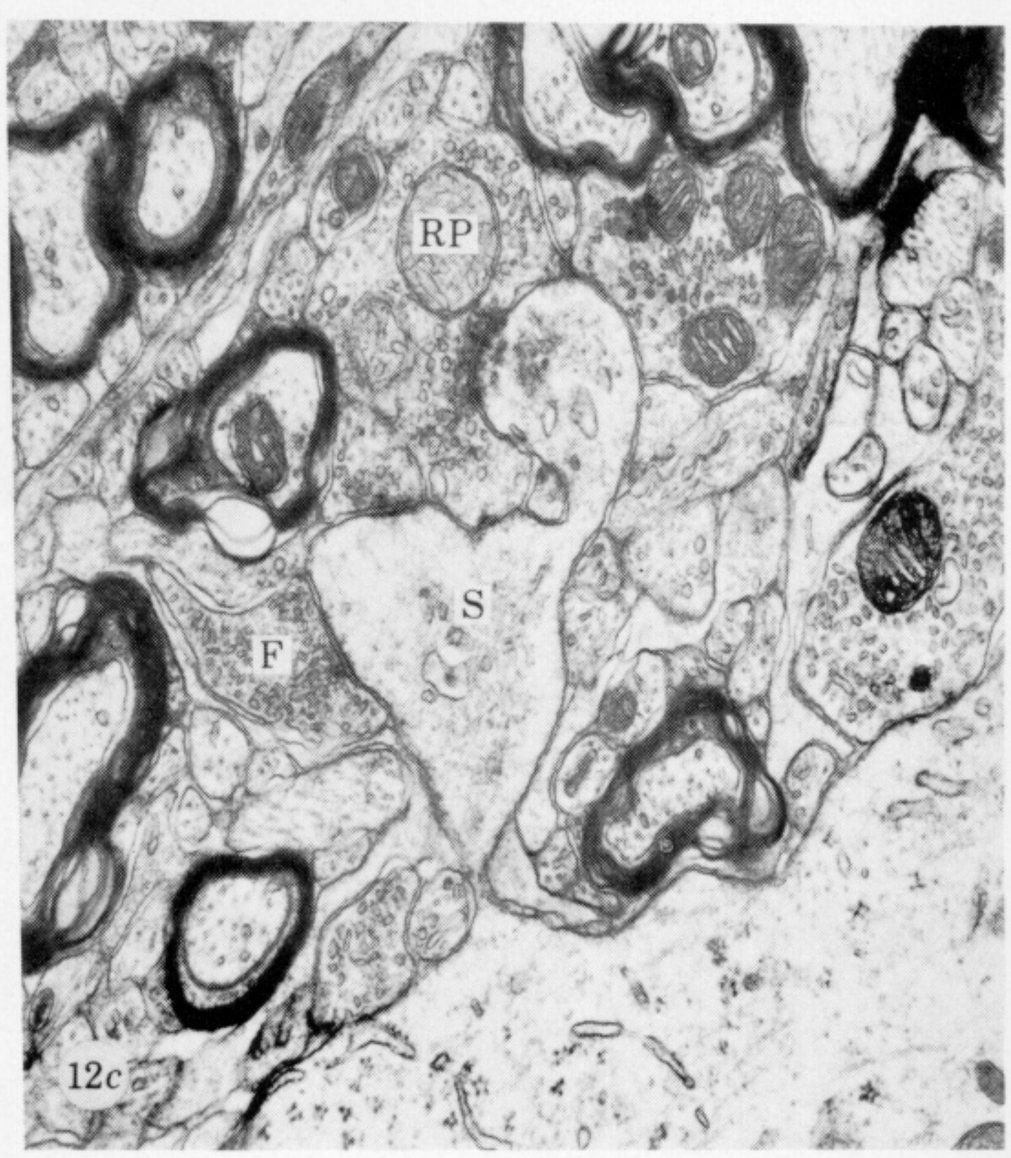

FIGURES 10–12. For description see facing plate 1.

13

F

S

F

S

F

D

F

14*a*

RP

14*b*

RP

RP

*

RP

14*c*

15*a*

m.a.

i.s.

as.

a.h.

c.b.

r.

g.e.r.

f.

15*b*

16

a.

a.

FIGURES 13–16. For description see facing plate 4.

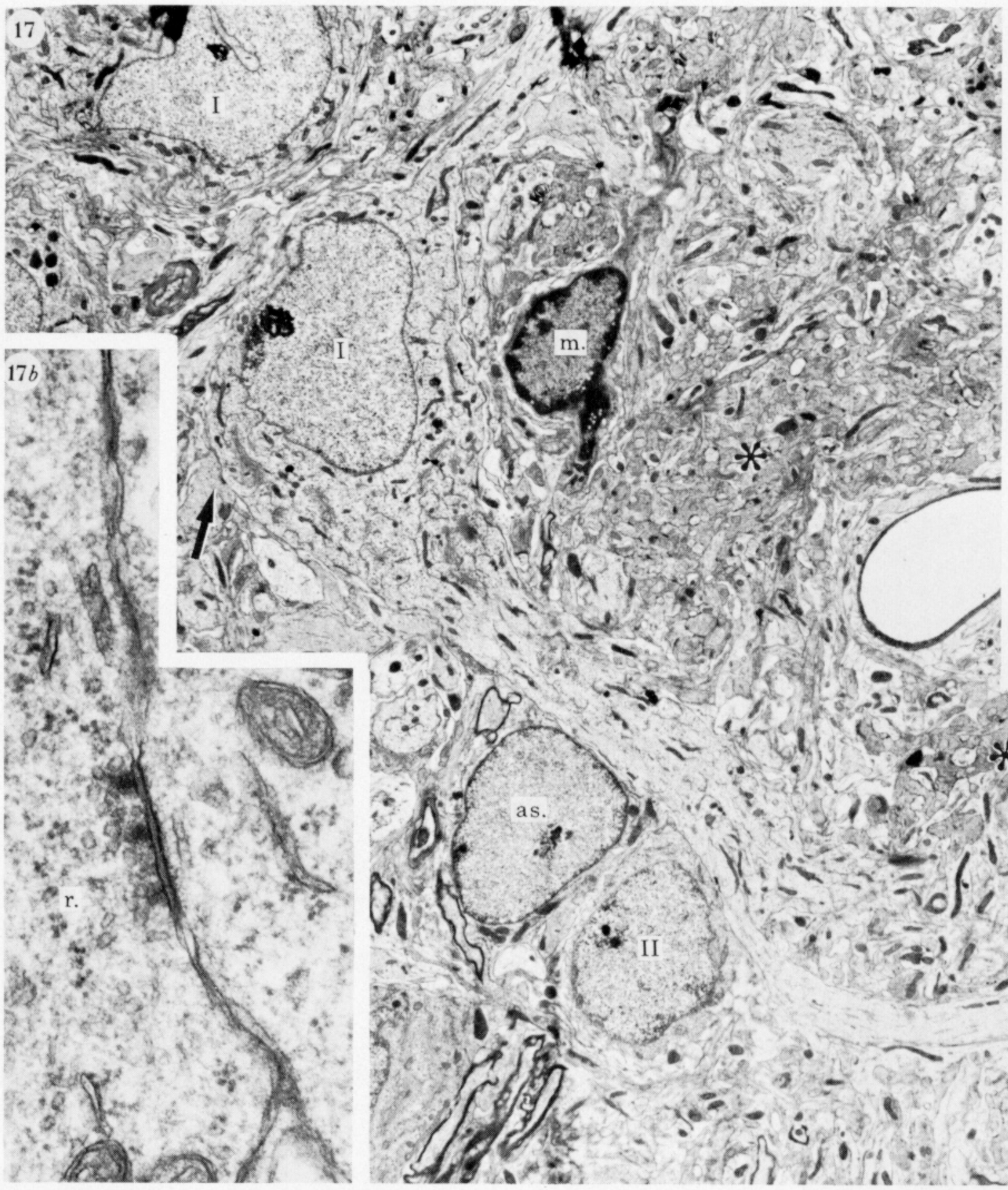

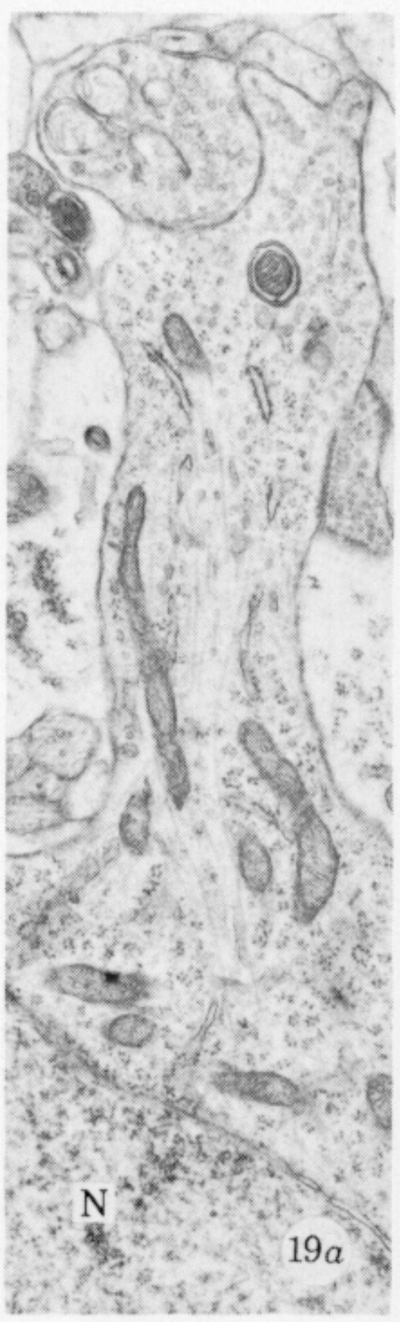

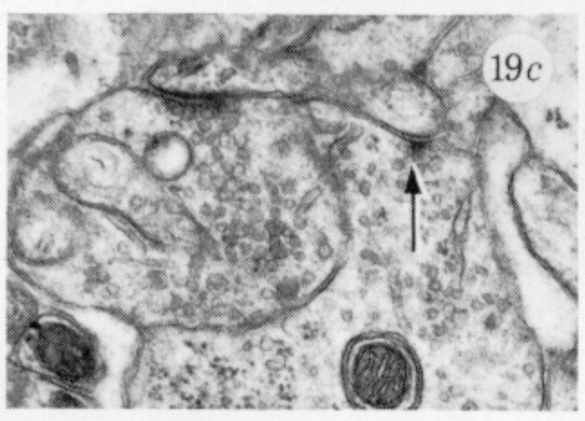

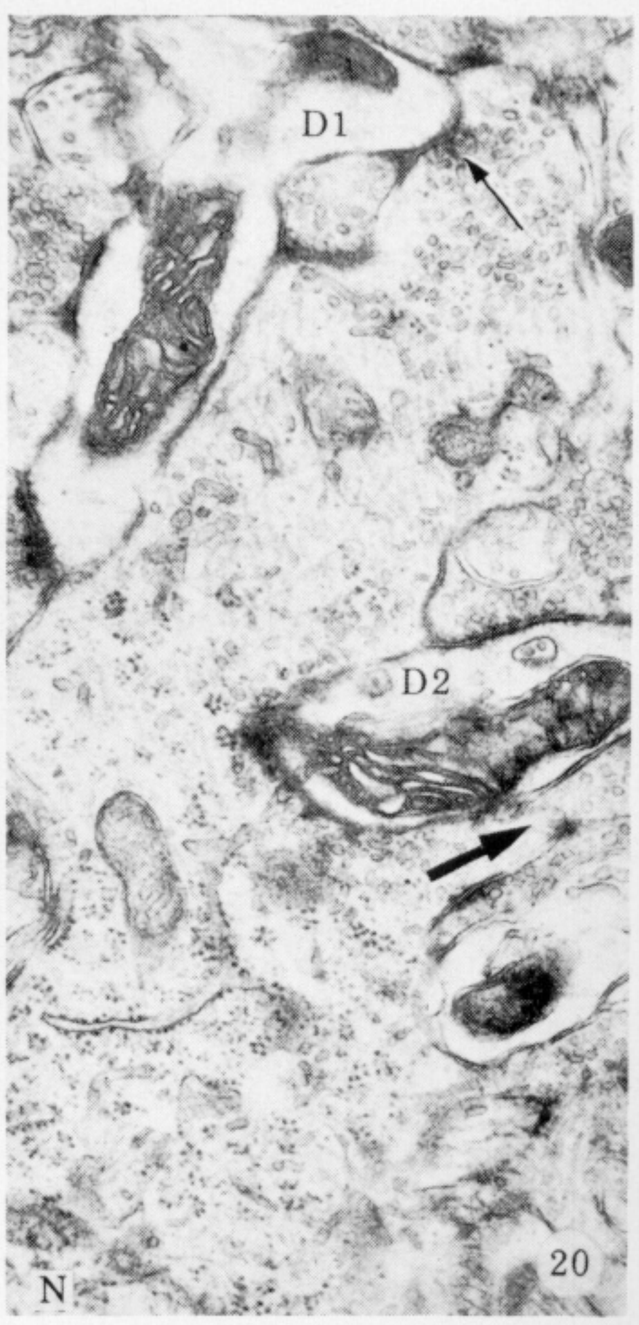

FIGURES 17–20. For description see facing plate 4.

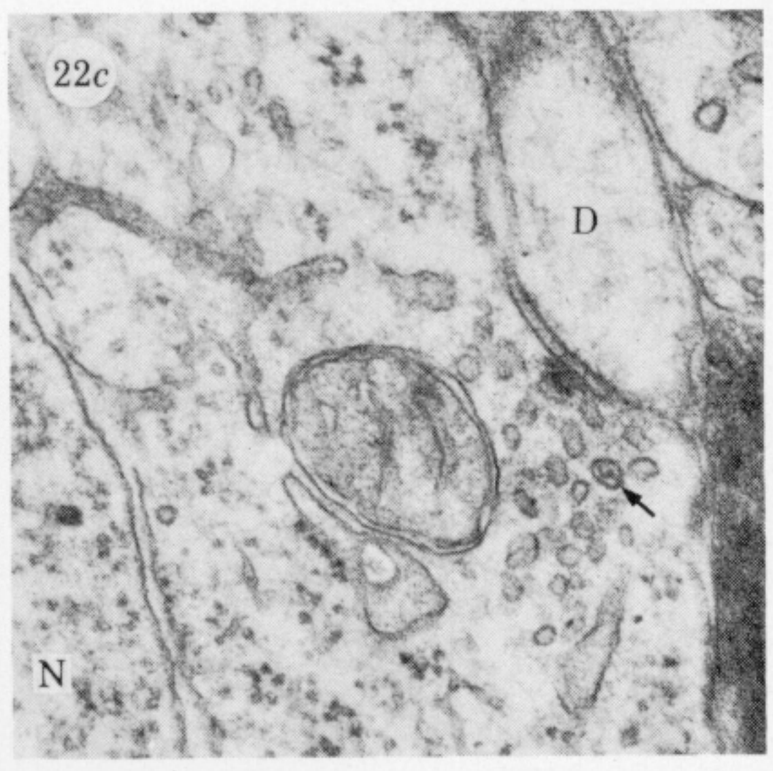

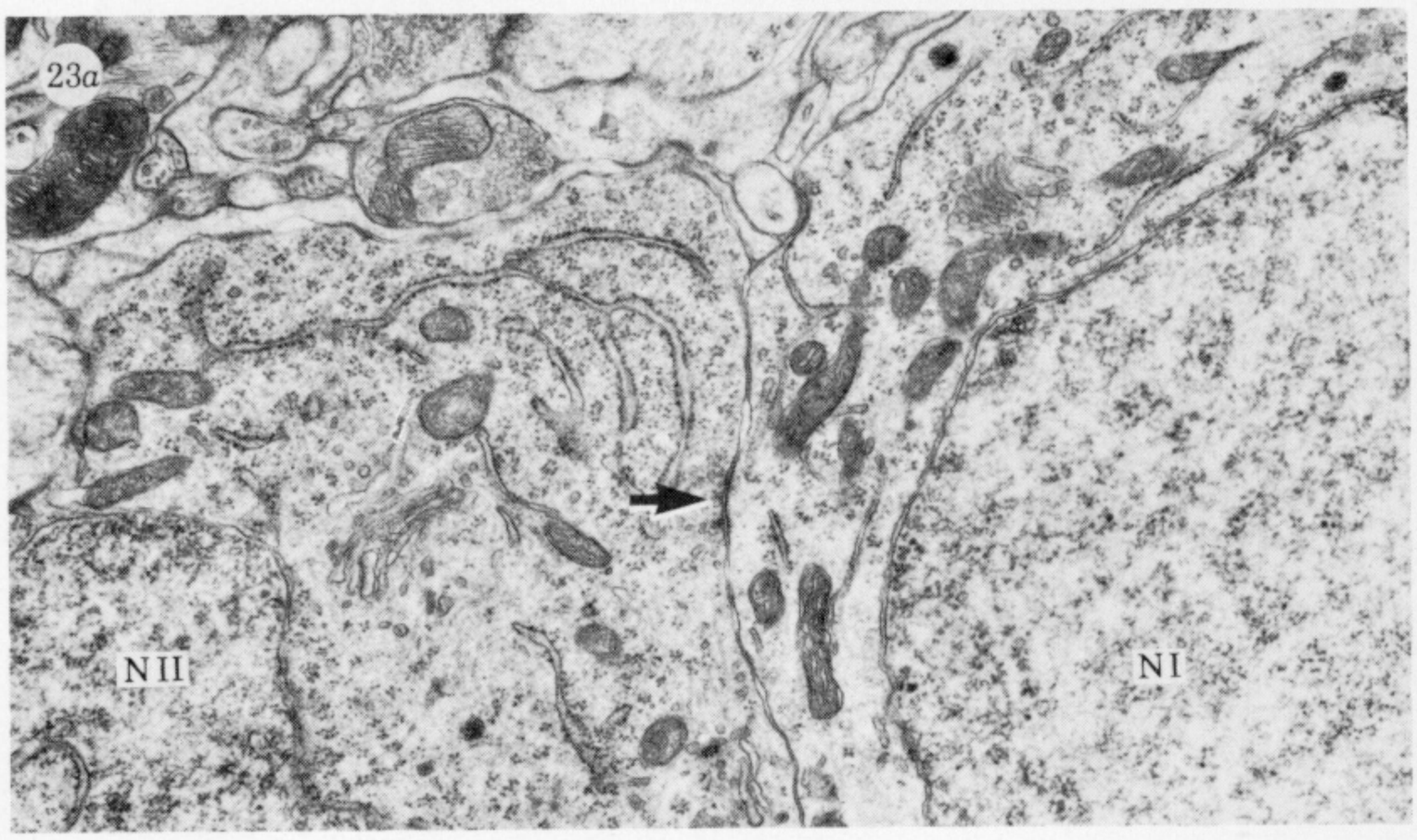

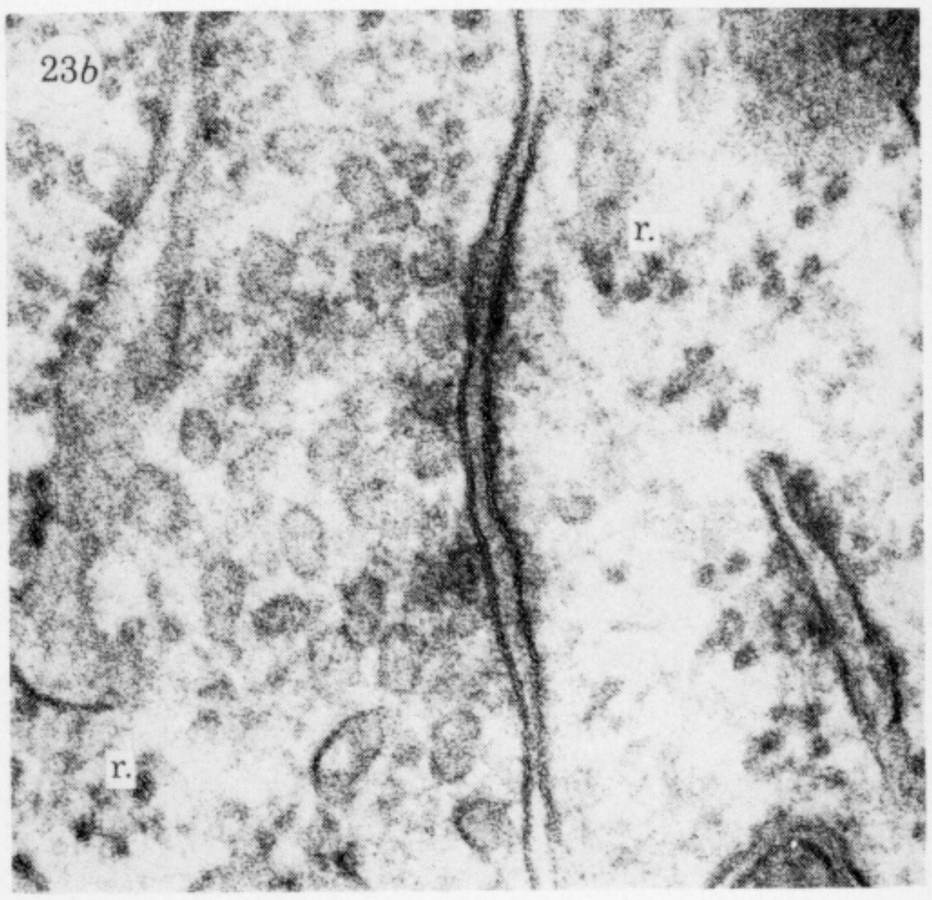

24

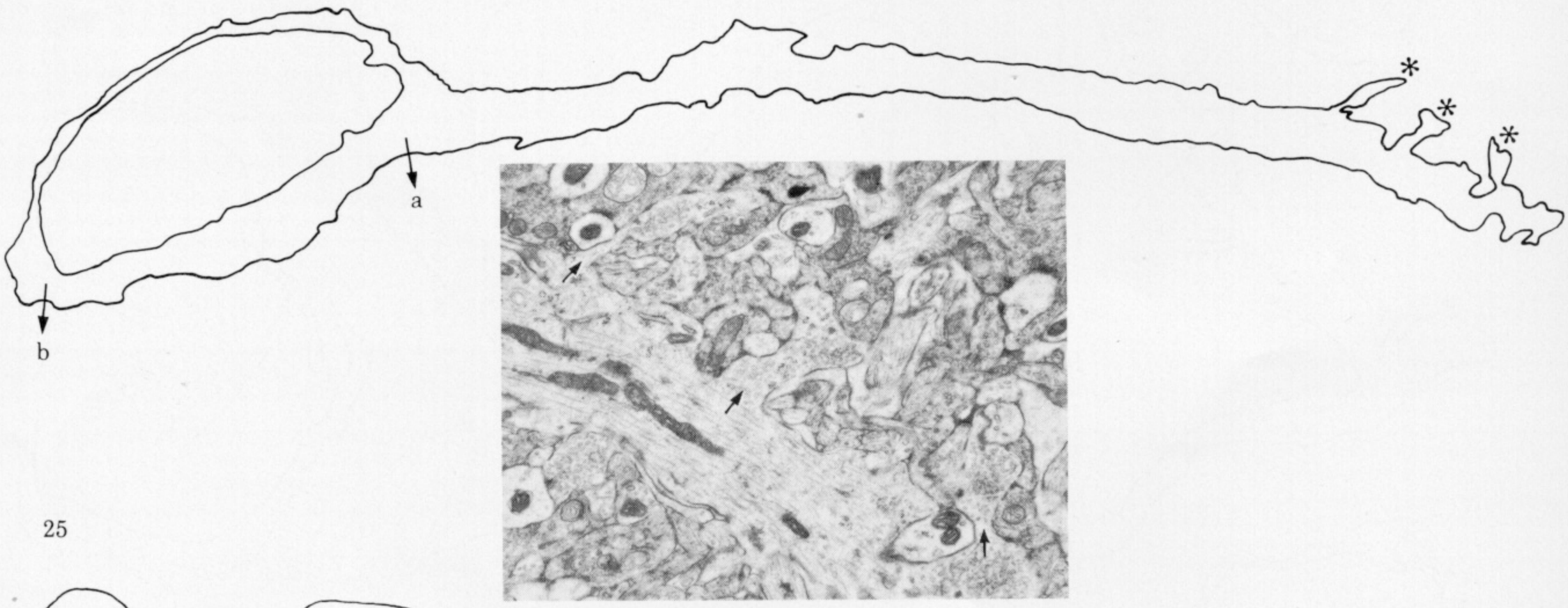

25

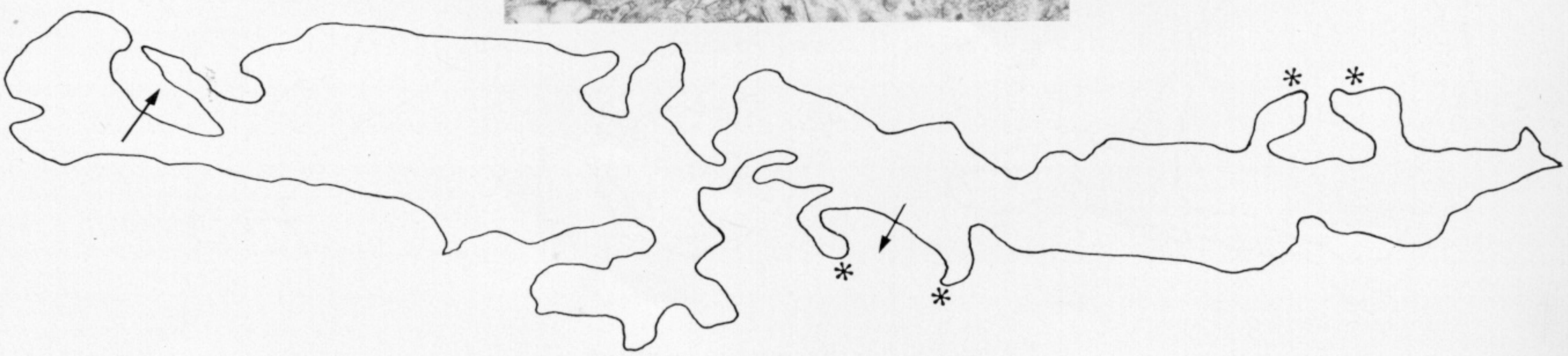

FIGURES 22–25. For description see facing plate 5.

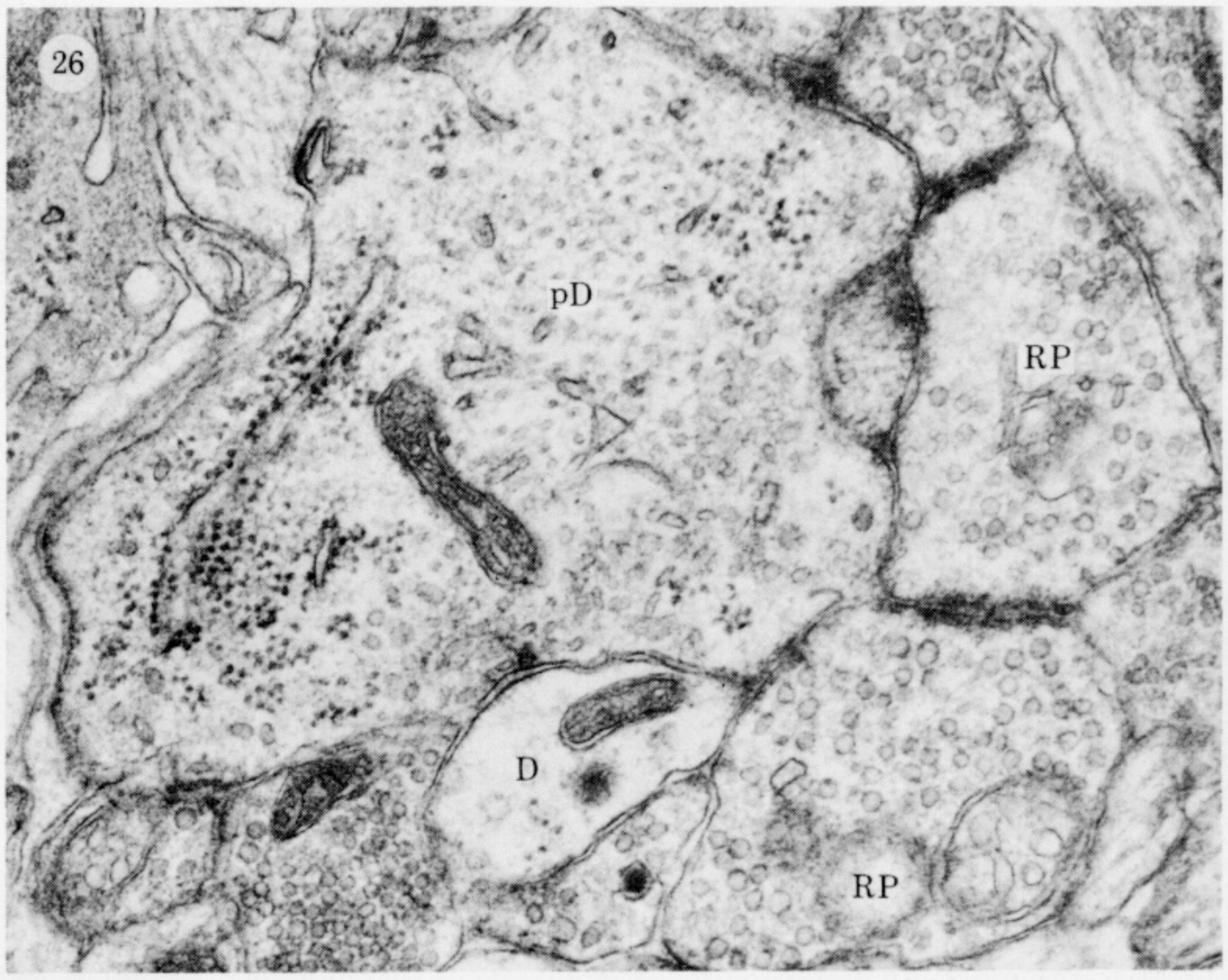

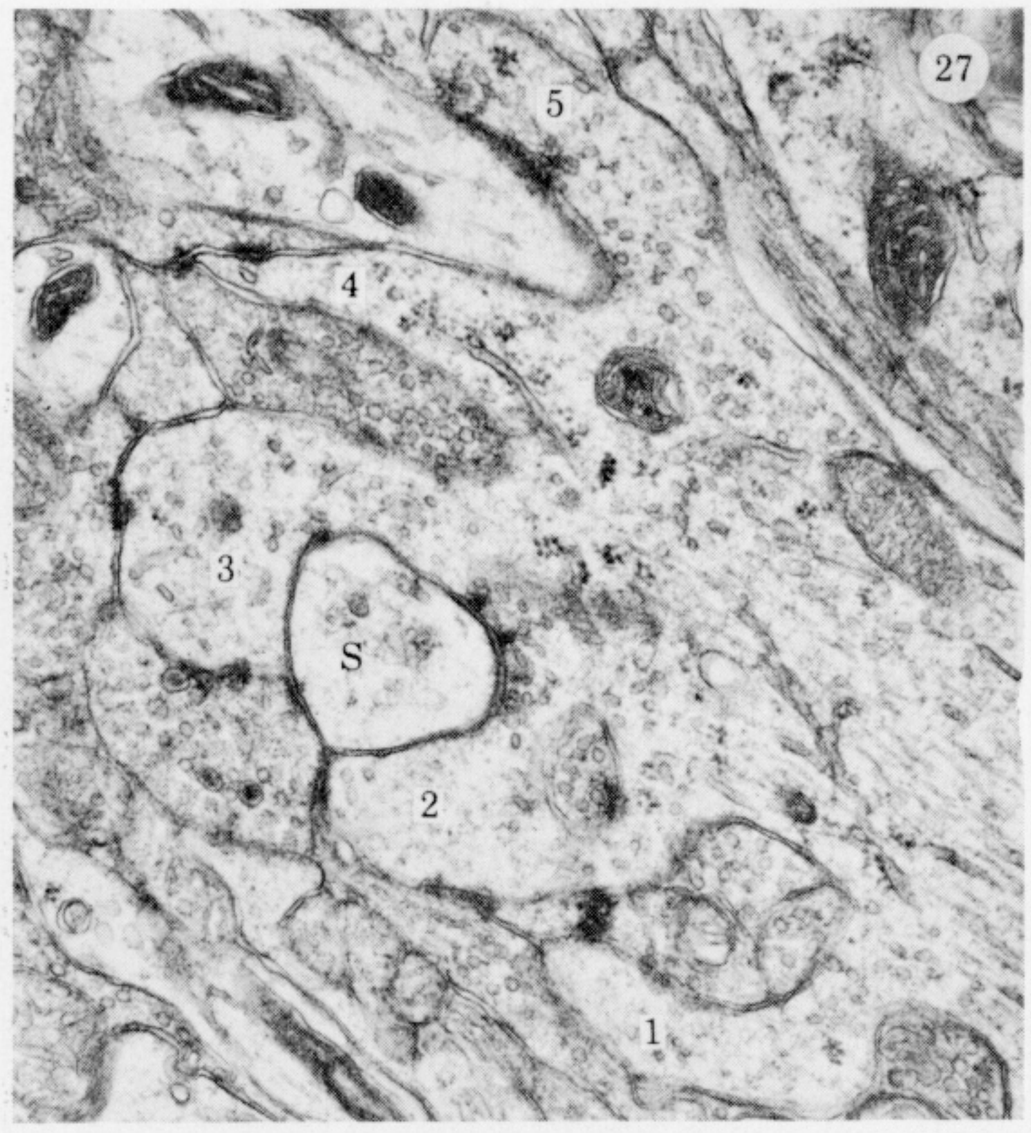

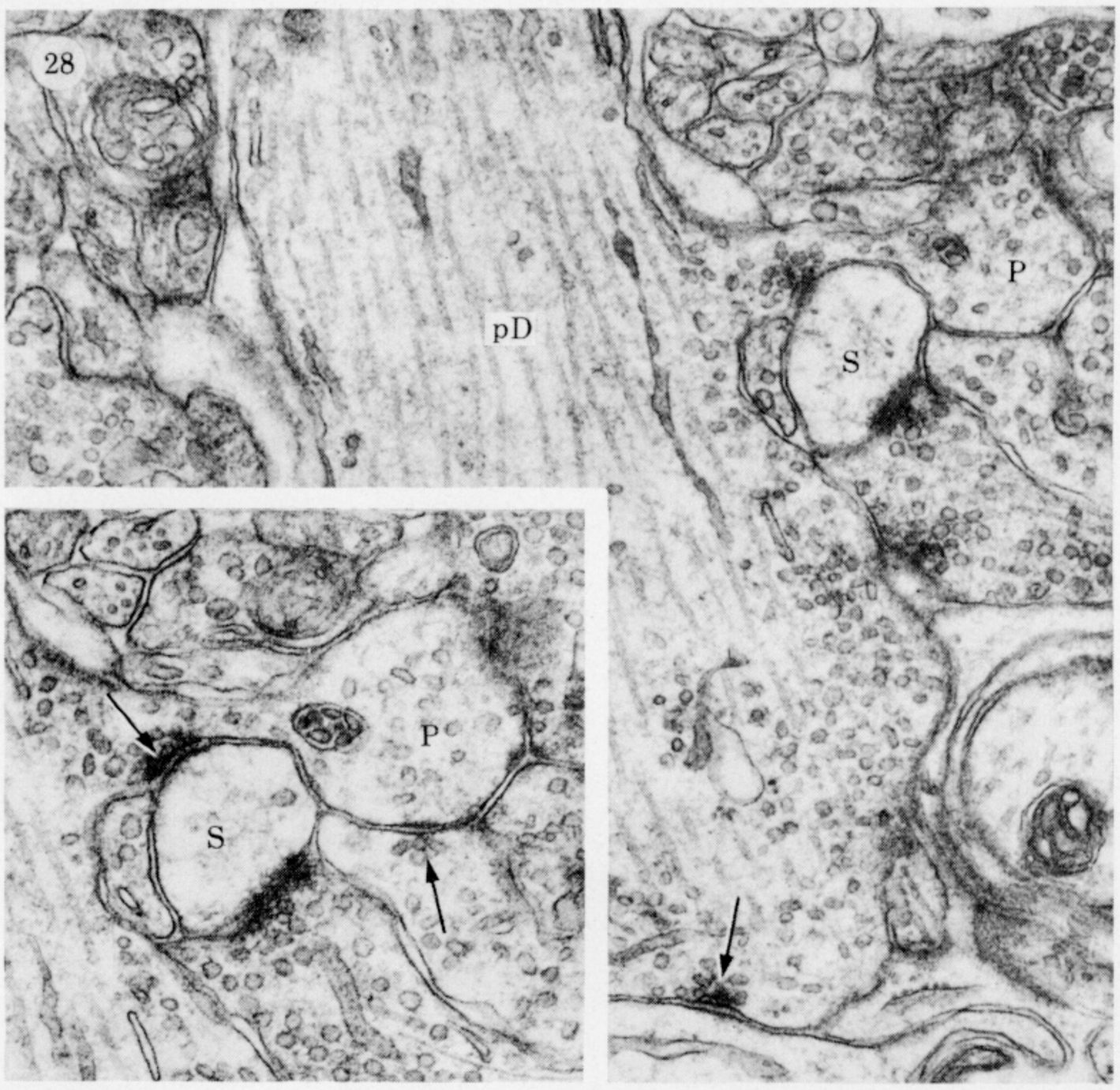

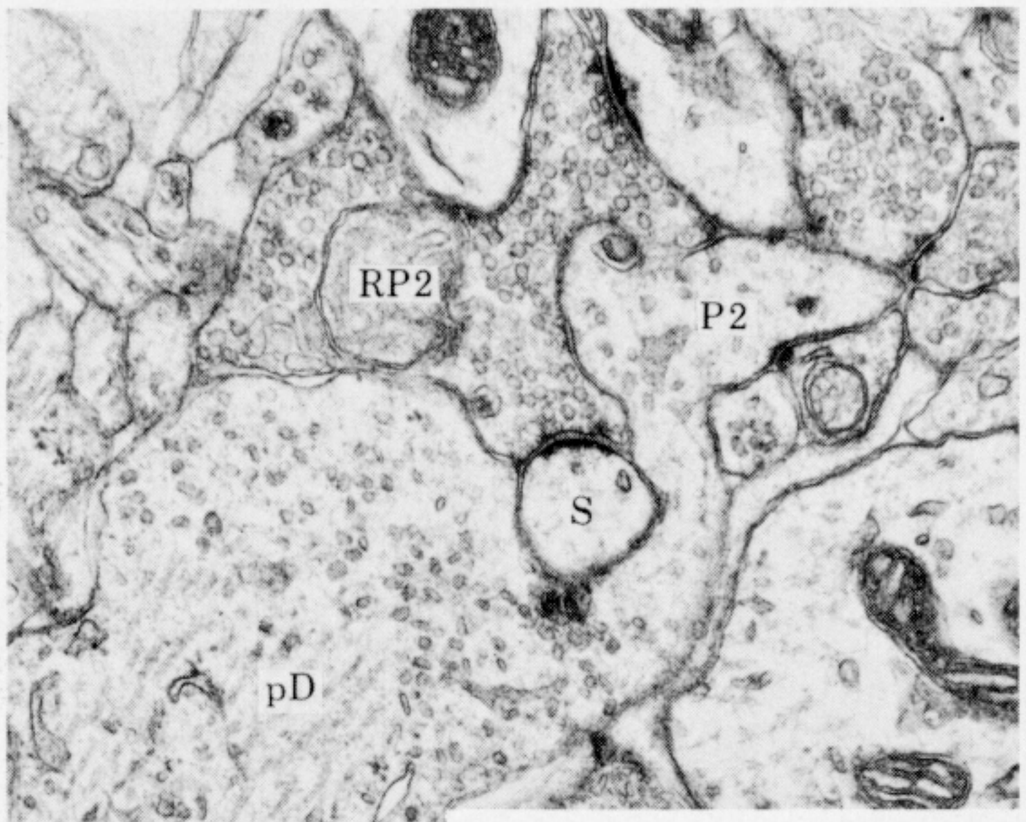

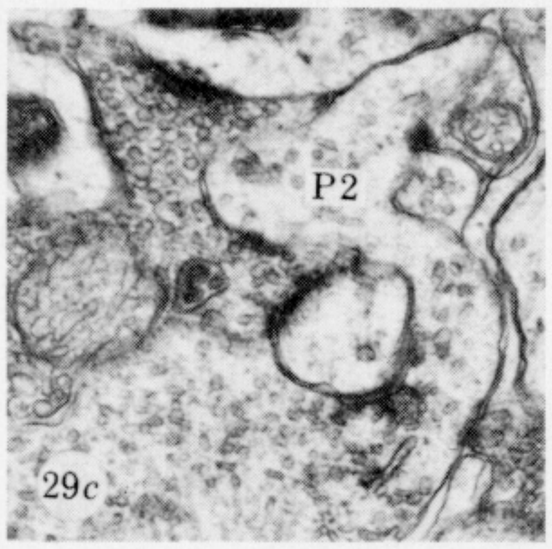

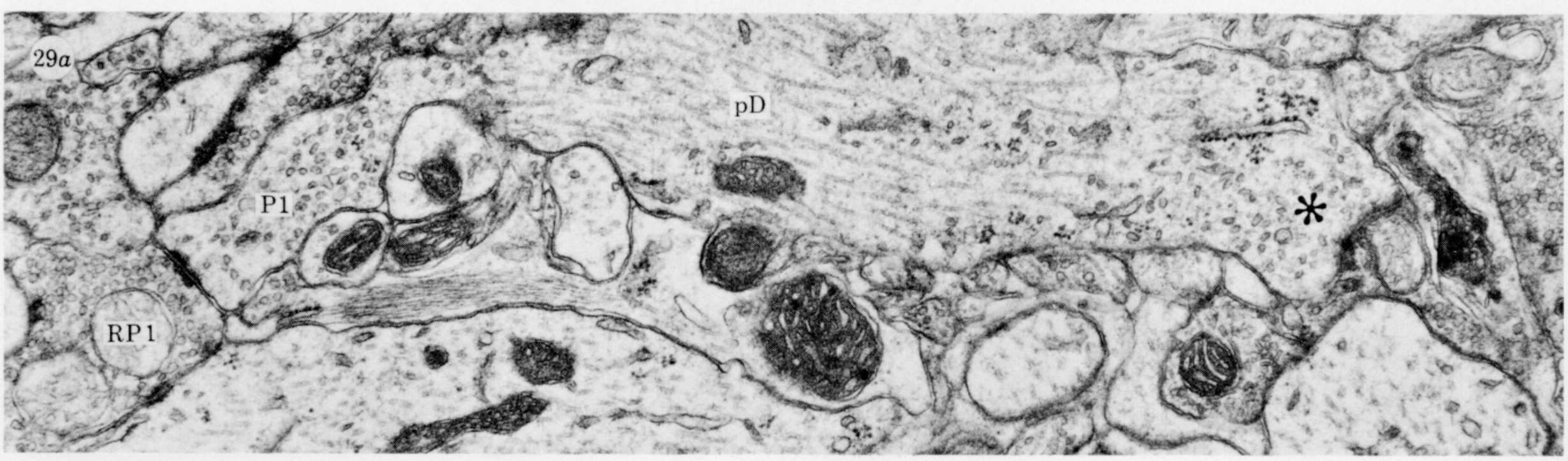

FIGURES 26–29. For description see opposite.

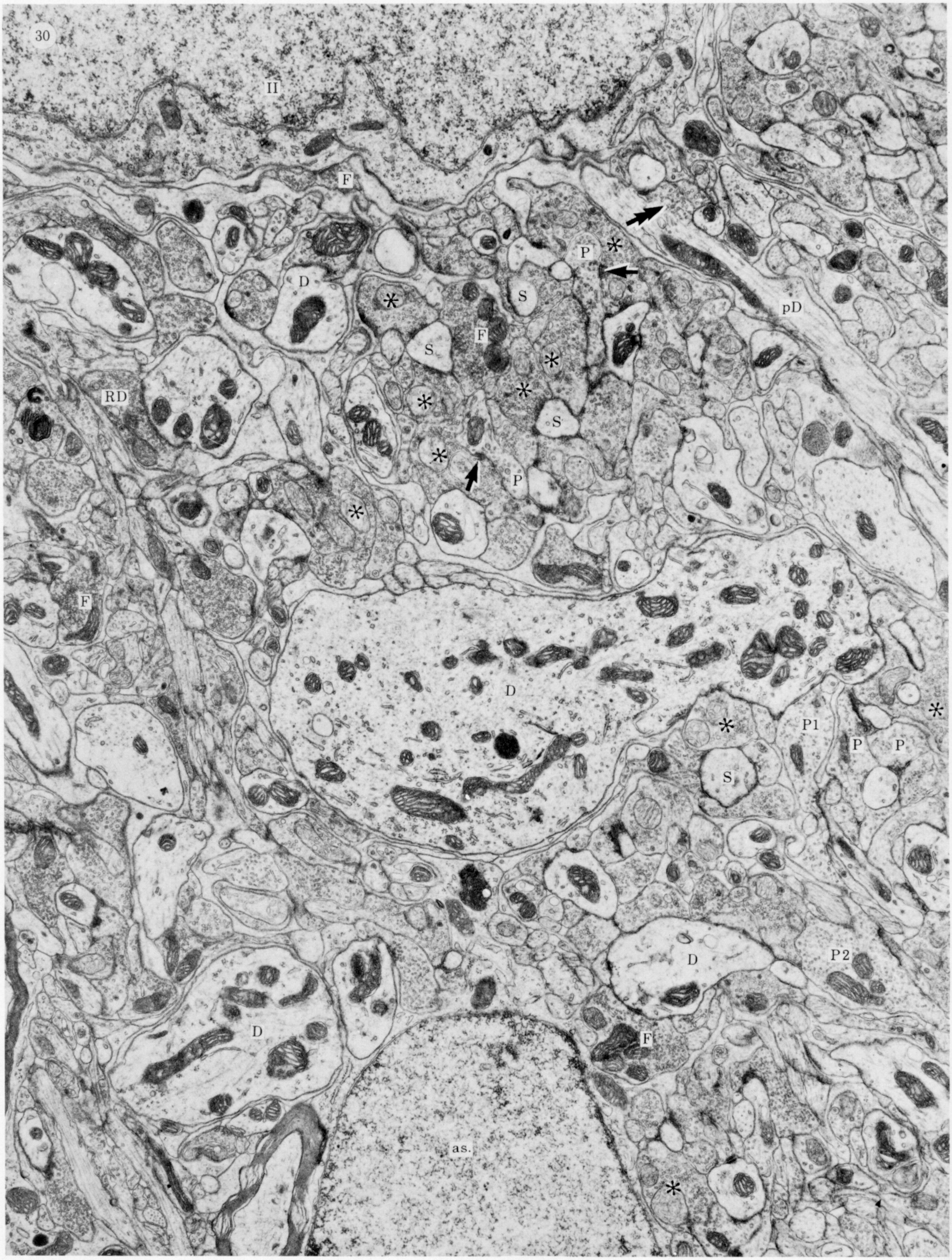

FIGURE 30. For description see p. 586.

FIGURES 31–37. For description see p. 587.

38*a*

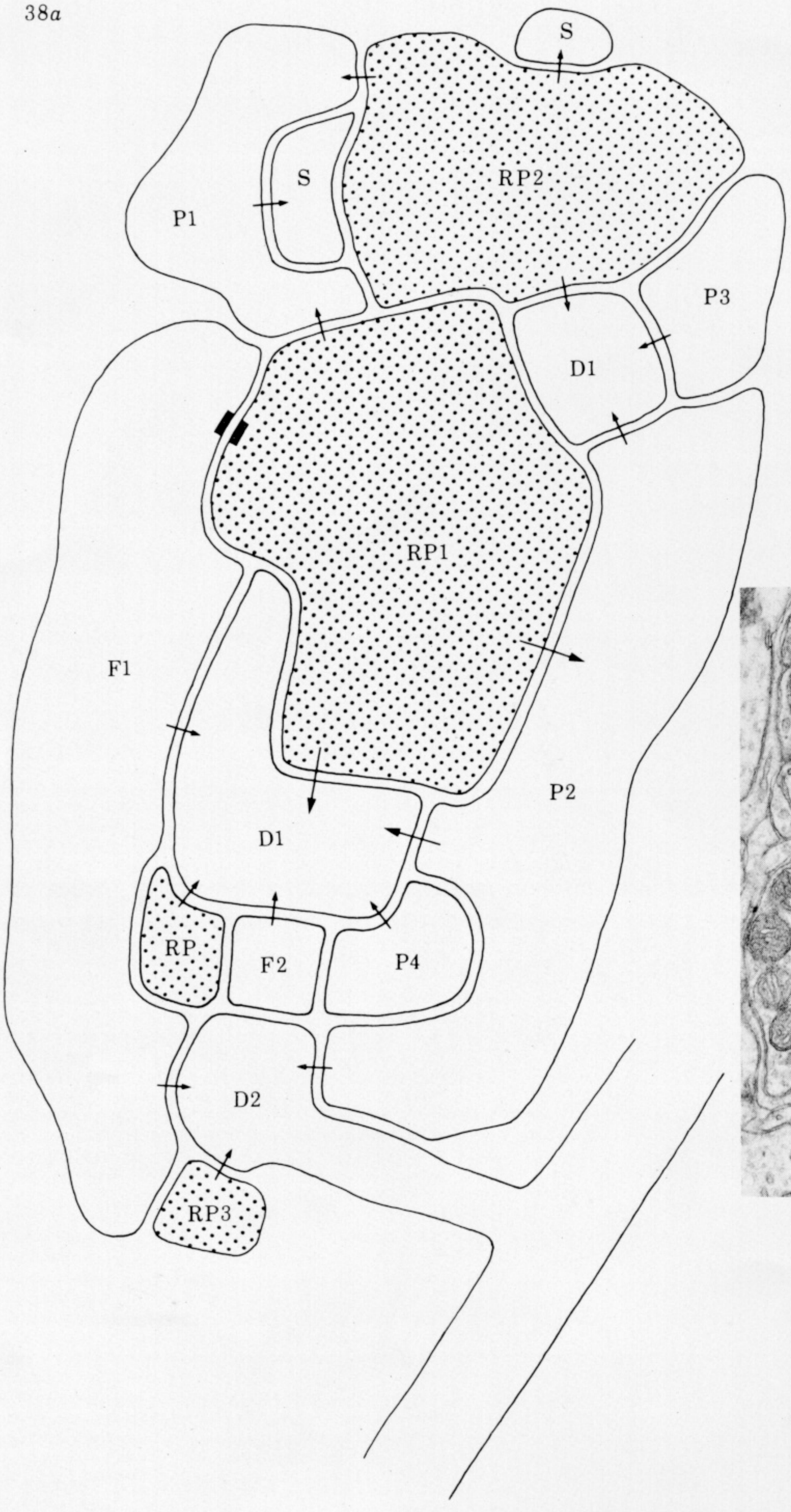

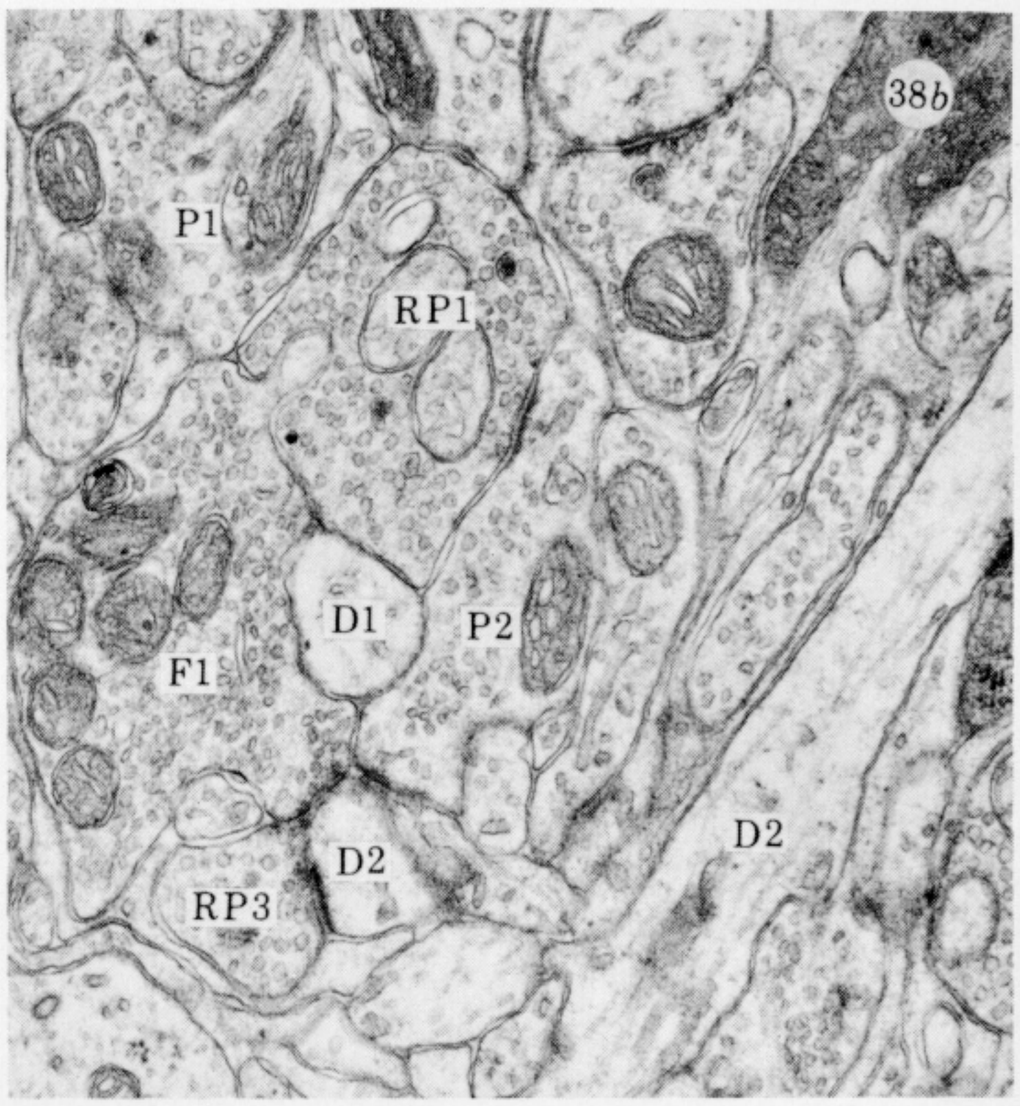

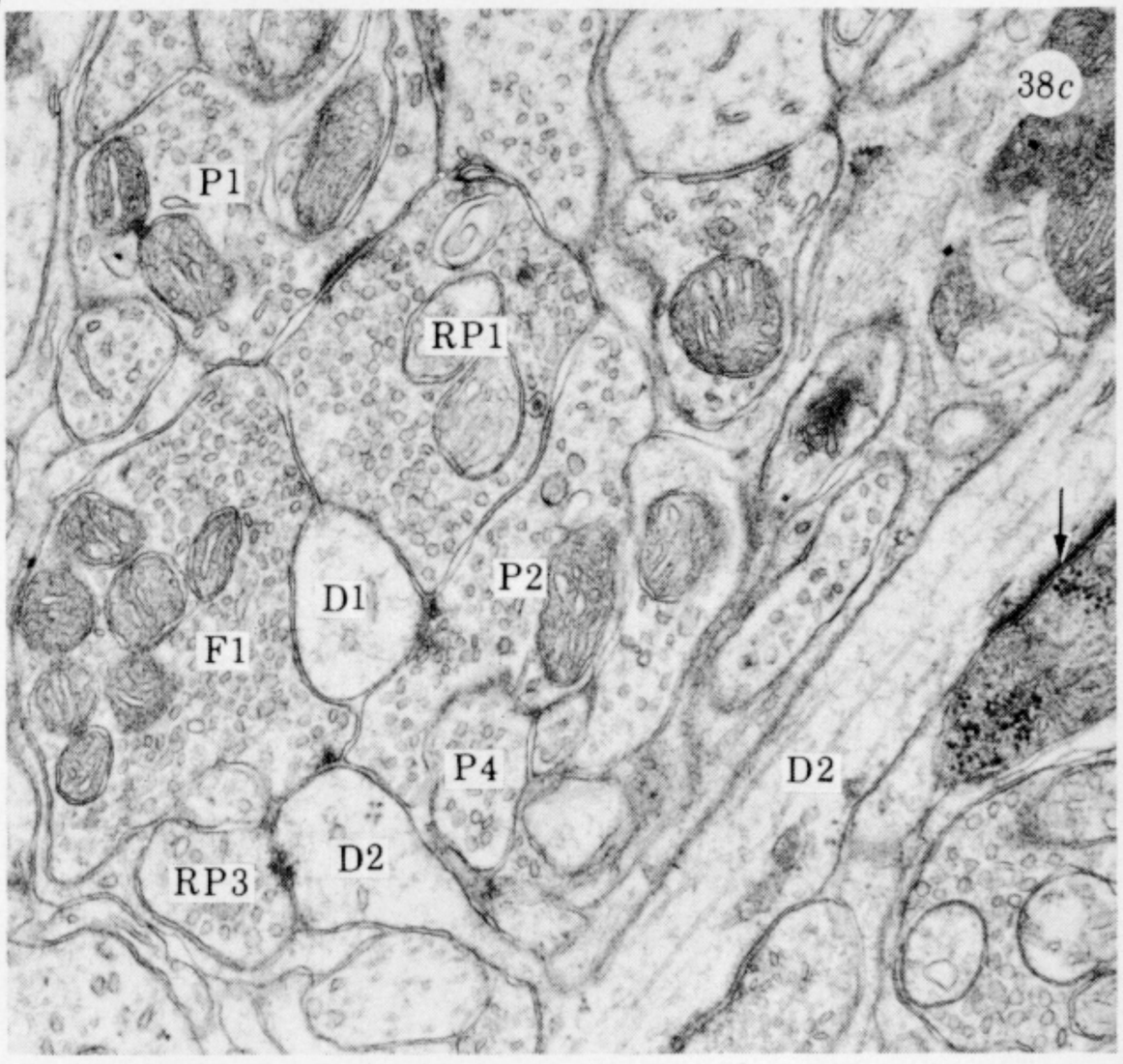

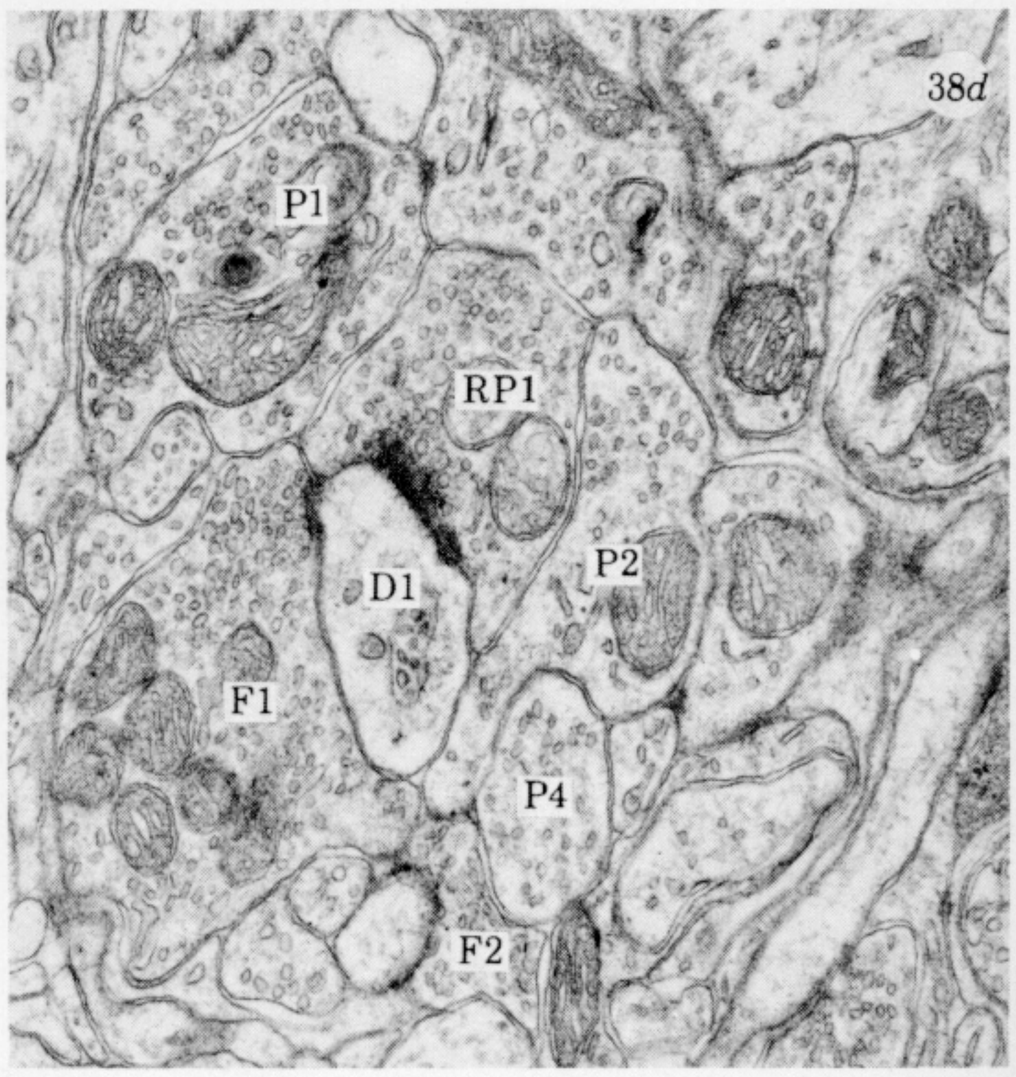

FIGURE 38. For description see opposite.

39*a*

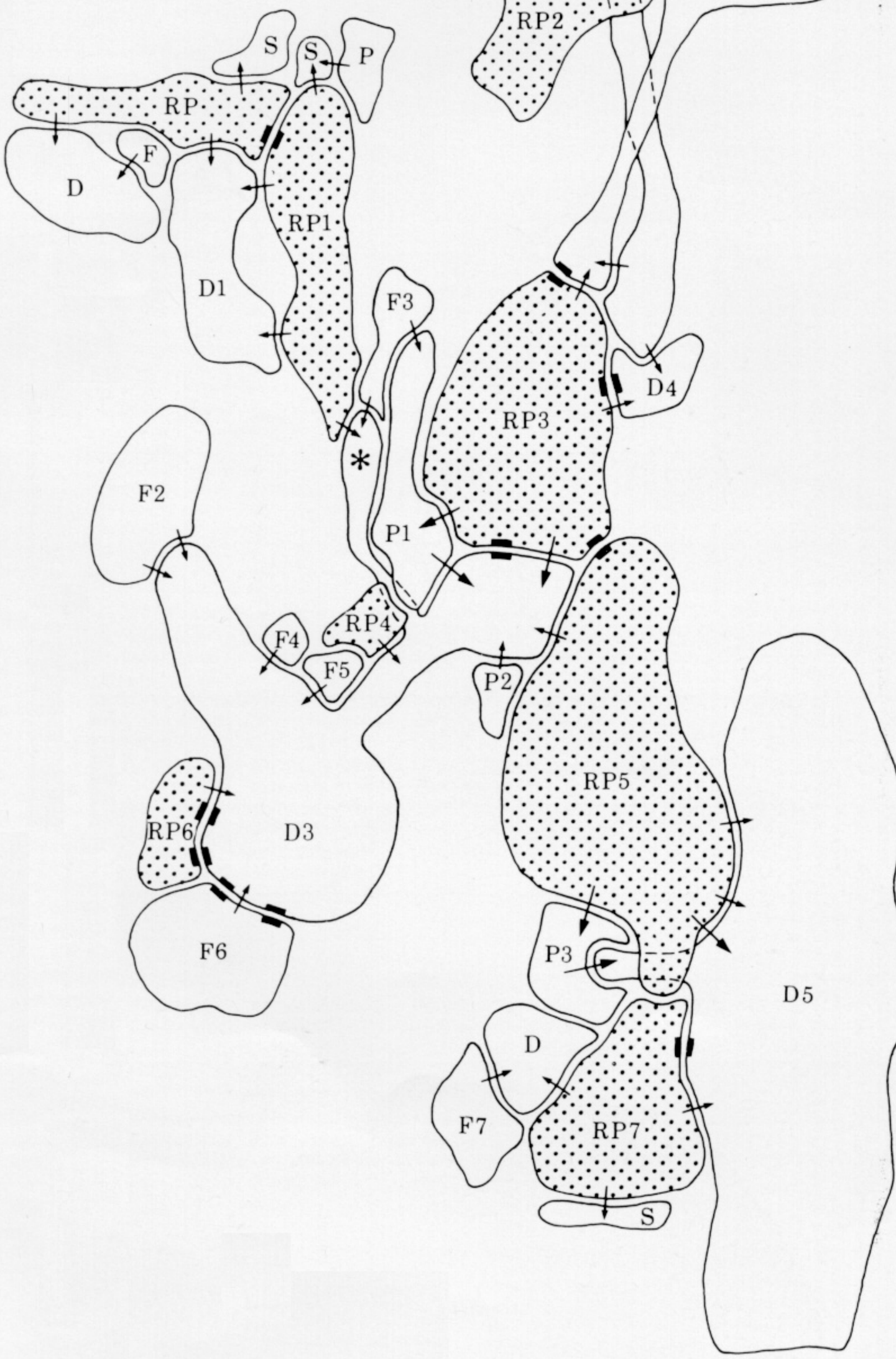

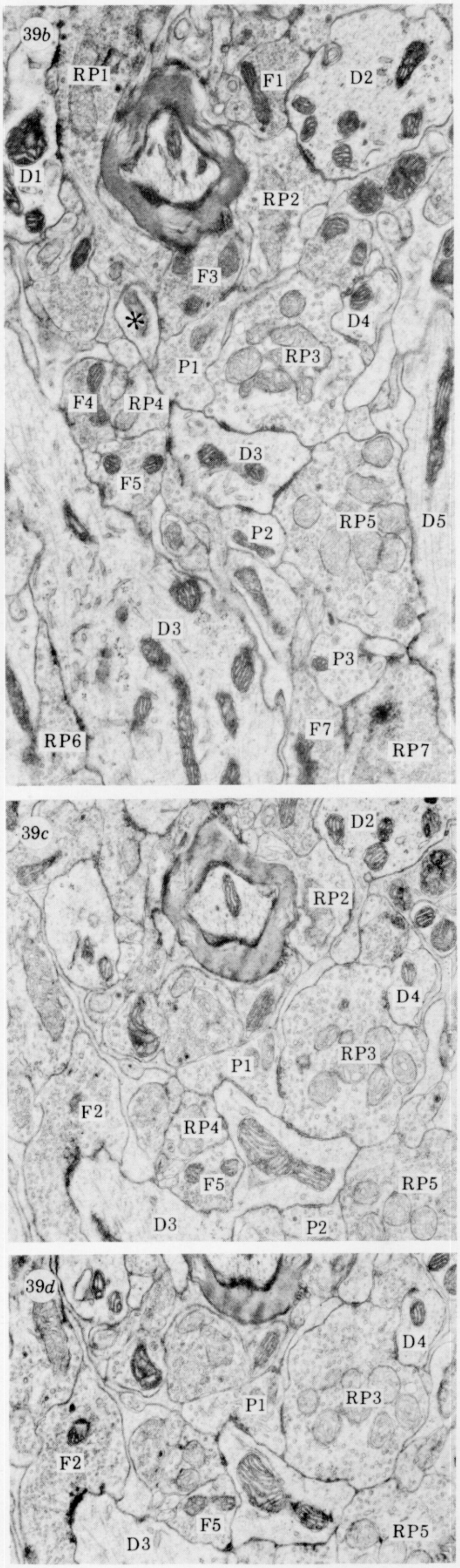

FIGURE 39. For description see opposite.

FIGURE 40. For description see p. 594.

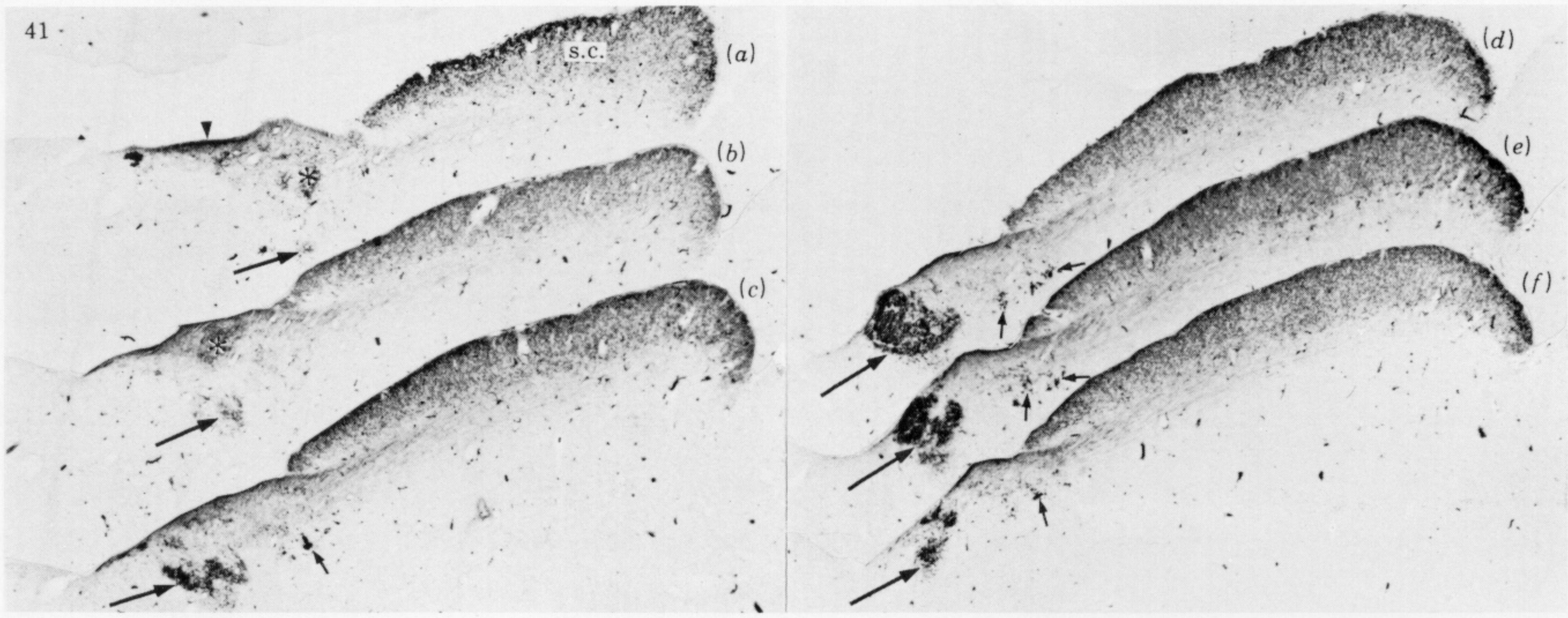

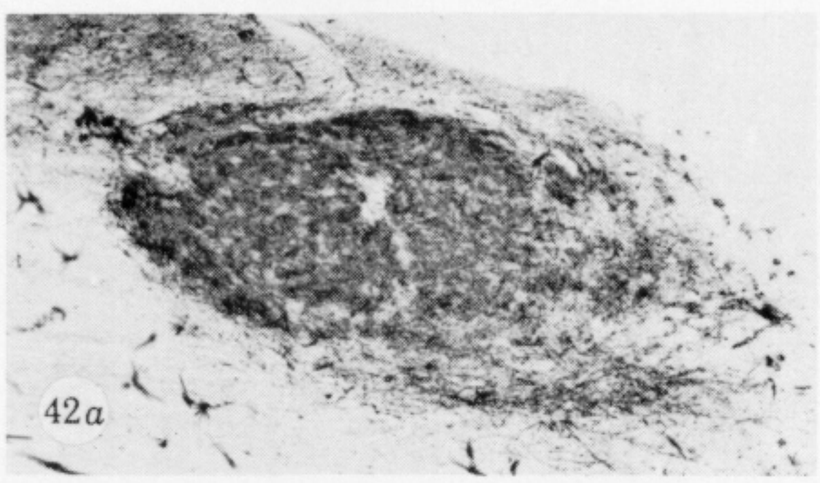
42a

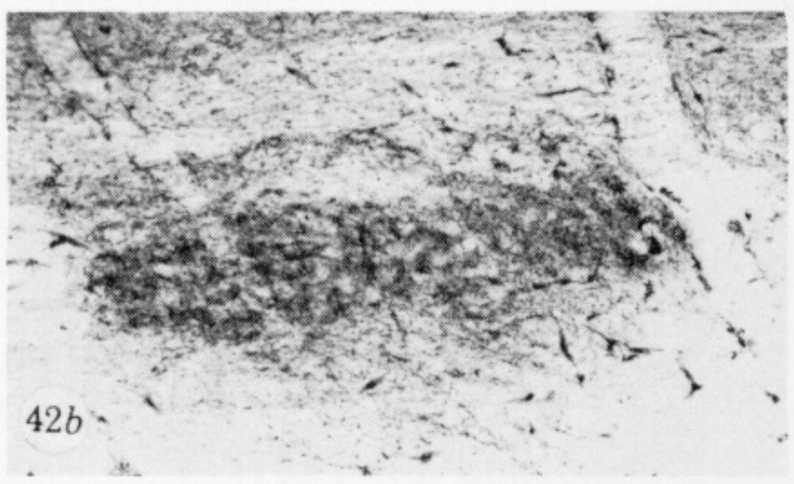
42b


42c


42d

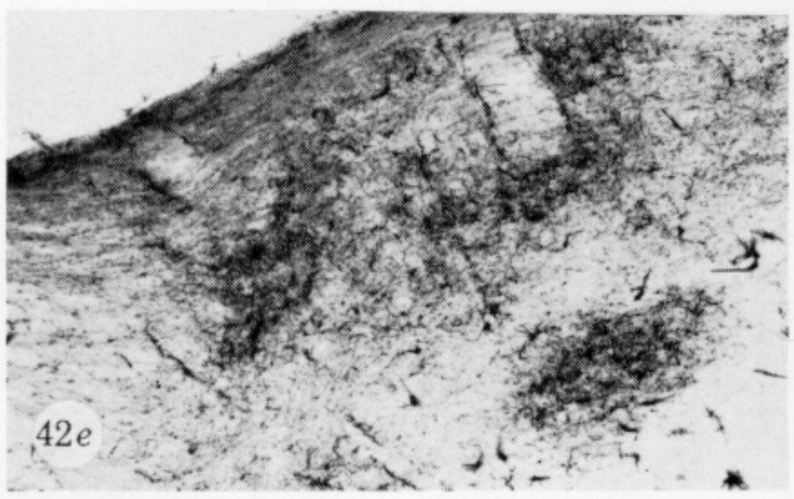
42e

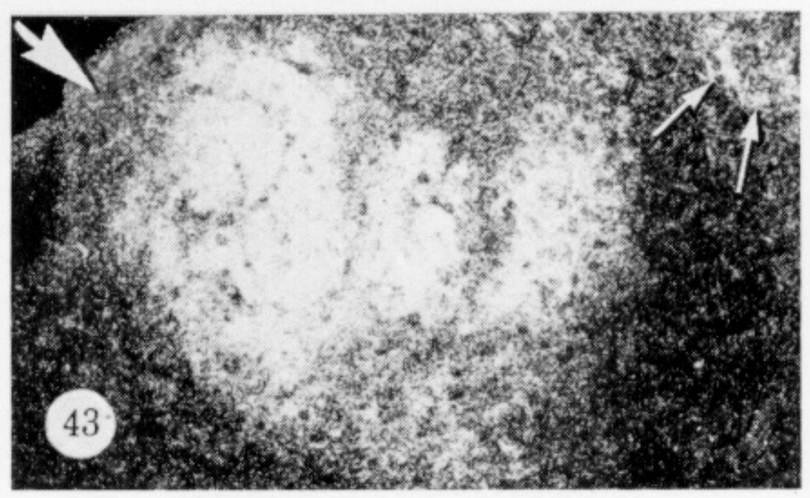
43

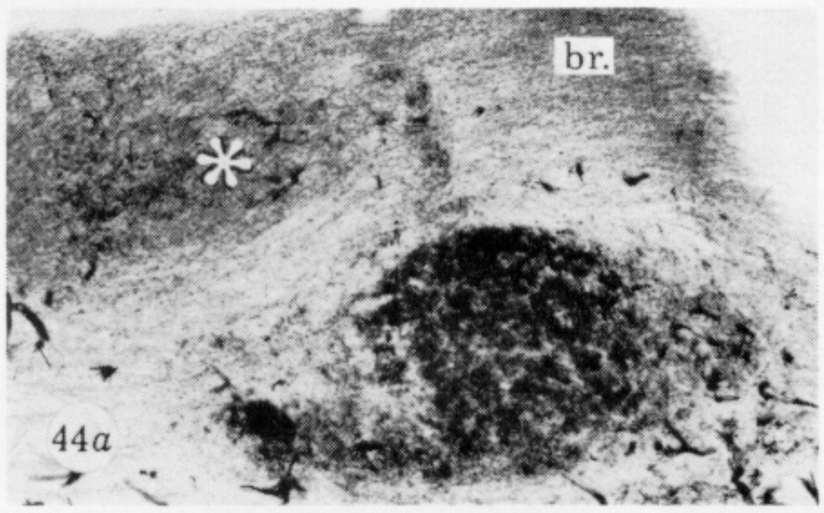

44a

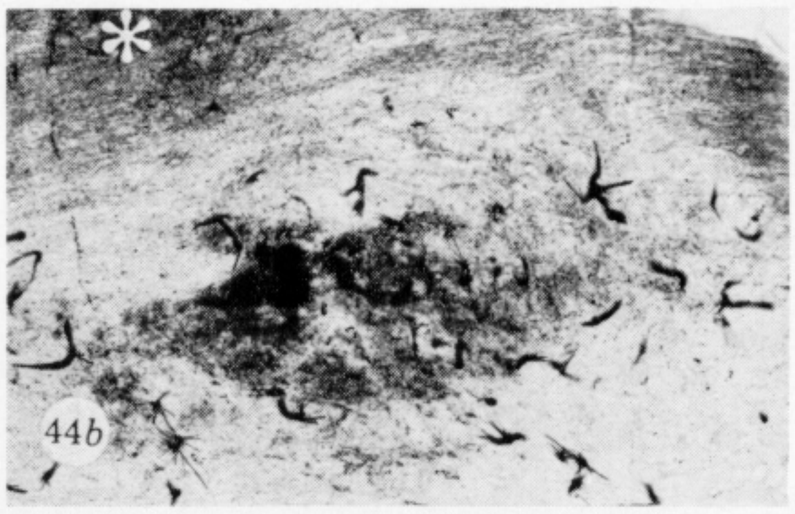
44b

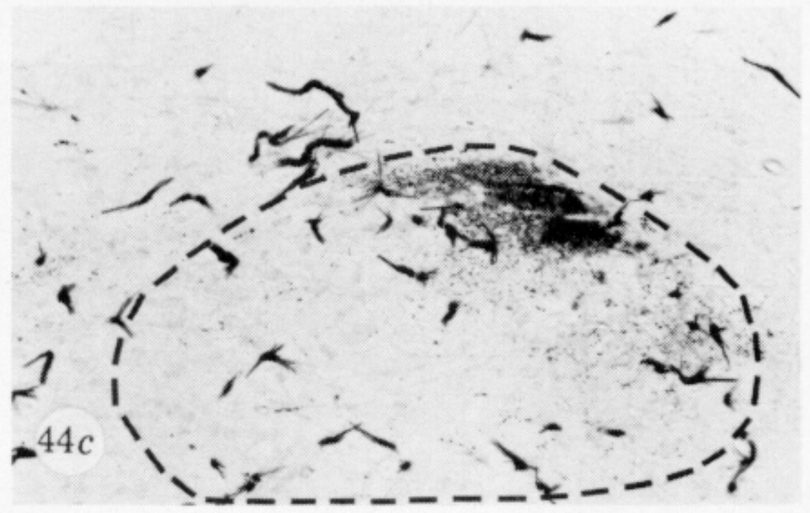
44c

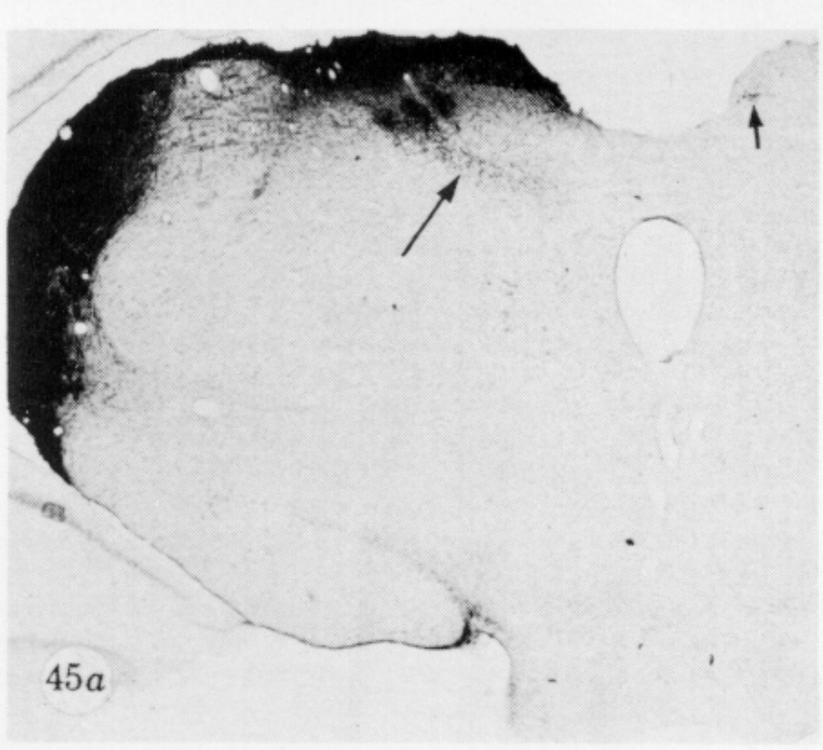
45a

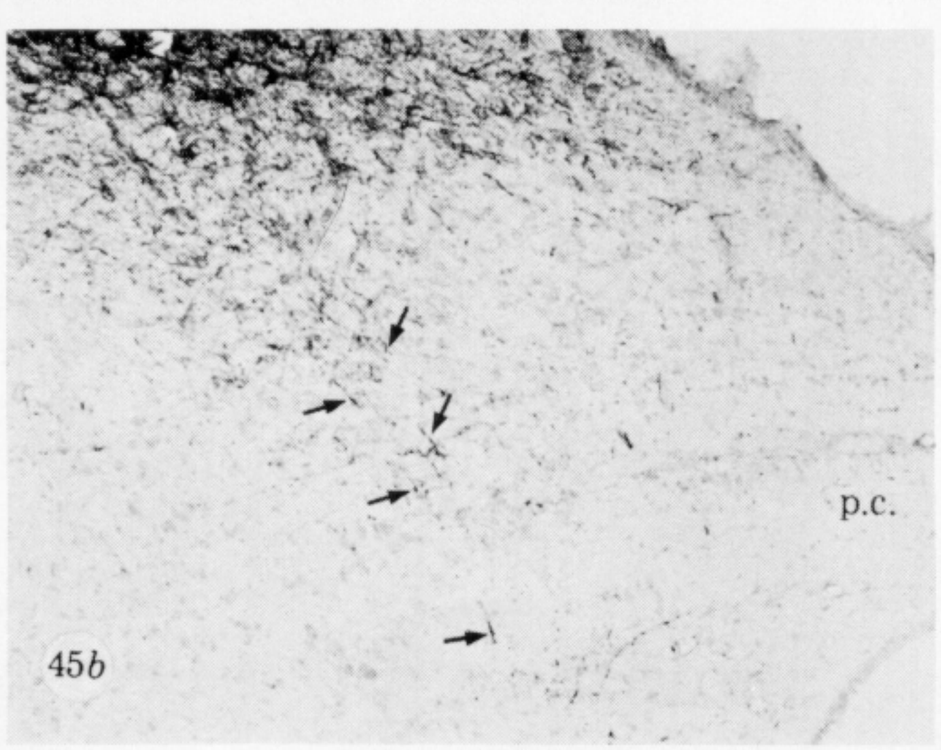

45b

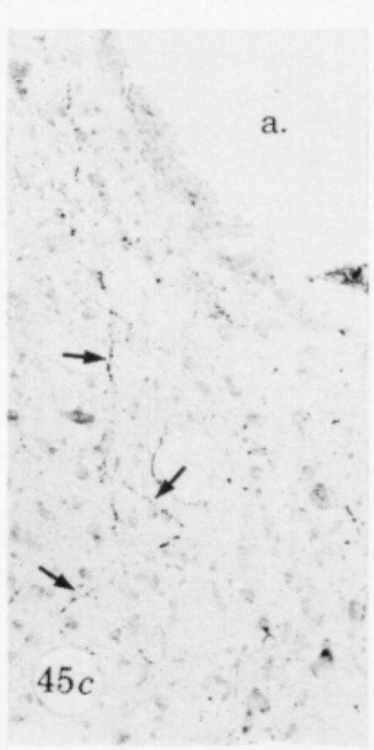

45c

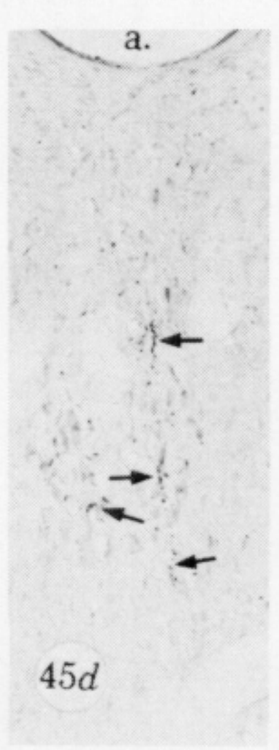

45d

FIGURES 41–45. For description see p. 594.

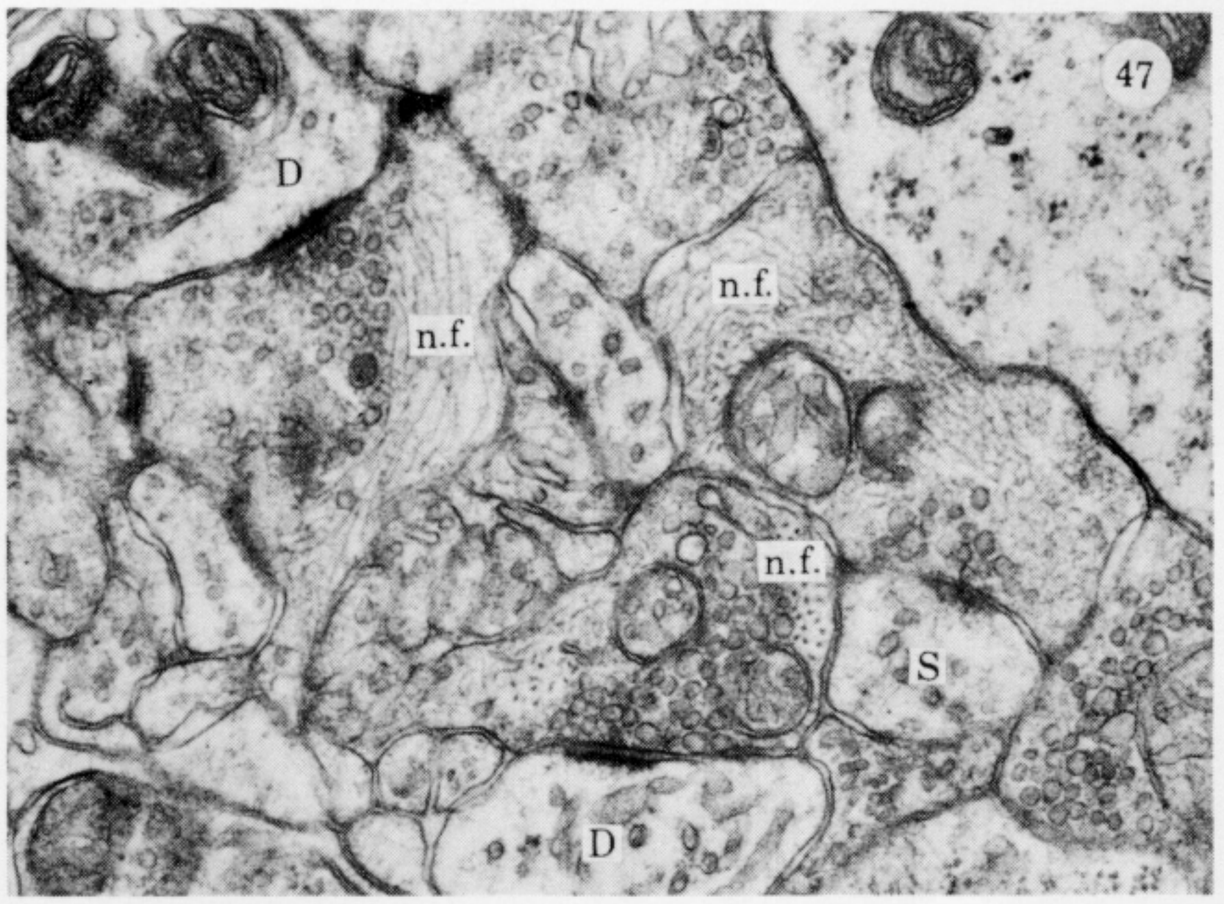

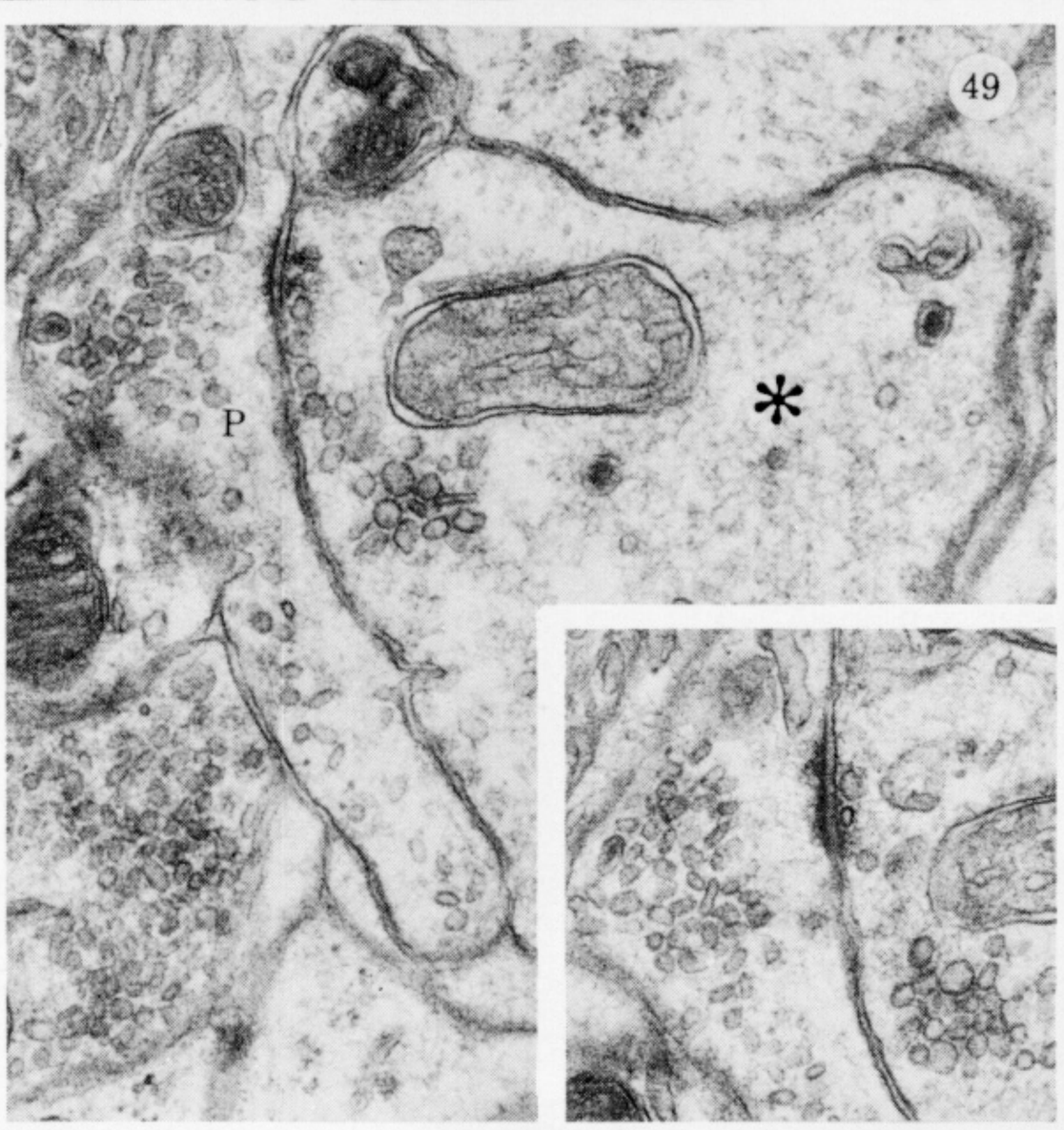

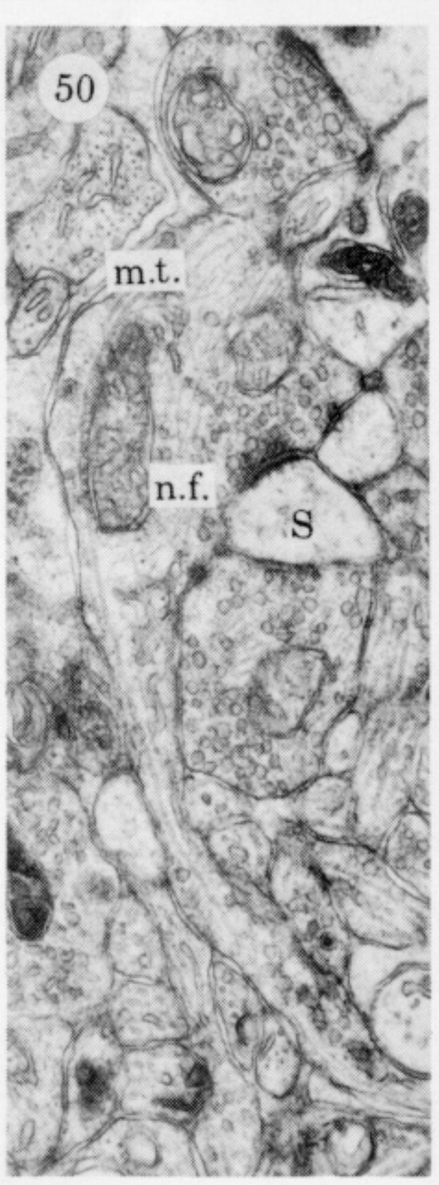

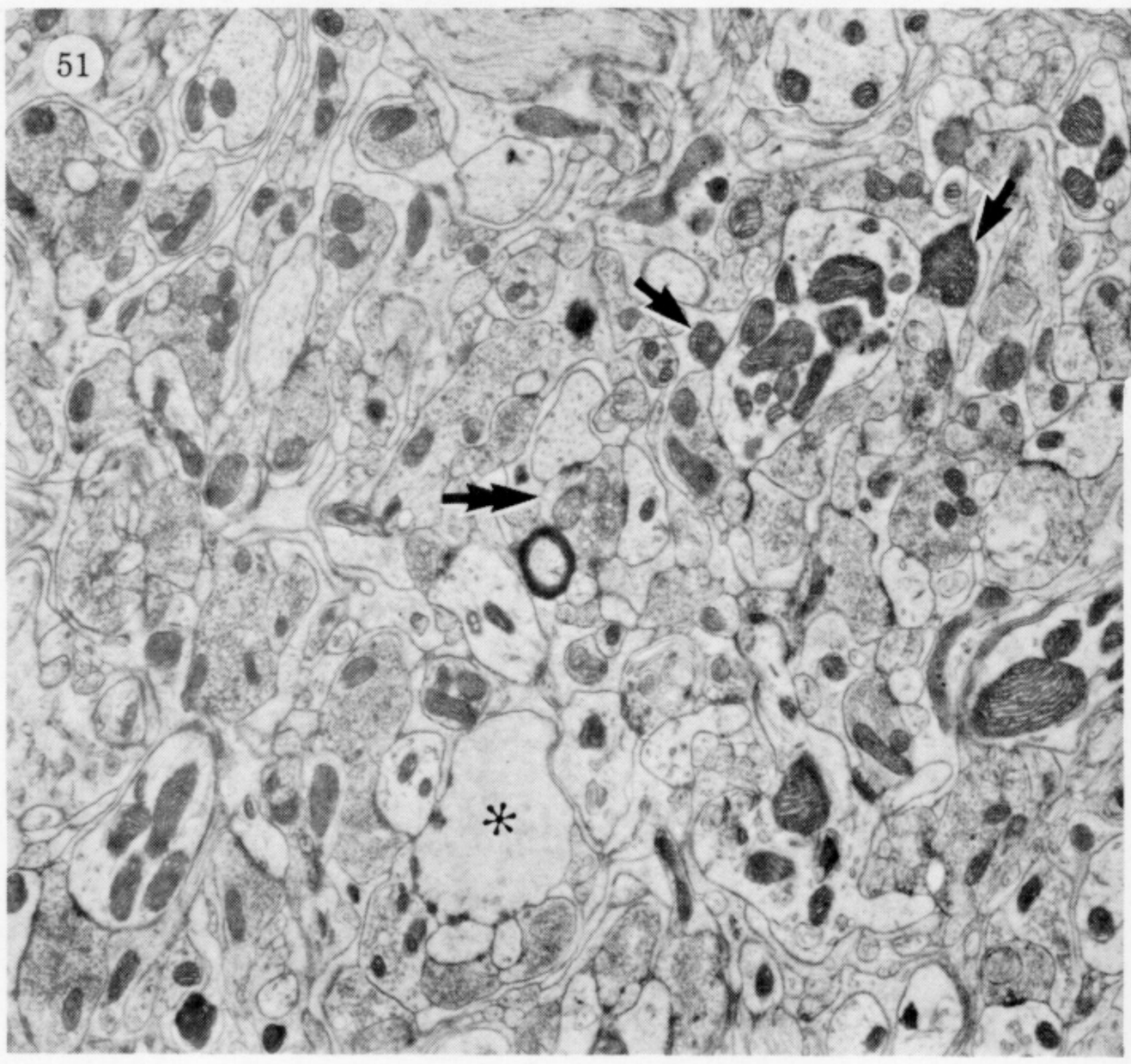

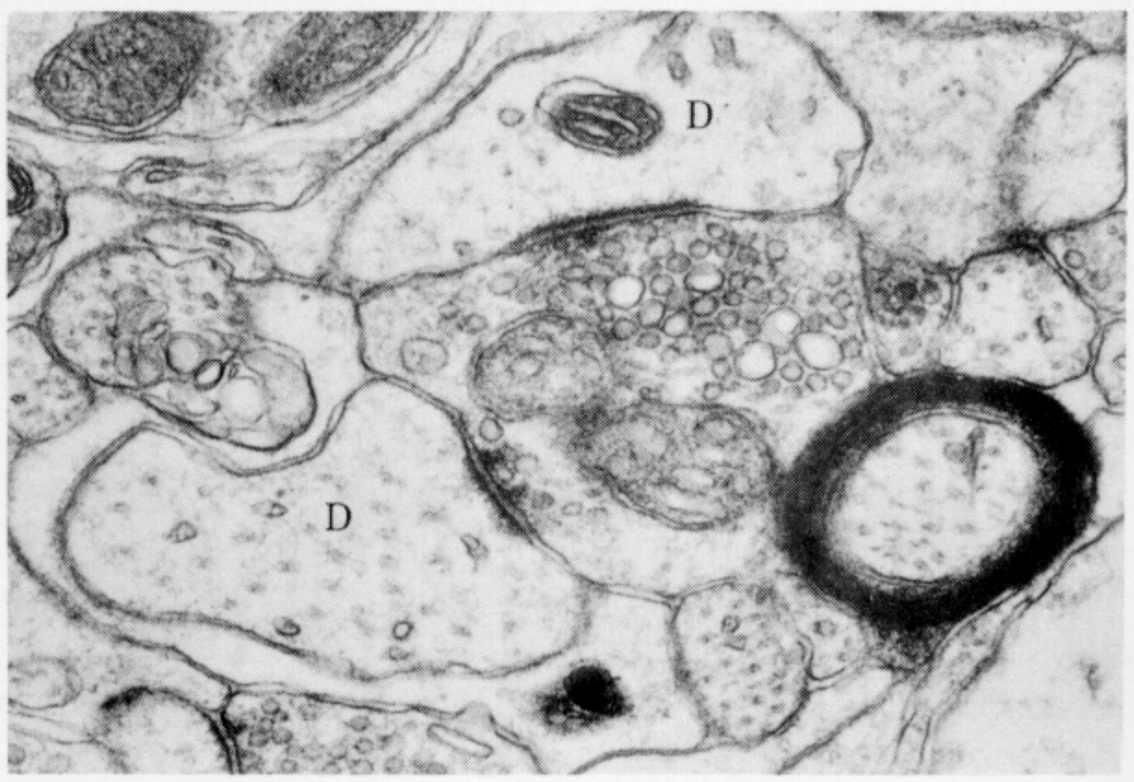

FIGURES 46–51. For description see opposite.

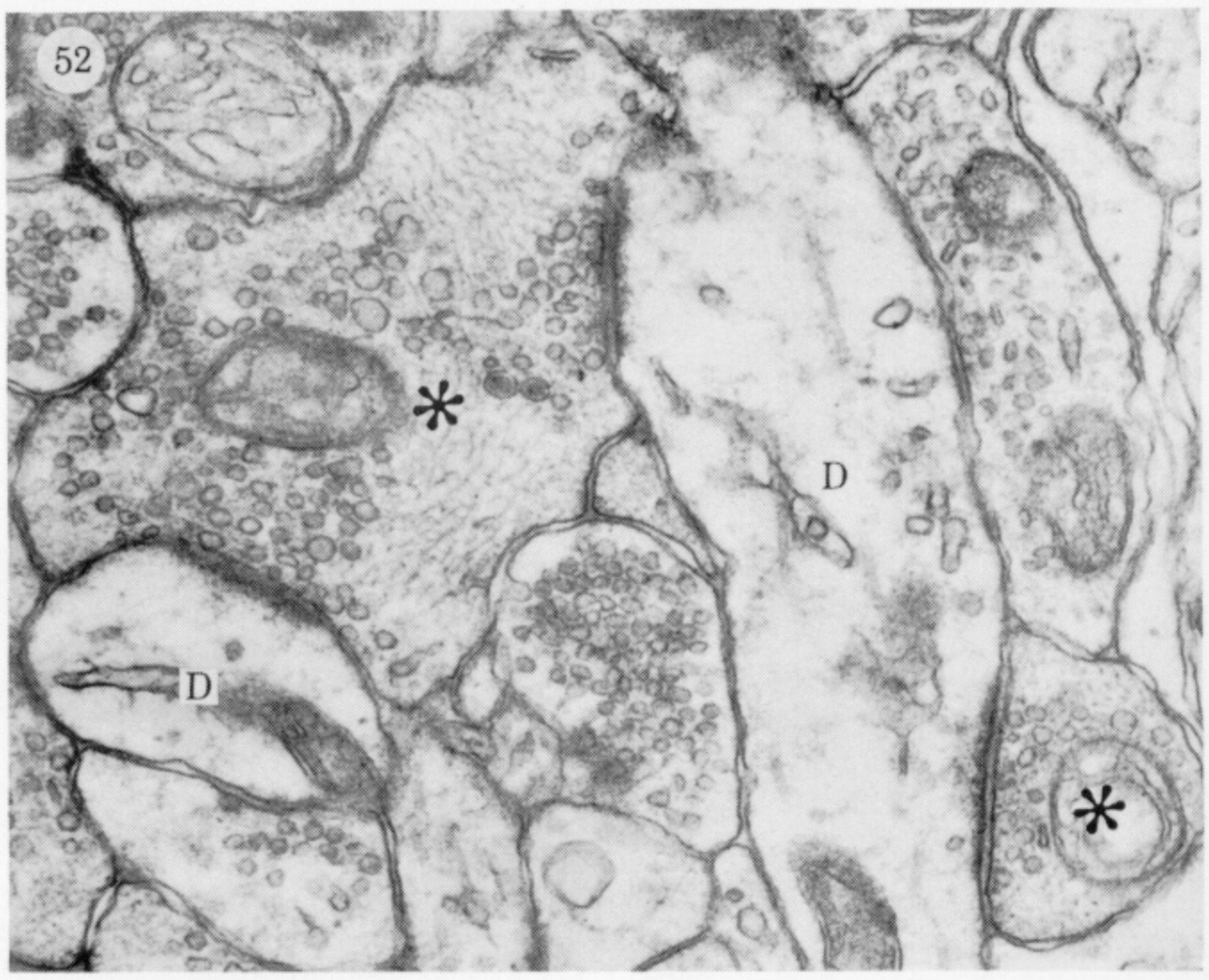

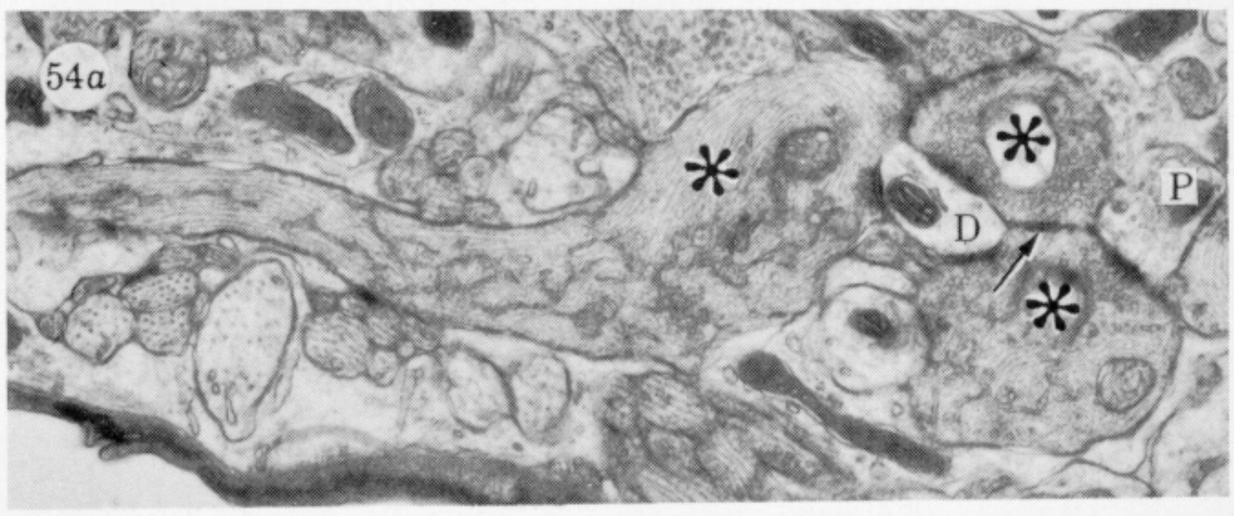

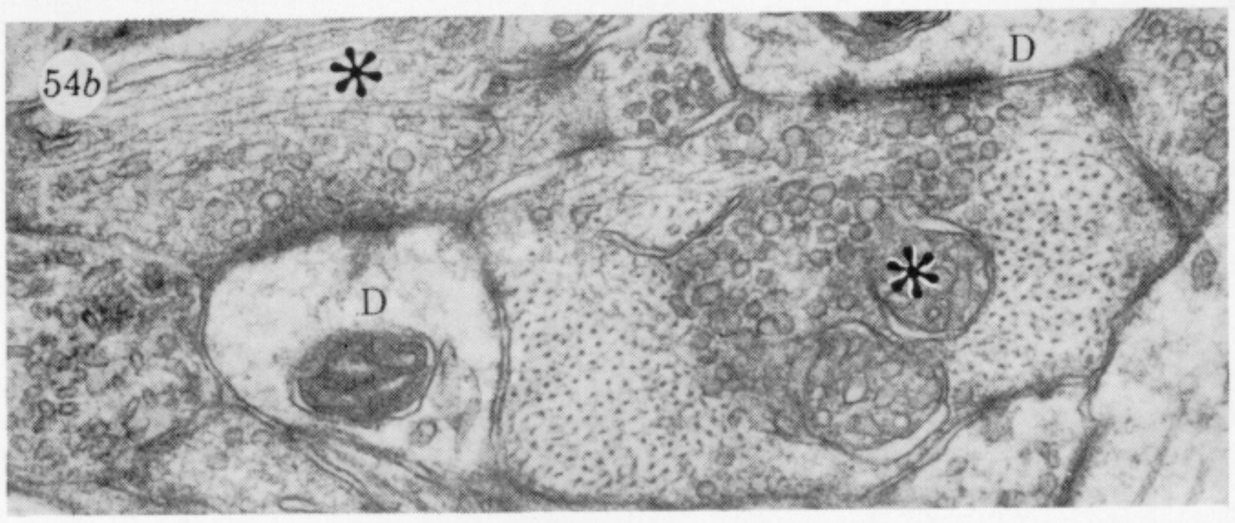

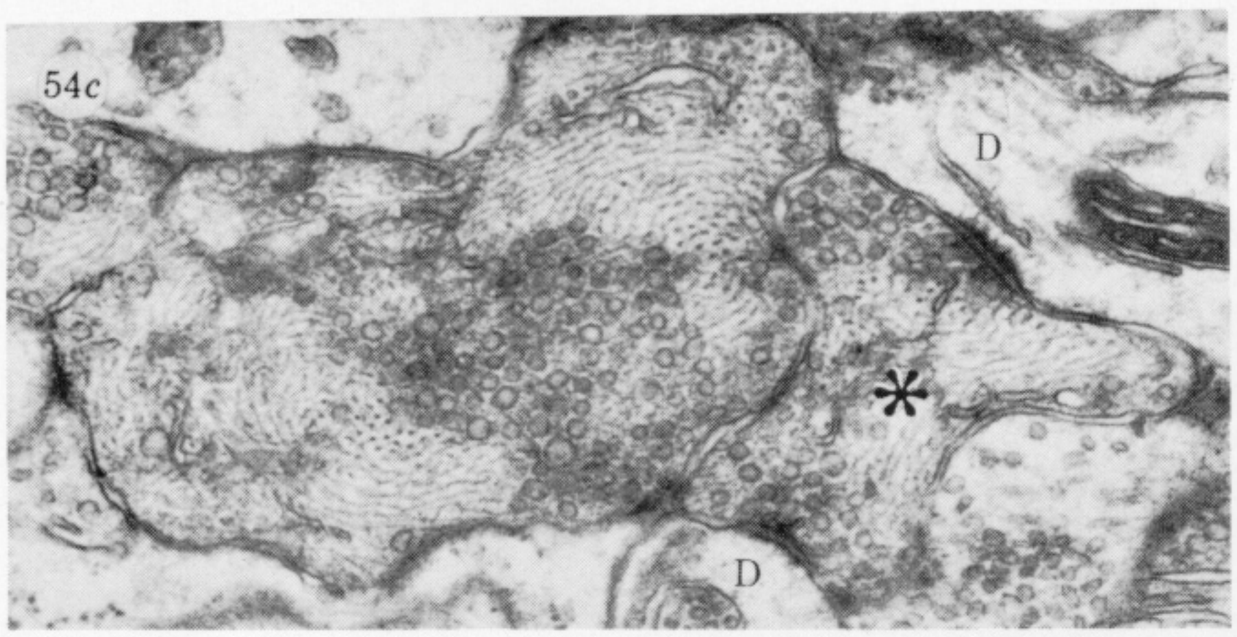

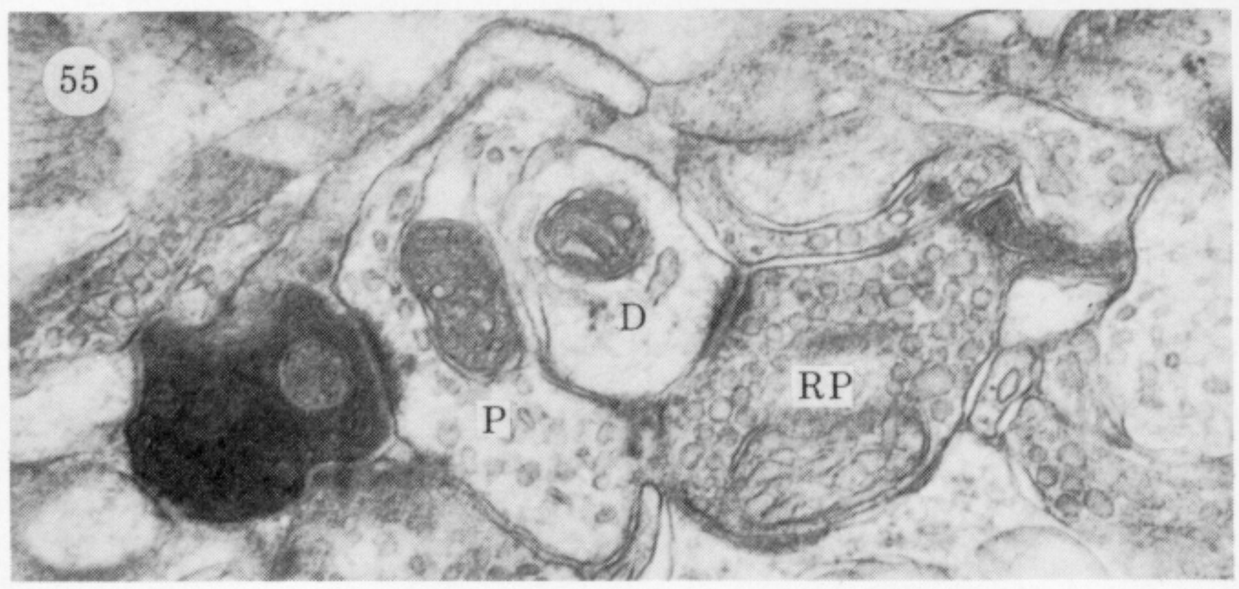

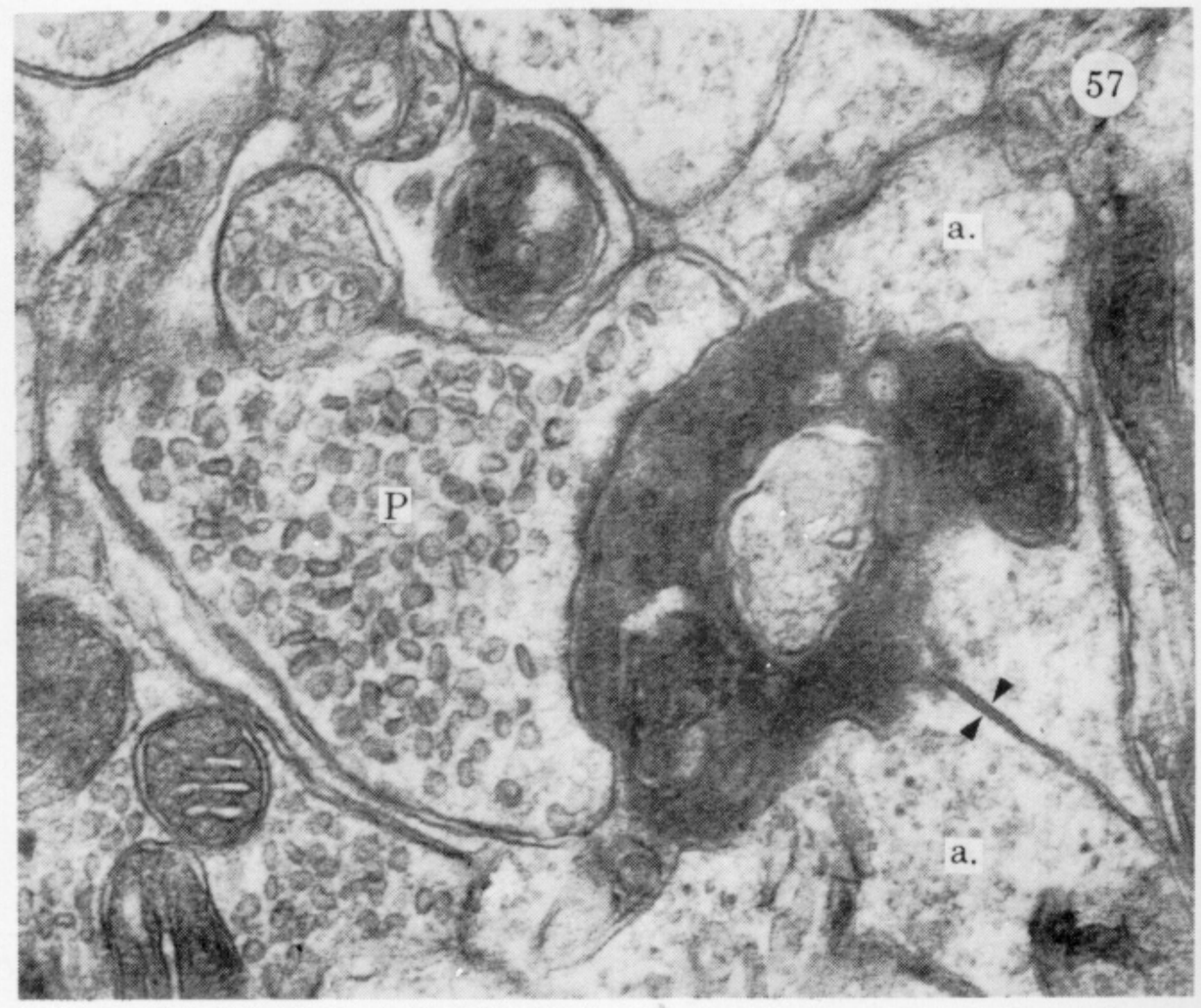

FIGURES 52–57. For description see facing plate 16.

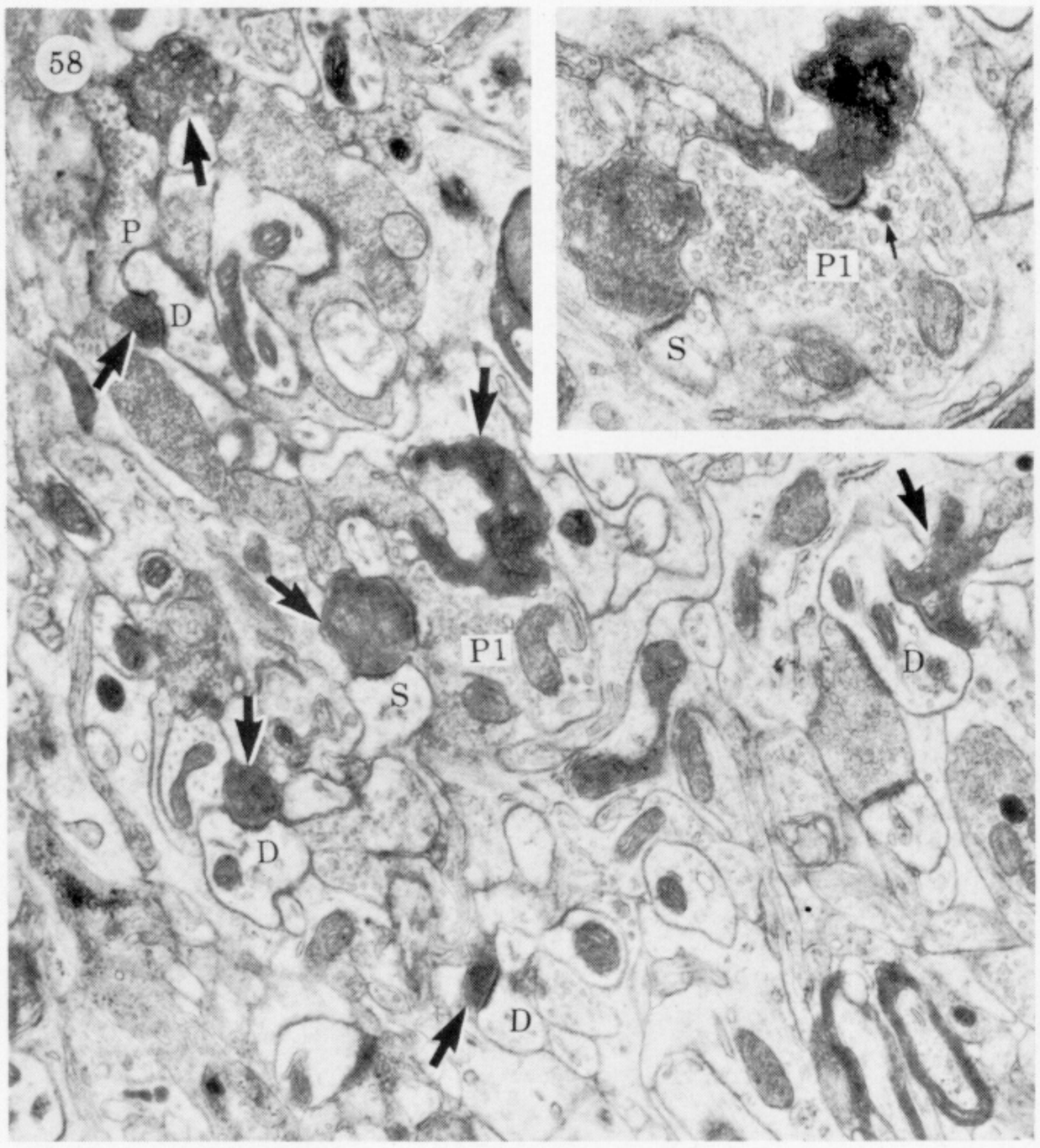

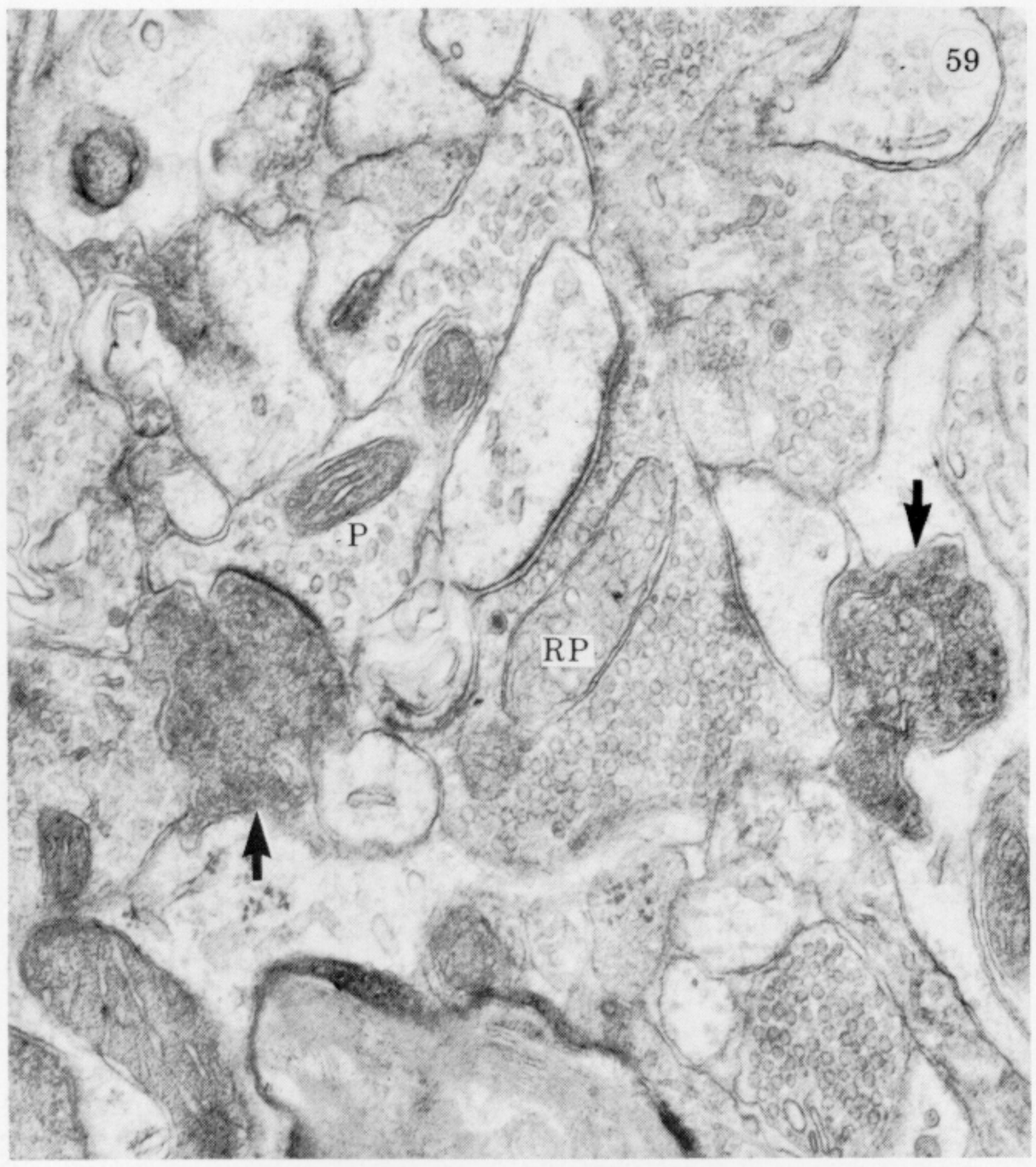

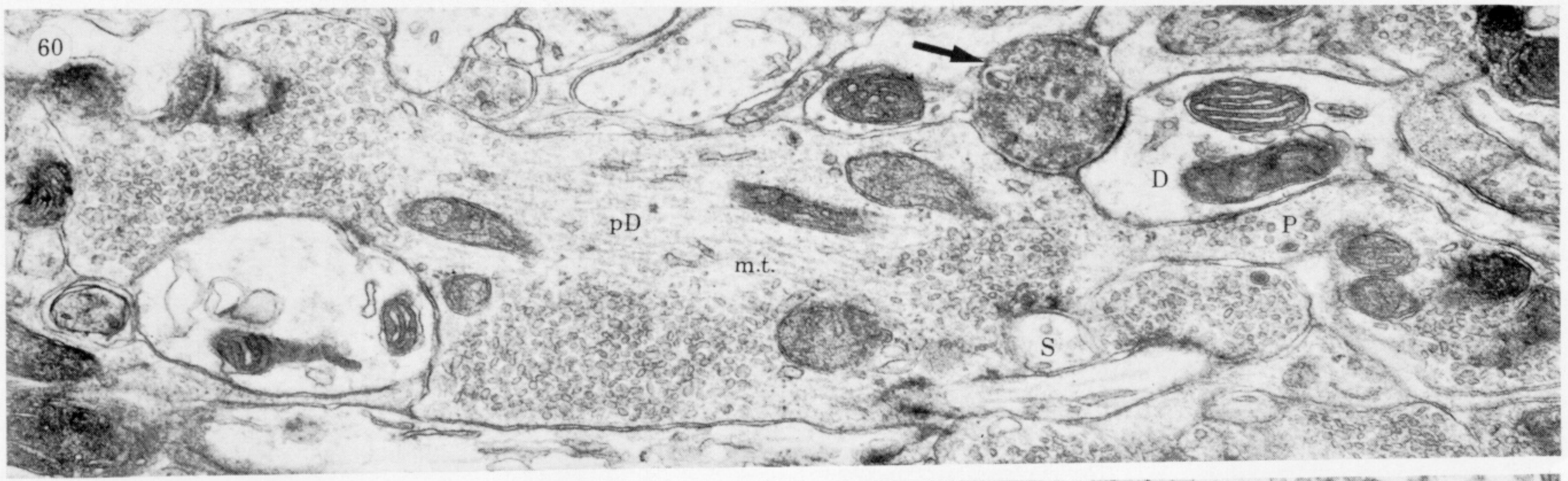

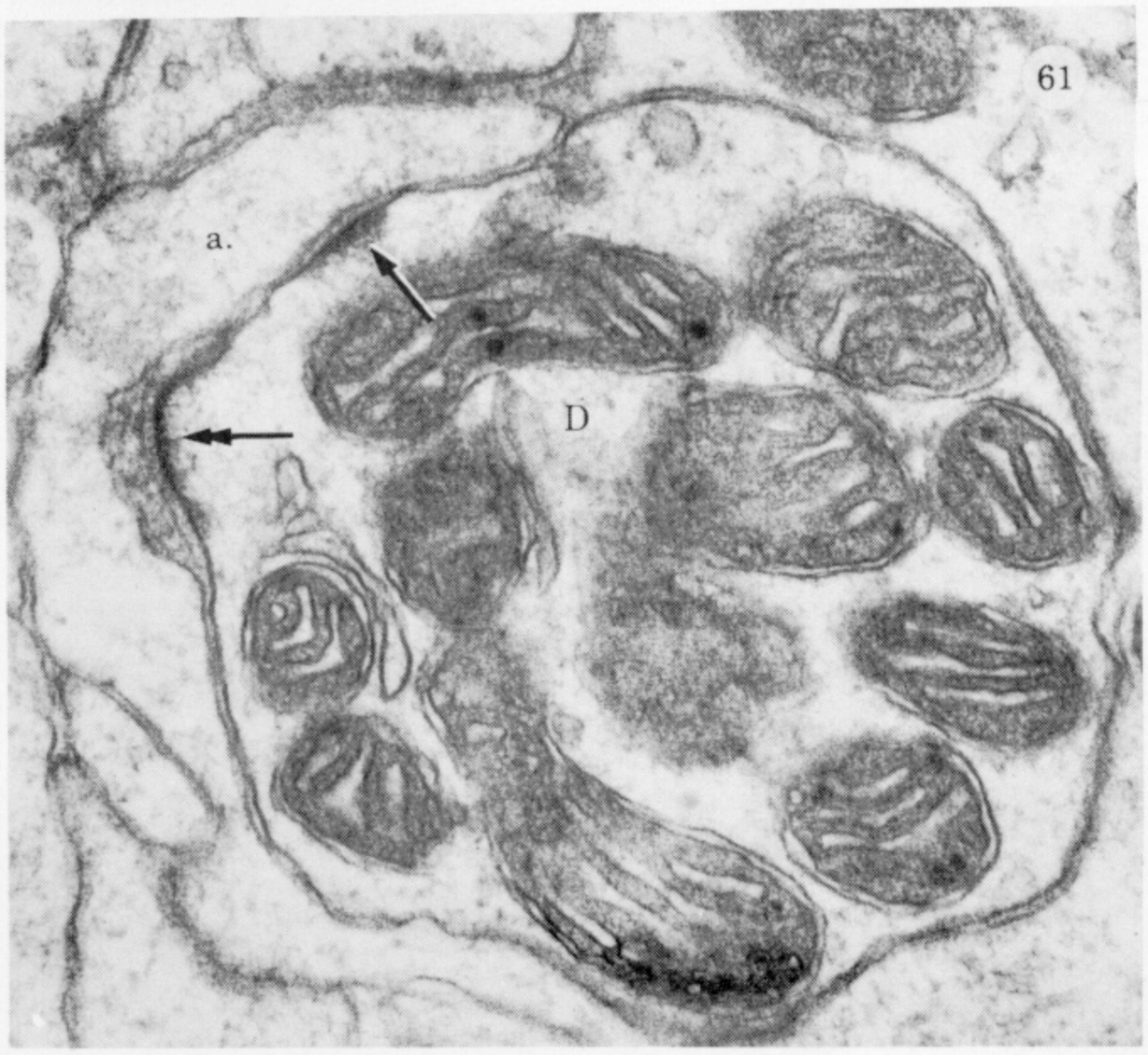

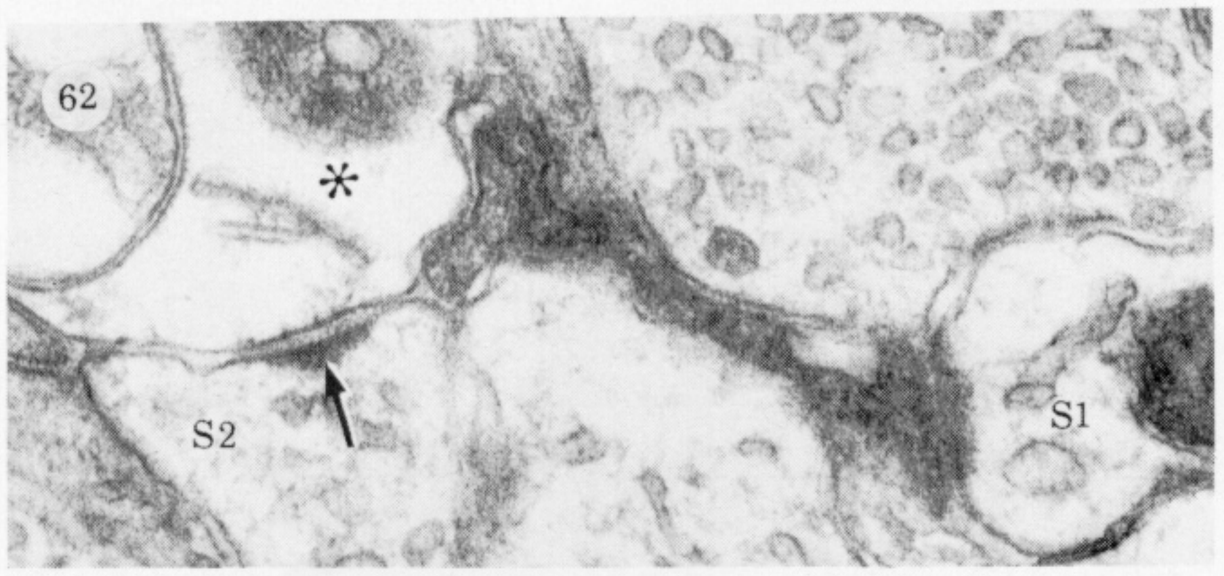

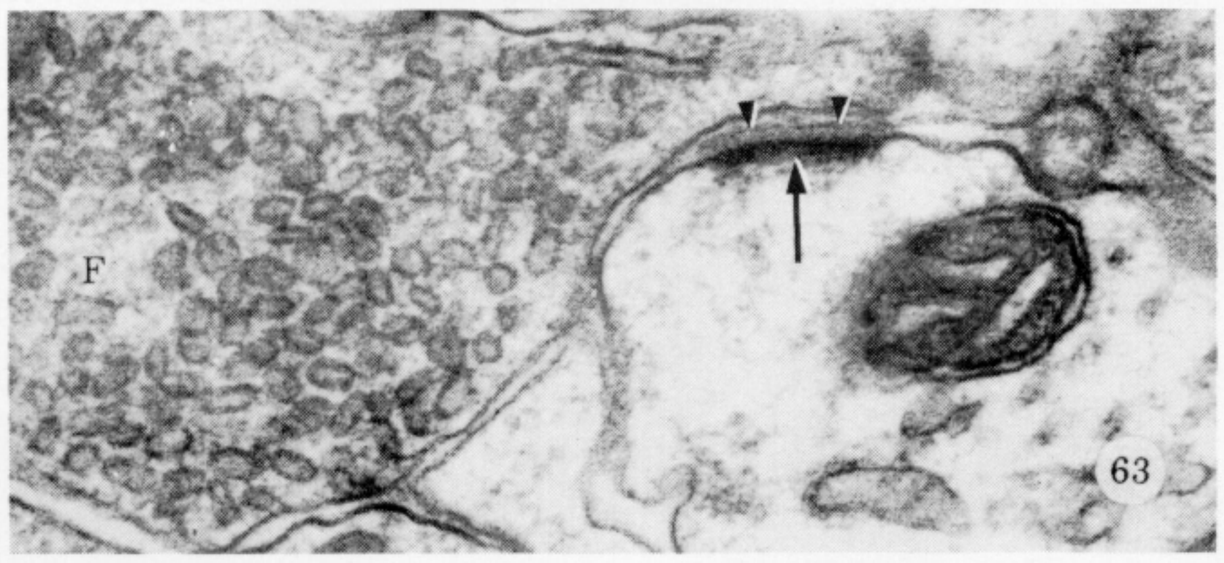

FIGURES 58–63. For description see p. 595.

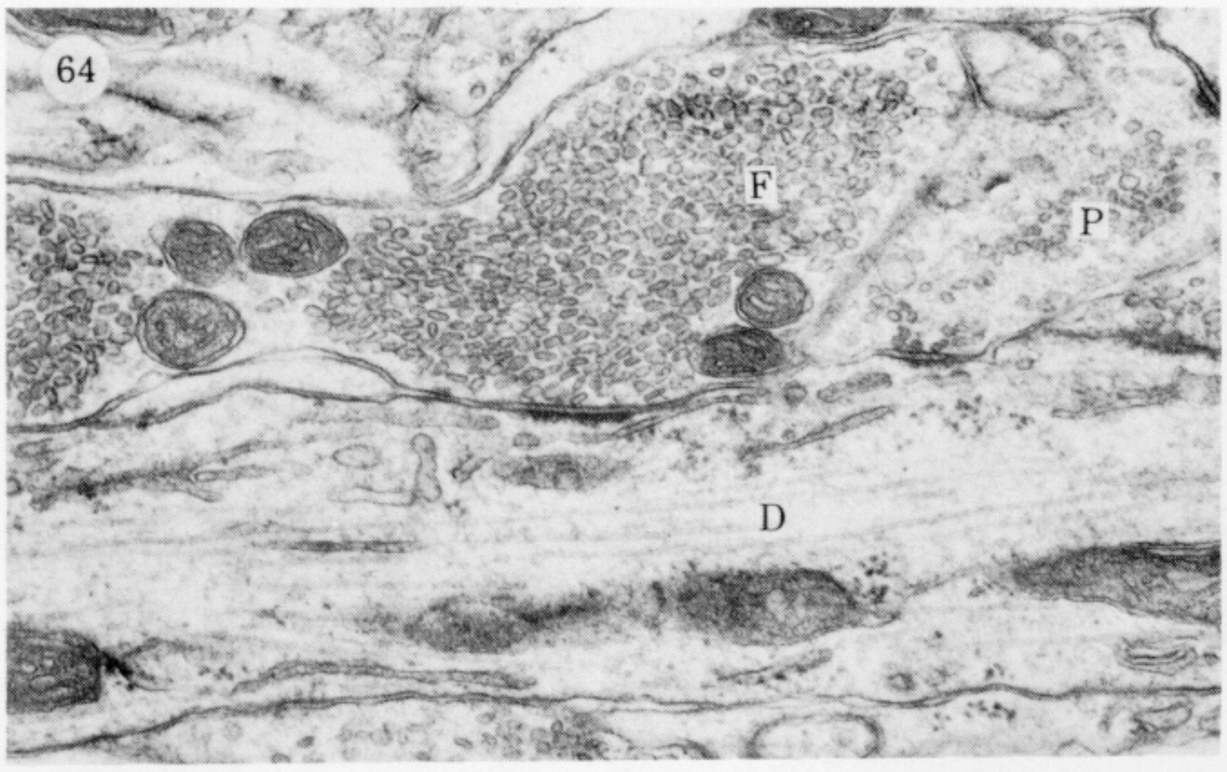

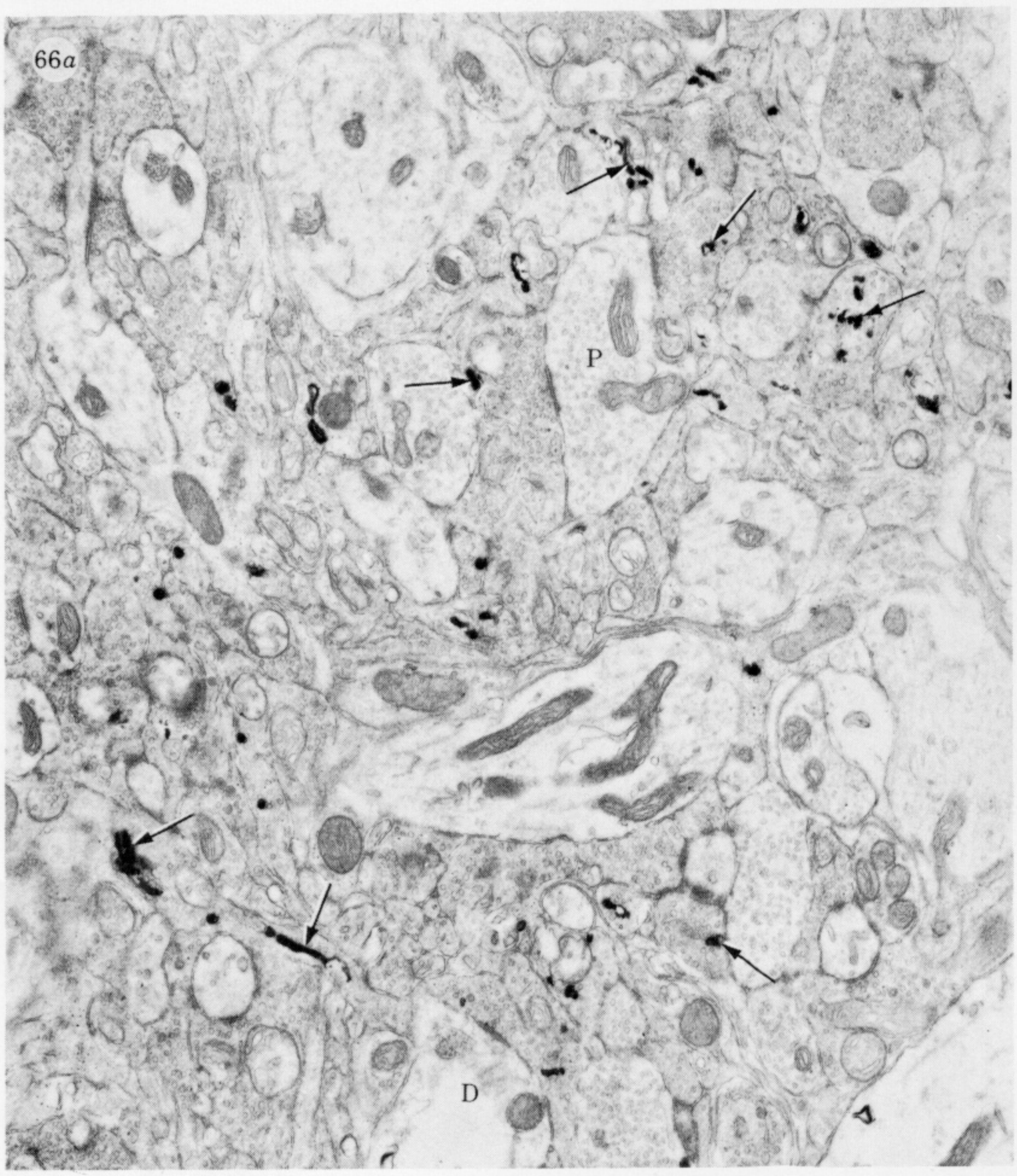

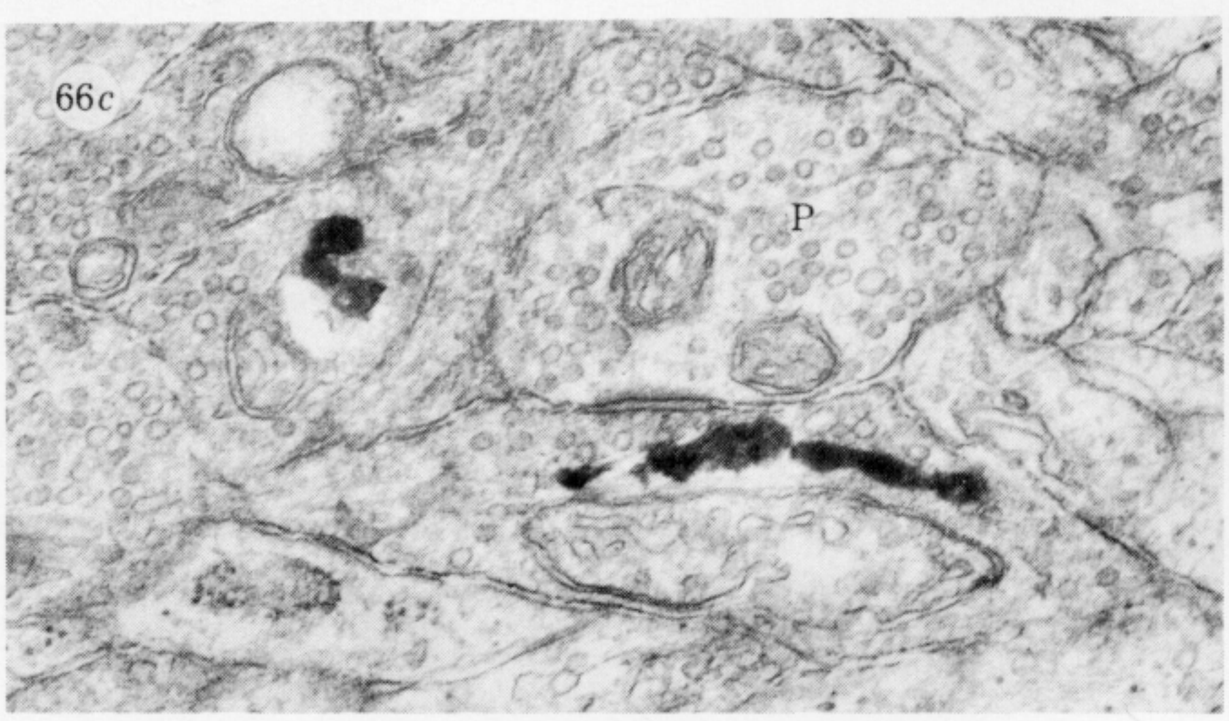

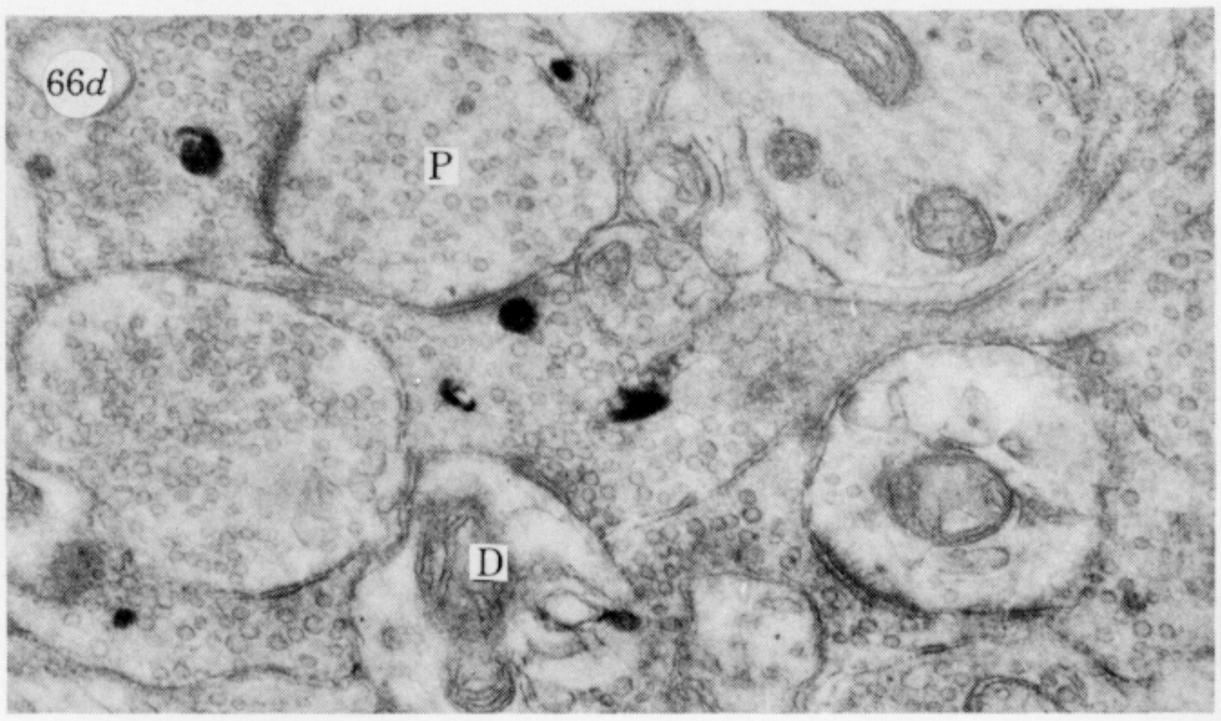

FIGURES 64–66. For description see p. 595.